

**Adaptation of Innovative CMC Fluid Film
Bearings for a Propellant Feeding Pump for
Cryogenic Space Propulsion Systems**

***Anwendungskonforme Anpassung innovativer
faserkeramischer Fluidlager an eine
Forschungstreibstoffförderpumpe für kryogene
Raumfahrtantriebe***

Bachelor Thesis from
cand. aer. Max Beitinger

IRS-24-S-005

University Professor:

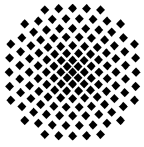
apl. Prof. Dr.-Ing. Georg Herdrich

Supervisor:

Dipl.-Ing. Markus Ortelt

German Aerospace Center, Stuttgart
Institute of Space Systems
University of Stuttgart

April 2024



Bachelor Thesis

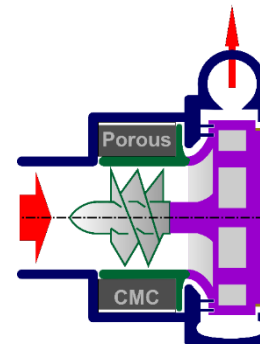
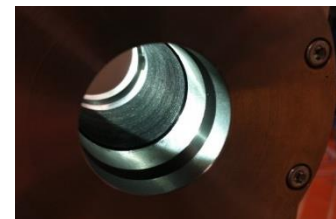
for Mr. Max Beitinger

Adaptation of innovative CMC fluid film bearings for a propellant feeding pump for cryogenic space propulsion systems

Motivation:

The Institute of Structures and Design of the DLR Stuttgart is currently transferring its innovative Ceramic Matrix Composite (CMC) fluid film bearing technology to the industrial application of cryogenic space propulsion systems. In collaboration with the research initiative Launch Canada and the German licensee space startup Black Engine Aerospace GmbH, the technology that has already been developed at DLR will be implemented in a specific turbopump demonstrator design.

The aim of this work is to use an existing engineering tool to adapt the bearing geometry based on the specifications and geometric constraints of the demonstrator application, as well as to design and construct a modular interchangeable bearing component for the research pump. Special attention and novelty will be given to evaluating the future consideration of potential particle emissions from the fiber ceramic into the hydraulic circuit.



CMC fluid film bearing technology (DLR)
 (Source: DLR)

Task:

- Literature research
- Collection of operative specifications for the bearing design
- Design and construction of the modular bearing component
- Preparational assessment of potential particle emission out of the CMC-component
- Presentation and discussion of the scientific results and report

The work is carried out at DLR Stuttgart

Supervisor, internal: apl. Prof. Dr. G. Herdrich

Supervisor, external: Dipl.-Ing. Markus Ortelt

Start of processing: 15.01.2024

Latest submission: 10.05.2024

Acknowledgment of receipt:

I hereby confirm that I have read and understood the task as well as the legal provisions and the study and examination regulations.

15.01.2024, gez. G. Herdrich
 Date
 apl. Prof. Dr.-Ing.
 Georg Herdrich
 (Responsible University lecturer)

10.01.2024, gez. M. Ortelt
 Date
 External supervisor

15.01.2024, gez. M. Beitinger
 Date
 Signature of student

Rechtliche Bestimmungen: Der/die Bearbeiter/in ist grundsätzlich nicht berechtigt, irgendwelche Arbeits- und Forschungsergebnisse, von denen er/sie bei der Bearbeitung Kenntnis erhält, ohne Genehmigung des/der Betreuers/in dritten Personen zugänglich zu machen. Bezüglich erreichter Forschungsleistungen gilt das Gesetz über Urheberrecht und verwandte Schutzrechte (Bundesgesetzblatt I/S. 1273, Urheberrechtsgesetz vom 09.09.1965). Der/die Bearbeiter/in hat das Recht, seine/ihre Erkenntnisse zu veröffentlichen, soweit keine Erkenntnisse und Leistungen der betreuenden Institute und Unternehmen eingeflossen sind. Die von der Studienrichtung erlassenen Richtlinien zur Anfertigung der Bachelorarbeit sowie die Prüfungsordnung sind zu beachten.

Professoren und Privatdozenten des IRS:

Prof. Dr.-Ing. Stefanos Fasoulas (Geschäftsführender Direktor) · Prof. Dr.-Ing. Sabine Klinkner (Stellvertretende Direktorin) · Hon.-Prof. Dr.-Ing. Jens Eickhoff · Prof. Dr. rer. nat. Reinhold Ewald · apl. Prof. Dr.-Ing. Georg Herdrich · Prof. Dr. rer. nat. Alfred Krabbe · Hon.-Prof. Dr. Volker Liebig · Hon. Prof. Dr. rer. nat. Christoph Nöldeke · Prof. Dr.-Ing. Stefan Schlechtriem · apl. Prof. Dr.-Ing. Ralf Srama

Erklärungen

Hiermit versichere ich, **Beitinger, Max**, dass ich diese **Bachelorarbeit** selbstständig mit Unterstützung des Betreuers / der Betreuer angefertigt und keine anderen als die angegebenen Quellen und Hilfsmittel verwendet habe. Die Arbeit oder wesentliche Bestandteile davon sind weder an dieser noch an einer anderen Bildungseinrichtung bereits zur Erlangung eines Abschlusses eingereicht worden.

Ich erkläre weiterhin, bei der Erstellung der Arbeit die einschlägigen Bestimmungen zum Urheberrecht fremder Beiträge entsprechend den Regeln guter wissenschaftlicher Praxis¹ eingehalten zu haben. Soweit meine Arbeit fremde Beiträge (z.B. Bilder, Zeichnungen, Textpassagen etc.) enthält, habe ich diese Beiträge als solche gekennzeichnet (Zitat, Quellenangabe) und eventuell erforderlich gewordene Zustimmungen der Urheber zur Nutzung dieser Beiträge in meiner Arbeit eingeholt. Mir ist bekannt, dass ich im Falle einer schuldhaften Verletzung dieser Pflichten die daraus entstehenden Konsequenzen zu tragen habe.

Stuttgart, 30.04.2024, gez. M. Beitinger

.....
Ort, Datum, Unterschrift

Hiermit erkläre ich mich damit einverstanden, dass meine **Bachelorarbeit** zum Thema:

Adaptation of innovative CMC fluid film bearings for a propellant feeding pump for cryogenic space propulsion systems

in der Institutsbibliothek des Instituts für Raumfahrtssysteme ohne Sperrfrist öffentlich zugänglich aufbewahrt und die Arbeit auf der Institutswebseite sowie im Online-Katalog der Universitätsbibliothek erfasst wird. Letzteres bedeutet eine dauerhafte, weltweite Sichtbarkeit der bibliographischen Daten der Arbeit (Titel, Autor, Erscheinungsjahr, etc.).

Nach Abschluss der Arbeit werde ich zu diesem Zweck meinem Betreuer neben dem Prüfaxemplar eine weitere gedruckte sowie eine digitale Fassung übergeben.

Der Universität Stuttgart übertrage ich das Eigentum an diesen zusätzlichen Fassungen und räume dem Institut für Raumfahrtssysteme an dieser Arbeit und an den im Rahmen dieser Arbeit von mir erzeugten Arbeitsergebnissen ein kostenloses, zeitlich und örtlich unbeschränktes, einfaches Nutzungsrecht für Zwecke der Forschung und der Lehre ein. Falls in Zusammenhang mit der Arbeit Nutzungsrechtsvereinbarungen des Instituts mit Dritten bestehen, gelten diese Vereinbarungen auch für die im Rahmen dieser Arbeit entstandenen Arbeitsergebnisse.

Stuttgart, 30.04.2024, gez. M. Beitinger

.....
Ort, Datum, Unterschrift

¹ Nachzulesen in den DFG-Empfehlungen zur „Sicherung guter wissenschaftlicher Praxis“ bzw. in der Satzung der Universität Stuttgart zur „Sicherung der Integrität wissenschaftlicher Praxis und zum Umgang mit Fehlverhalten in der Wissenschaft“

Abstract

In this thesis, simulations, constructive efforts and experiments are described in order to adapt and design innovative Ceramic Matrix Composite (CMC) Fluid Film Bearings for use in a research fuel pump for cryogenic fuels and to prepare them for safe operation in this application. For this purpose, the operating data of the pump and loads on the fuel pump bearings are collected and estimated, and a design model of the existing design of the turbopump is created. To develop the design, various bearing concepts for different configurations are created and systematically evaluated. The influence of various design and operating parameters on the load-bearing capacity of the bearings is then analysed using numerical simulation of the pressure distribution in the lubrication gap of the bearings. Subsequently, three selected concepts are designed in detail within the geometry of the housing using the design model. Possible advantages and disadvantages are discussed and one design is further developed as a prototype for experimental application testing. Particles from the CMC, pose a threat to the integrity of the spacecraft, especially when combining a carbon-based CMC-Material with liquid oxygen. Therefore the amount and size distribution of the particles occurring in the material is examined using a series of experiments in which CMC-Material samples are repeatedly cleaned using ultrasound and the extricated particles are filtered out and examined. The experiments show that particles are released from the material. These Particles are released in all size ranges relevant to limitation set for safe operation according to the normative specifications of the European Cooperation for Space Standardization (ECSS). Based on the investigations, suggestions are made for the further qualification process with regard to potential hazards caused by particle contamination.

Kurzfassung

In der vorliegenden Arbeit werden simulative, konstruktive und versuchspraktische Untersuchungen beschrieben, um innovative, faserkeramische Fluidlager für die Anwendung in einer Forschungstreibstoffförderpumpe für kryogene Treibstoffe anzupassen, auszulegen und für einen sicheren Betrieb besonders in Turbopumpen für Raumfahrtantrieben vorzubereiten. Dazu werden die Betriebsdaten und Belastungen der Treibstoffpumpenlager gesammelt und abgeschätzt sowie ein Konstruktionsmodell des bestehenden Entwurfs der Turbopumpe erstellt. Für die Auslegung werden verschiedene Lagerkonzepte für mögliche Konfigurationen erstellt und systematisch bewertet sowie der Einfluss verschiedener Designparameter auf die Tragfähigkeit der Lager mithilfe numerischer Simulation der Druckverteilung im Schmierpalt der Lager untersucht. Anschließend werden drei ausgewählte Konzepte mithilfe des Konstruktionsmodells in der Geometrie des Gehäuses detailliert konstruiert, mögliche Vor- und Nachteile diskutiert und eine Konstruktion für eine mögliche Anwendung als Versuchsträger weiterentwickelt. Da Partikel aus dem faserkeramischen Werkstoff, insbesondere bei der Kombination einer kohlenstoffbasierten Faserkeramik mit flüssigem Sauerstoff eine Gefahr für die Integrität des Raumfahrzeugs darstellen, wird die Partikelmenge und Größenverteilung der im Material vorkommenden Partikel mithilfe einer Versuchsreihe untersucht. Dazu werden Werkstoffproben wiederholt im Ultraschall gereinigt und die sich lösenden Partikel herausgefiltert und untersucht. Die Versuche resultieren in dem Ergebnis, dass sich Partikel in allen Größenbereichen, der für den sicheren Betrieb nach den normativen Vorgaben der Europäischen Kooperation für Raumfahrtnormung vorgegebenen Grenzen, aus dem Material auslösen lassen. Auf Basis der Untersuchungen werden Vorschläge für den weiteren Qualifikationsprozess hinsichtlich potentieller Gefahren durch Partikelkontamination gemacht.

Contents

1. Introduction and motivation	1
1.1. Work objectives	3
2. Theory and Fundamentals	5
2.1. Design and Calculation of Porous Fluid Film Bearings	5
2.1.1. Journal Bearing	6
2.1.2. Thrust Bearing	10
2.2. Ceramic Matrix Composite Materials	11
2.3. Particle Measurement Methods	13
2.3.1. Particle Definition and Limits	14
2.3.2. Continuous Procedures	15
2.3.3. Dicontinuous Procedures	17
3. Methodology	21
3.1. Systematic Selection Procedure	21
3.2. Numerical Fluid Mechanical Calculation of CMC Fluid Film Bearings	22
3.3. Experimental Investigation of Material-Inherent Particles	25
3.3.1. Sampling Method - Filtration	25
3.3.2. Microscopic Analysis	27
3.3.3. Gravimetric Analysis	30
4. Results and Discussion	31
4.1. Collection of Operative Specifications	31
4.1.1. Load requirements	31
4.2. Design and Construction	34
4.2.1. Initial Design	35
4.2.2. Concept Development and Selection	39
4.2.3. Detailed development of the selected concepts	44
4.3. Preliminary evaluation of potential particle emission risks	47
4.3.1. Experiment Results	47
4.3.2. Conclusions	50
4.3.3. Discussion and Outlook	52
5. Summary	55
5.1. Design and Construction of the Bearing Components	55
5.2. Evaluation of the Risk due to Particle Pollution	56
A. Excerpts from standards	IX
B. Technical Drawings	XI
C. Design Renderings	XIX
D. Experiment Documentation	XXI

List of Figures

1.1.	Launch costs into low Earth orbit	1
1.2.	Test setup of a CMC fluid film bearing developed at German Aerospace Center (Deutsches Zentrum für Luft- und Raumfahrt e.V.) (DLR)	2
1.3.	Three-quarter section of a turbopump developed by the Launch Canada Rocketry Association (LCRA)	2
2.1.	Schematic of the operation of the hydrostatically lubricated CMC bearing for use in a turbopump	6
2.2.	Geometry and designation of the parameters for the journal bearing	7
2.3.	Nomenclature for Reynolds Equation for Hydrodynamic Lubrication (REHL)	7
2.4.	Numerical grid for the solution of the model equation for journal bearings	9
2.5.	Geometry and designated parameters for the thrust bearing	10
2.6.	Numerical grid for the solution of the model equation for thrust bearings	11
2.7.	Schematic of the possible production methods of Polymer Infiltration and Pyrolysis (PIP) and Liquid Silicon Infiltration (LSI) for CMC-Materials	12
2.8.	X-ray Computer Tomography (CT) image of pore structure of Optimized Ceramic for Hypersonic Application with Transpiration Cooling (OCTRA)-Material in Carbon/Carbon (C/C) state	13
2.9.	Schematic of the orthotropic layered structure of a journal bearing	13
2.10.	Schematic of the states of a disperse two-phase flow dependent on the volume fraction of the disperse phase	16
2.11.	schematic of the LSAPC working principle	17
2.12.	Suitability of the various sieving methods for analysing different particle sizes [39]	19
3.1.	Illustration of the filtration procedure with a 3D-Printed filtration device.	26
3.2.	Counting pattern for ten locations According to the ISO 4407 standard	28
4.1.	Components of the shaft assembly for radial load assumptions	32
4.2.	Calculated Forces based on gravitational weight and unbalance	34
4.3.	Reference measurements of the current turbo pump design state	34
4.4.	First iteration cross section	35
4.5.	Load carrying capacities of the Initial Bearing Design	35
4.6.	Calculated pressure distribution within the Journal Bearing for the Initial Design	36
4.7.	Calculated pressure distribution within the Thrust Bearing for the Initial Design	36
4.8.	Effect of changing the supply pressure difference on the Load carrying capacities of the bearing	37
4.9.	Effect of increasing the lubricating film area by increasing z_J or $R_{T,3}$	37
4.10.	Effect of changing permeability.	37
4.11.	Effect of changing the thickness of the bearings z_T and $R_{J,2}$	38
4.12.	Effect of changing the viscosity μ	38
4.13.	Effect of changing the gap height h_0	38
4.14.	Various concepts developed for the combination of journal and thrust bearings for absorbing radial forces and axial forces in both directions within one bearing setup.	40

4.15. Comparison of the Load bearing capacities of the bearing designs.	44
4.16. Integration of concept C into the design.	45
4.17. Integration of concept I into the design.	46
4.18. Integration of Design Concept A	47
4.19. Results of particle mass quantity measurements using the gravimetric method. . .	49
4.20. Digital microscopic image with three-dimensional image capture, Filter residues from Sample 1, Ultrasonic cleaning time of 64 min (total of 128 min).	50
4.21. Particle distribution of the cleaning fluid of sample 1, ultrasonic cleaning time 30 s (total of 240 s).	51

List of Tables

2.1. Categorisation of particle measurement methods	14
2.2. Particle cleanliness requirements of the Vulcain	15
3.1. Input values for numerical calculation of the pressure distribution within the bearings lubrication gaps	24
3.2. Geometry changes for numerical calculation the journal and thrust bearing design variants C,I and A.	25
4.1. Basic specifications of the electric turbopumps developed by the LCRA.	31
4.2. Specifications of the Bearings used in the original design.	32
4.3. Determination of the weight of the shaft assembly	33
4.4. Reference measurements for the turbopump housing.	35
4.5. Evaluation criteria selected to identify the best suitable concepts.	39
4.6. Results of the preference analysis.	42
4.7. Selection results of the selection procedure with the total utility values K_l highlighted in red.	43
4.8. Filtration times	48
4.9. Material sample weights before and after ultrasonic cleaning tests.	48
4.10. Measured filter weights before and after filtration	48
4.11. Parameters a and b for the fitted function and comparison of factor a with actual weight difference m_d of the material samples.	49
4.12. Fluid properties at different potential operation points for future liquid flush tests.	53

Nomenclature

Formula symbols

Latin Letters

b	[m]	Non-porous length of the bearing
C	[-]	Weighting factor
e	[m]	Eccentricity
F	[N]	Load
h	[m]	Gap height
K	[-]	Total utility value
L	[-]	Load multiplication factor
m	[kg]	Mass
n	[1/s]	Rotational speed
nx	[-]	Number of nodes in x-direction
ny	[-]	Number of nodes in y-direction
N	[-]	Number of particles
NR	[-]	Number of nodes in radial direction
$N\varphi$	[-]	Number of nodes in circumferential direction
p	[Pa]	Pressure
p	[-]	Partial utility value
P	[-]	Evaluation points
R	[m]	Radius
s	[-]	Safety factor
S	[-]	Rank
T	[K]	Temperature
u	[m/s]	Seepage velocity
U	[m/s]	Fluid velocity in circumferential direction
V	[m/s]	Fluid velocity in axial direction
W	[m/s]	Fluid velocity in radial direction
x	[m]	Distance
z	[m]	Porous length of the bearing

Greek Letters

μ	[Pa · s]	Dynamic viscosity
ρ	[kg/m ³]	Density
α	[-]	Permeability coefficient
β	[1/m ³]	Particle concentration
φ	[°]	Circumferential angle

Indices

0	Initial value
a	Shaft surface
b	Inner sleeve surface
d	Difference
e	Exhaust
g	Gravitational
i	Node counter in φ -direction
J	Journal
j	Node counter in x/r-direction
k	Counter of selection criteria
l	Counter of created concepts
m	Mass
n	Number
p	Particle
s	Supply
T	Thrust
u	Unbalance

Constants

g_0	9,81 m ² /s	Gravity factor
-------	------------------------	----------------

Acronyms and Abbreviations

BC Boundary Condition

BEA Black Engine Aerospace GmbH

C/C Carbon/Carbon

C/C-SiC Carbon Fibre Reinforced Silicon Carbide Ceramics

CAD Computer Aided Design

CMC Ceramic Matrix Composite

CT Computer Tomography

CVD Chemical Vapour Deposition

DLR German Aerospace Center (Deutsches Zentrum für Luft- und Raumfahrt e.V.)

ECSS European Cooperation for Space Standardization

Fig. Figure

GN2 Gaseous Nitrogen

LCRA Launch Canada Rocketry Association

LEPC Light Extinction Particle Counter

LN2 Liquid Nitrogen

LOX Liquid Oxygen

LSAPC Light Scattering Airborne Particle Counter

LSI Liquid Silicon Infiltration

NIST National Institute of Standards and Technology

OCTRA Optimized Ceramic for Hypersonic Application with Transpiration Cooling

PIP Polymer Infiltration and Pyrolysis

REHL Reynolds Equation for Hydrodynamic Lubrication

RLV Reusable Launch Vehicles

RP-1 Rocket Propellant 1

SiC Silicon Carbide

SiCFRP Silicon Carbide Fibre Preform

Tab. Table

VDI Association of German Engineers (Verein deutscher Ingenieure)

1. Introduction and motivation

Growing global competition due to the increasing number of private space transport companies has caused the number of space transports to rise for years. The development summarised under the term “New Space” has shown that there is an increasing demand for ever cheaper space transport. Figure (Fig.) 1.1 shows that launch costs per kilogramme into low Earth orbit have constantly declined for decades.

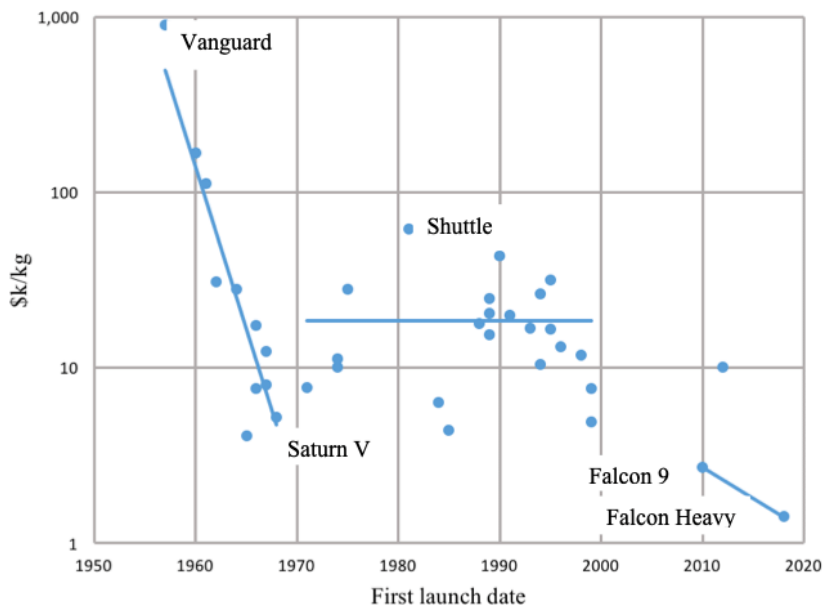


Fig. 1.1.: Launch costs into low Earth orbit [1]

Today, it seems obvious that reuse is the decisive factor in increasing the economic efficiency of space transport systems. Critical components for reusable rocket stages are among others the combustion chamber and the turbopumps of the fuel supply system. State-of-the-art technology uses mainly metallic materials for the combustion chamber.

The porous CMC-Materials developed at the DLR are a promising alternative that should enable the construction of high-performance and in particular, highly reusable rocket combustion chambers for Reusable Launch Vehicles (RLV) while also offering significant advantages by reducing weight and manufacturing costs [2, 3, 4].

In order to keep up with increased lifetimes of future generations of rocket engines for RLV, the turbopumps used will also have to be operated over longer lifetimes in order to be economical [5]. Turbopumps are an elementary component of liquid rocket propulsion systems. They ensure a high combustion chamber pressure despite low tank pressure, which leads to an increased maximum payload due to a higher achievable specific impulse and a lower tank mass [6]. The critical components for a long service life and reusability of these turbopumps are their bearings [7].

Previous studies have shown that transpiration-lubricated hydrostatic fluid film bearings made of

1 Introduction and motivation

porous CMC can be operated in a higher temperature range compared to conventional bearings. They have shown promising characteristics like high thermal shock resistance and low thermal expansion and can be operated at both cryogenic and high temperatures [8]. In addition, the CMC-Materials have a very homogeneous microporosity, which leads to a very uniform flow through the material. For this reason, they are seen as a promising technology for use in turbopumps for rocket engines

Fig. 1.2 shows a picture of a test setup of such a bearing.

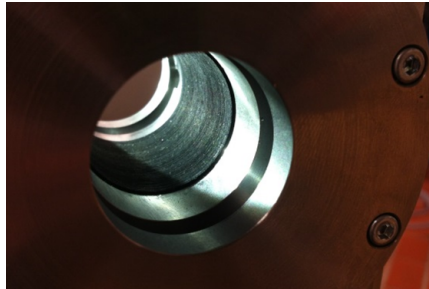


Fig. 1.2.: Test setup of a CMC fluid film bearing developed at DLR [2]

Building on the research and development results of DLR and its partners, this work is intended to take further steps in the development of a fluid film bearing made of microporous CMC which will replace the two-part ball bearing of an existing rocket turbopump design.

The investigated turbopump is a research project from LCRA, an industry-supported Canadian research initiative in the field of rocket technology. Fig. 1.3 shows a three-quarter section of a turbopump developed by the LCRA.

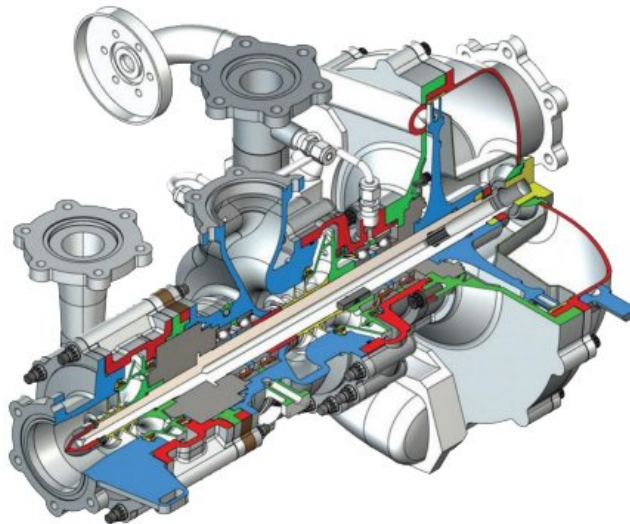


Fig. 1.3.: Three-quarter section of a turbopump developed by the LCRA [9]

The work is also being carried out in collaboration with the start-up Black Engine Aerospace GmbH (BEA), which aims to transfer the CMC-technology from DLR to industry. Part of this endeavour is also the implementation of CMC-Bearings in real world applications.

The CMC-Material contains particles that are generated during the production process and may be released when the material is used as a transpirationally lubricated bearing. These particles

pose a potential risk to trouble-free operation. Particles are not only a risk for the functionality of the bearing, but also in the propellant lines of the rocket-engine in particular. For this reason, particular attention should be paid to the consideration of particle ejection from the CMC-Components of the bearing design.

1.1. Work objectives

The goal of the work can be divided into three main objectives:

1. Operational specifications for the bearing design are to be compiled using the data provided by the LCRA.
2. The design and construction of the modular bearing component is to be carried out with the help of the specifications determined and the given geometry of the pumps housing. The basis for this includes calculation with numerical tools for the fluid mechanical simulation of the pressure distribution within the bearing gap based on [10].
3. Evaluation of particle emissions with aim of a preparatory assessment, considering applicable regulations and possibilities for particle measurement methods.

2. Theory and Fundamentals

In the following chapter, the calculation and design of hydrostatically lubricated CMC fluid film bearings and the basics of the CMC-Materials, which are used as a material in this application, and their manufacturing process are explained. The results of the literature research on regulations regarding particle contamination of spacecraft hardware and particle measurement methods are then presented.

2.1. Design and Calculation of Porous Fluid Film Bearings

The purpose of a bearing is to support and guide parts that move relative to each other, in particular rotating parts in machines or devices. They absorb the external forces acting on the supported parts in order to transfer them to housings or similar components. The friction that occurs in bearings between the moving parts under load is minimised by small contact surfaces and lubricants (for example in ball bearings), by large sliding surfaces with separating fluids (for example in fluid film bearings) or by magnetic fields that keep the shaft in suspension.

Bearings can be divided into axial or thrust bearings, which absorb forces in the axial direction, and radial or journal bearings, which absorb forces in the radial direction. They can also be categorised according to their function as fixed bearings (absorbing longitudinal forces in both directions), support bearings (absorbing longitudinal forces in only one direction and radial forces) and floating bearings (absorbing only transverse forces and allowing displacement in the longitudinal direction). [11, 12].

The CMC-Bearings which are assessed in this work are fluid film bearings. Fluid film bearings are characterised by a sliding movement between the bearing and the supported part; lubricated by an either gaseous or liquid fluid.

They can be divided into hydrostatic and dynamic fluid film bearings based on their working principle. Hydrostatic fluid film bearings operate with an external pressure supply to provide the lubrication gap with lubricant. The necessary lubricant pressure is therefore generated outside the bearing. In the case of dynamic fluid film bearings, a load-bearing lubricating film is formed solely by the relative movement between the shaft and bearing shell [11].

A schematic representation of the setup for employing a CMC fluid film bearing to support a turbopump shaft is shown in Figure 2.9. The bearing components (green, grey) of the turbopump are used to transfer the forces, which are caused by the fluid flow within the pump (red arrows) and the rotating parts (purple), to the non spinning casing (blue). In this way, the bearing holds the shaft of the turbopump in place, which ensures its proper functioning.

An important equation used as a foundation to calculate CMC fluid film bearings is Darcy's law coupled to the corresponding fundamental Reynold's equation of fluid film bearings. Darcy's law provides a linear relation to describe fluid flow through a porous material (equation 2.1) [14, 15]. Darcy's law states that the average seepage velocity u in m/s through a porous material is proportional to the pressure gradient through the porous sample dp/dx . The pressure gradient describes the loss of pressure p in Pa along a distance x in m. The proportionality factor is

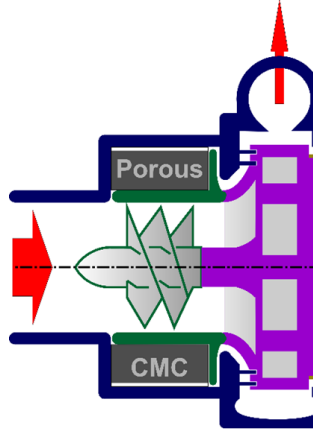


Fig. 2.1.: Schematic of the operation of the hydrostatically lubricated CMC bearing for use in a turbopump [13]

dependent on the dynamic viscosity of the lubricating fluid and the permeability of the CMC-Material. The dynamic viscosity is defined as μ in Pa·s and the permeability as α [-].[10, 8]

$$\frac{dp}{dx} = -\frac{u \cdot \mu}{\alpha} \quad (2.1)$$

The permeability α is a material constant, influencing the flow through the material and therefore the pressure distribution and load-carrying capacity of the bearing. As it is dependent on the specific material used and the production process chosen, the specific basics for CMC-Materials and the production of the bearing sleeves out of the material are described in chapter 2.2.

In addition to Darcy's law, the Forchheimer term can be added to the equation for higher Reynolds numbers, accounting for inertial forces [16]. It has been shown that this extension is not necessary for use in fluid film CMC-Bearing [10].

For CMC fluid film bearings, the two basic configurations for journal bearings (absorbing radial forces) and thrust bearings (absorbing axial forces) are presented below. The basics of the numerical calculation of the pressure distribution within the lubrication gap are also explained.

2.1.1. Journal Bearing

In a Journal CMC fluid film bearing, the fluid flows mainly radially through a porous bearing sleeve, forming a lubricant layer between the shaft and the CMC-Sleeve which absorbs radial forces. Proof of concept of this bearing type has already been demonstrated experimentally [17]. Fig. 2.2 shows the main dimensions for such a bearing with the nomenclature used in this work. Visualisation and naming of the parameters are based on [18]. The parameter designations used for this work are as follows:

b denotes the length of the non-porous part of the journal bearing in m, z_j the length of the porous part of the bearing sleeve in m. R_1 describes the radius of the mounted shaft. R_2 describes the inner radius of the bearing sleeve. The difference between the two values forms the gap height for the lubricant film to form and is calculated as $h_0 = R_2 - R_1$. The index zero refers to the initial value of the gap height, which changes during operation due to movement of the shaft within the bearing. R_3 describes the outer radius of the bearing sleeve. The thickness of the sleeve results from the difference between its inner radius R_2 and the outer radius R_3 . All radii and the gap

heights are given in m. The circumferential angle ϕ is given in degrees.

Another important parameter of the journal bearing is its eccentricity e in m describing the deviation of the shaft's axis from the centre line [19].

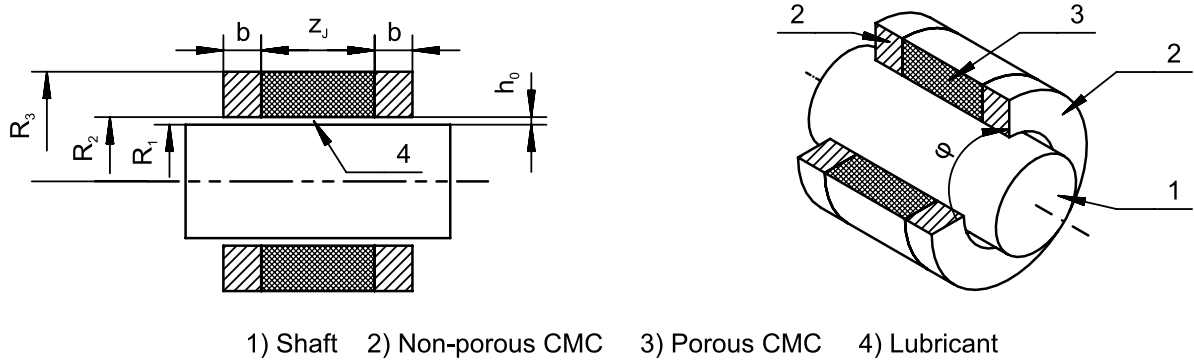


Fig. 2.2.: Geometry and designation of the parameters for the journal bearing

The approach for calculating the bearings fluid dynamics is based on an equation developed by O. Reynolds in 1886 called the REHL. Its full form is:

$$\frac{\partial}{\partial x} \left(\frac{\rho \cdot h^3}{12 \cdot \mu} \cdot \frac{\partial p}{\partial x} \right) + \frac{\partial}{\partial y} \left(\frac{\rho \cdot h^3}{12 \cdot \mu} \cdot \frac{\partial p}{\partial y} \right) = \frac{\partial}{\partial x} \left(\rho \cdot \frac{U_a + U_b}{2} \cdot h \right) + \frac{\partial}{\partial y} \left(\rho \cdot \frac{V_a + V_b}{2} \cdot h \right) \quad (2.2)$$

$$+ \rho \cdot (W_a - W_b) - \rho \cdot U_a \cdot \frac{\partial h}{\partial x} - \rho \cdot V_a \cdot \frac{\partial h}{\partial y} + \frac{\partial \rho}{\partial t} \cdot h$$

The nomenclature is shown in fig. 2.3. ρ describes the density of the fluid in kg/m^3 . The velocities U_a , U_b , V_a , V_b , W_a and W_b stand for the velocities of fluid at the shaft and bearing in m/s in the according coordinate direction of a xyz-coordinate system. Index a stands for velocities at the shaft surface, b for the velocities at the inner surface of the non rotating bearing sleeve.

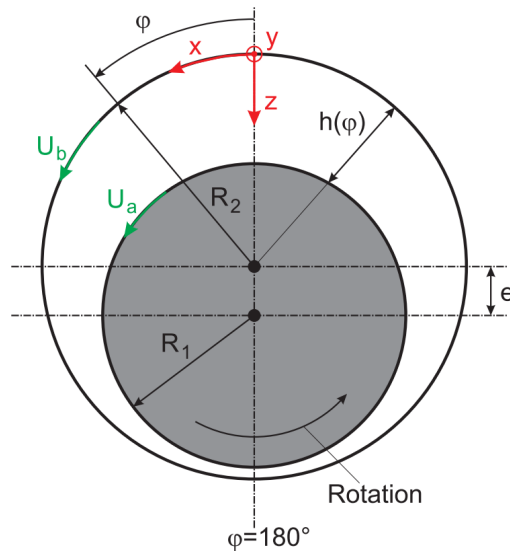


Fig. 2.3.: Nomenclature for REHL [18]

The boundary conditions described in the following allow for a simplification of the REHL-Equation. For the journal bearing, the velocities in the direction of the shaft at the shafts surface V_a and the bearings sleeve surface V_b are assumed to be zero. The velocity in z-direction at the

2 Theory and Fundamentals

sleeves surface U_b is also assumed to be zero as the bearing is not rotating. This is called the no slip condition:

$$U_b = V_a = V_b = 0. \quad (2.3)$$

The velocity U_a can be calculated as the circumferential velocity of the shaft dependent on the rotational speed of the shaft n in 1/s:

$$U_a = 2 \cdot \pi \cdot n \cdot R_1. \quad (2.4)$$

For journal bearings the velocity of the fluid in radial direction W_a is dependent on the movement of the shaft within the bearing, and can therefore be written dependent on the changing of the gap height as:

$$W_a = U_a \cdot \frac{\partial h}{\partial x}. \quad (2.5)$$

Combining the REHL equation with the assumptions made in 2.3 and 2.5 and additionally assuming that the flow is steady, incompressible and of constant viscosity, the REHL reduces to

$$\frac{\partial}{\partial x} \left(\frac{\rho \cdot h^3}{12 \cdot \mu} \cdot \frac{\partial p}{\partial x} \right) + \frac{\partial}{\partial y} \left(\frac{\rho \cdot h^3}{12 \cdot \mu} \cdot \frac{\partial p}{\partial y} \right) = -W_b + \frac{U_a}{2} \cdot \frac{\partial h}{\partial x}, \quad (2.6)$$

which can be rewritten by mathematical transformation if there is no change in the gap in y-direction as

$$\frac{1}{12 \cdot \mu} \cdot \left(3 \cdot h^2 \cdot \frac{\partial h}{\partial x} \cdot \frac{\partial p}{\partial x} + h^3 \cdot \frac{\partial^2 p}{\partial x^2} + h^3 \cdot \frac{\partial^2 p}{\partial y^2} \right) = -W_b + \frac{U_a}{2} \cdot \frac{\partial h}{\partial x}. \quad (2.7)$$

[18] [20]

In order to take the specific requirements of porous CMC journal bearings where the lubricant is supplied perpendicular to the surface through the bearing sleeve into account, the Darcy equation is integrated into the derivation. Darcy's law can therefore be rewritten to calculate the velocity W_b by integrating Darcy's law in cylindrical coordinates over the bearings thickness which results in 2.8 (Details see [18]).

$$W_b = \frac{\alpha}{\mu \cdot R_2 \cdot \ln\left(\frac{R_s}{R_2}\right)} \cdot (p_s - p(\varphi)) \quad (2.8)$$

The interface between the REHL equation describing the fluid mechanics within the lubrication gap and Darcy's law describing the flow through the CMC-Sleeve is the velocity of the fluid perpendicular to the sleeve on the inside of the bearing sleeve W_b . For this connection it is assumed that the flow inside the porous sleeve is only moving radially through the sleeve. This assumption can be made, because the pressure gradient in radial direction is a lot higher than the pressure gradient in circumferential direction, which is neglected for this reason.

Combining the simplified REHL equation with this equation derived from Darcy's law (2.1) to calculate W_b results in the final model equation (2.9) for a simple flow model for modelling the pressure distribution in the gap of a journal bearing with porous material [18].

$$\frac{1}{12 \cdot \mu} \cdot \left(3 \cdot h^2 \cdot \frac{\partial h}{\partial x} \cdot \frac{\partial p}{\partial x} + h^3 \cdot \frac{\partial^2 p}{\partial x^2} + h^3 \cdot \frac{\partial^2 p}{\partial y^2} \right) - \frac{\alpha}{\mu \cdot R_{J,2} \cdot \ln\left(\frac{R_{J,3}}{R_{J,2}}\right)} \cdot p = \quad (2.9)$$

$$\frac{U_a}{2} \cdot \frac{\partial h}{\partial x} - \frac{\alpha}{\mu \cdot R_2 \cdot \ln\left(\frac{R_s}{R_2}\right)} \cdot p_s$$

This model equation is subsequently numerically solved by a finite difference method. For this purpose a numerical grid is introduced for the calculation with a number of nx nodes in x-direction and ny nodes in y-direction. The grid is shown in Fig. 2.4. Then, the differential quotients are replaced by second order accurate finite difference quotients. The difference quotients used for the calculation are:

$$\frac{\partial h}{\partial x} \approx \frac{h_{i+1} + h_{i-1}}{2 \cdot \Delta x} \quad (2.10)$$

$$\frac{\partial p}{\partial x} \approx \frac{p_{i+1,j} - p_{i-1,j}}{2 \cdot \Delta x} \quad (2.11)$$

$$\frac{\partial^2 p}{\partial x^2} \approx \frac{p_{i+1,j} - 2 \cdot p_{i,j} + p_{i-1,j}}{\Delta x^2} \quad (2.12)$$

$$\frac{\partial^2 p}{\partial y^2} \approx \frac{p_{i,j+1} - 2 \cdot p_{i,j} + p_{i,j-1}}{\Delta y^2} \quad (2.13)$$

These finite difference quotients are applied for all grey and red grid points (fig. 2.4). This leads to a linear equation system which is solved by the Gauss Seidel algorithm.

For all nodes with $j=0$ and $j=ny-1$ a Dirichlet Boundary Condition (BC) is set. This means that the static pressure is prescribed.

For all nodes with $i=0$ and $i=nx-1$ periodic BC are imposed. [18]

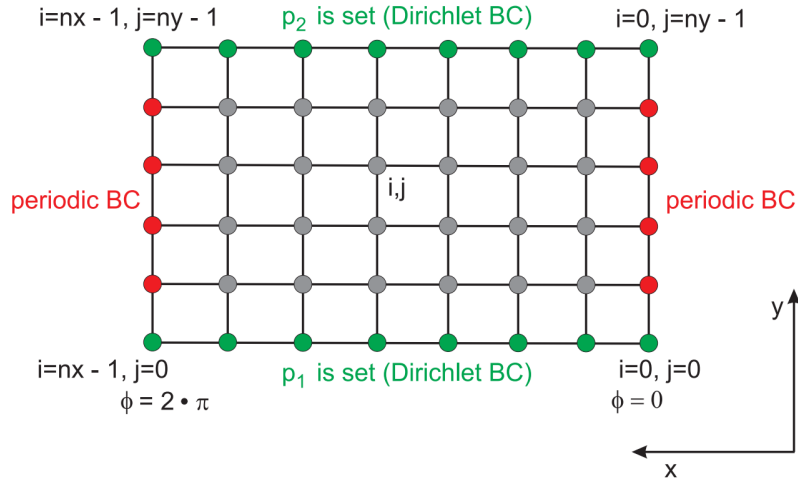


Fig. 2.4.: Numerical grid for the solution of the model equation for journal bearings [18]

This numerical calculation models the pressure distribution within the bearing in the direction of its length (y-axis) and in circumferential direction (x-axis). Additional details of the calculation process and the theoretical background of the calculation of the journal bearings as well as Details of the numerical solution process can be found in [18, 10, 8]. More refined calculation models than the described above have been developed by Schimpf, but the simple model has proven its accuracy in experimental investigations [10].

2.1.2. Thrust Bearing

In a CMC fluid film thrust bearing the fluid flows mainly axially through a porous bearing sleeve, forming a lubricant layer between a surface of the shaft, which is orthogonal to the axial direction of the shaft (shaft shoulder), and the surface of the bearings CMC-Ring. This configuration can absorb axial forces. Fig. 2.5 shows the main dimensions for such a bearing with the nomenclature used in this work. Visualisation and designation of the parameters are based on [19]. The parameter designations used for this work are as follows:

z_T denotes the radial length of the bearing ring. h denotes the gap height of the lubrication gap. The radii R_0 and R_1 denote the inner and outer radius of the inner non-porous ceramic sleeve whose radial thickness results from the difference. The radii R_2 and R_3 denote the inner and outer radius of the outer non-porous ceramic sleeve, the radial thickness of which results from their difference. The radial thickness of the porous ceramic sleeve results from the difference between R_2 and R_1 . All heights and radii are given in m.

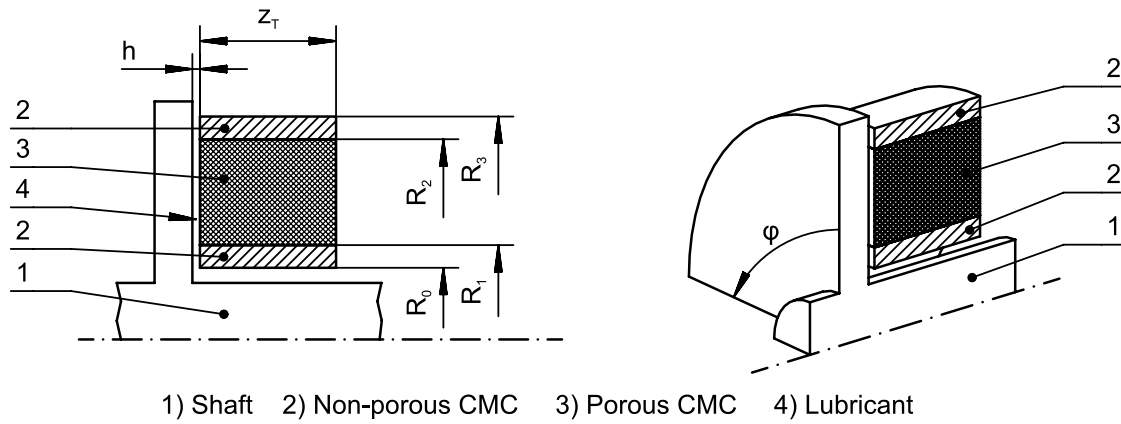


Fig. 2.5.: Geometry and designated parameters for the thrust bearing

Similar to journal bearings, the REHL is simplified and combined with Darcy's law. This results in the following equation in cylindrical coordinates:

$$h^3 \cdot \frac{\partial p}{\partial r} + h^3 \cdot r \cdot \frac{\partial^2 p}{\partial r^2} + \frac{h^3}{e} \cdot \frac{\partial^2 p}{\partial \varphi^2} = -p_s \cdot \left(\frac{12 \cdot \alpha \cdot r}{z_T} \right) + p \cdot \left(\frac{12 \cdot \alpha r}{z_T} \right). \quad (2.14)$$

The equation is subsequently solved numerically in a similar manner as in 2.1.1. The numerical grid for the calculation is shown in 2.6, with NR describing the number of nodes in radial direction and $N\varphi$ describing the number of nodes in circumferential direction. [19]

This calculation models the pressure distribution within the bearing in the radial direction (r -axis) and in circumferential direction (φ -axis). Additional details of the calculation process and theoretical background of the numerical calculation as well as details of the numerical solution process can be found in [19].

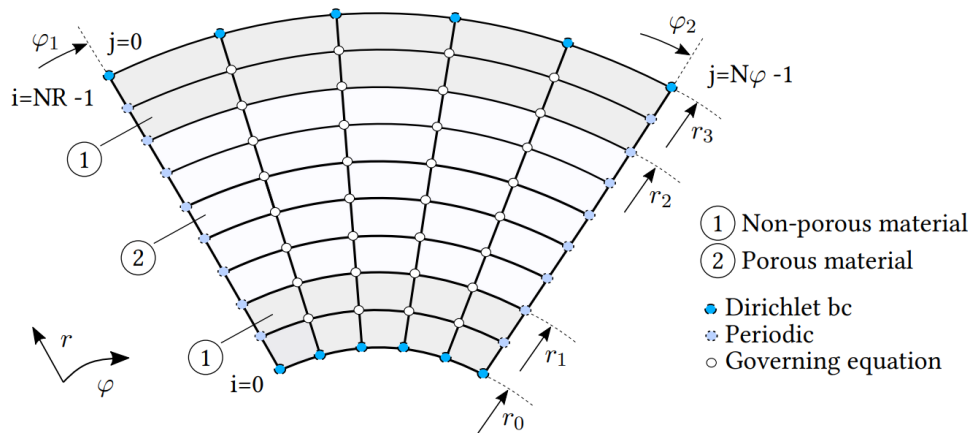


Fig. 2.6.: Numerical grid for the solution of the model equation for thrust bearings [19]

2.2. Ceramic Matrix Composite Materials

Porous CMC-Materials have been developed especially for use in high-temperature environments, as they meet requirements such as high temperature, thermal shock and oxidation resistance and low coefficient of thermal expansion.

The CMC-Materials required for use in hydrostatically lubricated fluid film bearings must be porous in order to ensure that the bearing functions properly. From the range of materials developed at DLR, the porous C/C CMC-Materials and the Carbon Fibre Reinforced Silicon Carbide Ceramics (C/C-SiC) ceramics developed by Dittert under the name OCTRA are suitable for this purpose. OCTRA was originally especially developed with applications for hypersonic vehicles in mind. [21]

C/C CMC-Materials have found applications for several uses at high temperatures, e.g. as heat shields for re-entry vehicles, aircraft brakes, hot-pressing dies and parts which are exposed to high temperatures such as nozzles. They combine high temperature applicability in inert environments with superior specific strength; a characteristic property often found in composite materials. As all composite materials the C/C CMC-Materials consist of fibres embedded in a matrix. In this specific case carbon fibres are combined with a carbonaceous matrix. A major drawback of C/C CMC-Materials is their reaction with oxygen, forming gaseous oxides of carbon and furthermore high production costs due to long processing times. For C/C-Materials the porosity evolves during the production process: Due to volume shrinkage within the matrix internal stresses built up, leading to microcracks within the material, making the material porous. To mitigate the low oxidation resistance of the C/C CMC-Material the C/C-SiC based OCTRA-Material is suitable for the application.

C/C-SiC Materials consist of carbon fibers embedded into a Silicon Carbide (SiC) matrix. There are three common processing routes for producing C/C-SiC composites which are explained below:

1. Polymer Infiltration and Pyrolysis (PIP)

A preform made out of carbon fibre is impregnated under heat and pressure with thermoplastic pitch, followed by pyrolysis of components of the pitch into SiC. Pyrolysis is the decomposition of the carbohydrates at high temperatures in the absence of oxygen.

The cycle is repeated until the desired density is obtained. Pitches are preceramic polymers of different molecular weights. The yield from the pitch precursor rises as the average molecular weight of the hydrocarbons in the pitch increases. The disadvantage of higher

molecular weight is that it increases viscosity which makes the penetration of the preform more difficult.

2. Liquid Silicon Infiltration (LSI)

For the LSI-Process silicon is melted on top of the porous C/C-Material. This liquid silicon then diffuses into the pores of the material. The carbon matrix reacts with the liquid silicon, forming SiC. This process has to be executed at temperatures exceeding the melting point of silicon.

3. Chemical Vapour Deposition (CVD)

The process of CVD is made through blowing a gaseous phase of chemical vapour in between and onto the carbon fibres in a preform. SiC is depositing on the fibres, forming an inherent SiC-Coating.

[21, 23, 24]

The schematic of the described LSI and PIP processes for a CMC-Material based on SiC-fibres instead of carbon fibres forming an Silicon Carbide Fibre Preform (SiCFRP) is shown in fig. 2.7.

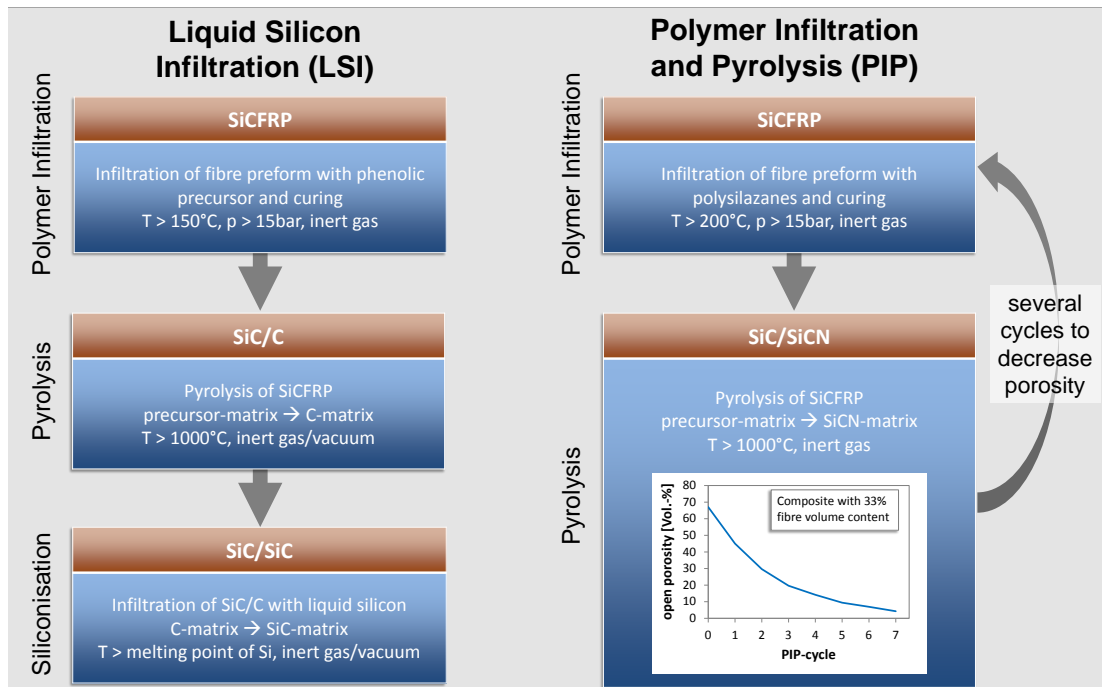


Fig. 2.7.: Schematic of the possible production methods of PIP and LSI for CMC-Materials [22]

The OCTRA-Material is a modified C/C-SiC-Material. When producing C/C-SiC-Material using a procedure carried out according to one of the production processes described above, the process normally causes the material to lose most of its porosity. With PIP, LSI and CVD the process is only made possible through the porosity, but is closing those pores. [25, 24, 21]

To regain and adjust the porosity of OCTRA-Materials a selective insertion of cavities into the C/C-Material is done. In order to achieve this carbon fibres are replaced by the non-stable aramid fibres before pyrolysis. During pyrolysis, these fibres are then degraded, leaving porosities in the material. Fig. 2.8 shows an X-ray CT image of the pore structure of the OCTRA-Material in C/C state. In the development process at DLR up to 38.80% have been replaced by aramid fibres to reach porosities of up to 9% compared to the porosity of pure C/C-SiC-Material of around 3%. These porosities can be seen as tunnel like structures in fig. 2.8. In this way OCTRA is closing the gap between C/C and C/C-SiC Material properties. [21].

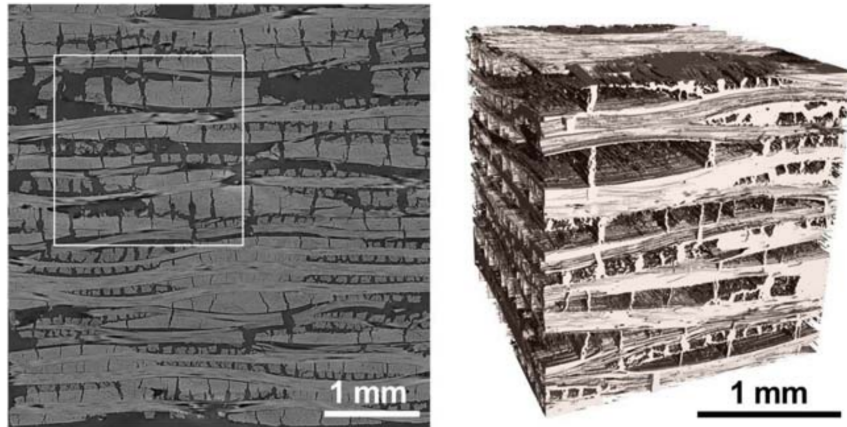


Fig. 2.8.: X-ray CT image of pore structure of OCTRA-Material in C/C state [21]

To produce the bearing sleeve for the journal bearing, sheets of fabric are first layered with an orientation alternating between $0^\circ/90^\circ$ and $\pm 45^\circ$. This plate is then pyrolyzed. Once the CMC-Material production steps have been completed, a bearing sleeve can be drilled out of the plate. The maximum length z_J of the ceramic parts of the bearing is therefore dependent on the thickness of the manufactured plate, as long as the porous part of the bearing is to consist of only one part. The layer structure for manufacturing a bearing sleeve from CMC-Material, as already used in experimentally realised bearings, is shown in Fig. 2.9.

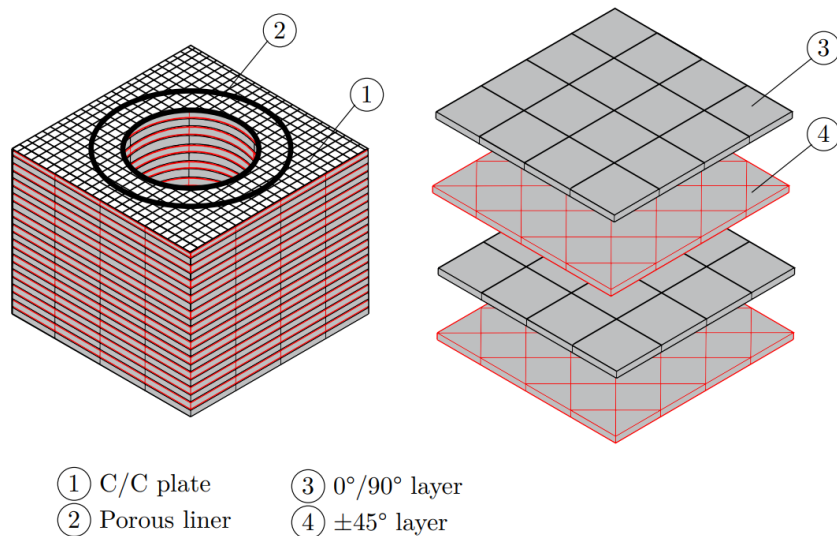


Fig. 2.9.: Schematic of the orthotropic layered CMC-Structure of a journal bearing [17]

2.3. Particle Measurement Methods

As rocket engines are sensitive to pollution, pollution control is an important aspect within the operation of a rocket engine. Particle pollution has to be faced and the impact to the operational aspects of the rocket engines has to be considered, to ensure a good performance. [26]

A measurement of particle contamination is required to ensure that the pollution limits of a specific system are not exceeded. The selection of one or more methods for measuring particle emissions is a challenge, as the methods differ greatly in terms of effort and cost as well as

informative value and accuracy.

In order to determine a suitable method for carrying out particle measurements for the CMC-Bearing, the various common particle measurement methods are first presented. In addition to the basic explanation of the measurement method, operating and resolution limits are briefly discussed.

The ISO 5884 standard, which deals with methods for sampling and measuring contamination by solid particles in hydraulic fluids, is referred to for comparison. The particle measurement methods presented are categorised in Table (Tab.) 2.1. [27]

Continuous methods are categorised as those in which measurement is possible in a fluid flow during a test. In this way, a time-dependent evaluation of the particle output is directly enabled by the measurement method. Discontinuous methods are categorised as those in which the measurement requires the particles to be removed from collection containers or filters after operation. Here, a time-dependent evaluation of the particle output is also possible, but only by intermediate evaluation of the results through interruption and intermediate evaluation of the collected particles. In general, it should also be possible to use continuous methods to analyse samples taken from fluids containing particles by passing the sample through an appropriate measuring apparatus. This is not possible the other way around.

A further categorisation is done into manual and automatic methods. The subdivision here refers to the type of evaluation. While the manual method requires manual counting and measuring of particles by an observer, in automatic methods the particle quantities and sizes are analysed automatically. In order to obtain comparable results, an automatic method requires the measuring device to be calibrated beforehand with samples containing particles of known properties. The evaluation differs depending on the measuring method. This is discussed separately in the presentation of each method.

The results of different automatic measuring methods can only be compared with each other to a limited extent. A comparison can only be made on the basis of the results obtained with the same method [27].

The continuous methods are presented in chapter 2.3.2 and the discontinuous methods in chapter 2.3.3.

Continuous Procedures		Discontinuous Procedures	
Automatic		Manual	Automatic
LEPC		Microscopic Method	Gravimetric Method
LSAPC		-	Sieving

Tab. 2.1.: Categorisation of particle measurement methods

2.3.1. Particle Definition and Limits

In order to be able to present the various particle measurement methods below, the properties of the particles should first be defined.

According to the ECSS definition in the Cleanliness Requirements for Spacecraft Propulsion Hardware (ECSS-E-ST-35-06C), a particle is a unit of solid matter of observable size. Fibres are also considered to be particles and are defined as a flexible structure with a length-to-width ratio of ten to one or more.

The particle size determined by the measuring method does not correspond exactly to the actual particle size. For automatic methods, the diameter of a particle measured by an automatic measuring device is the particle size considered for regulations. For the manual methods, the

apparent maximum linear dimension of a particle in the plane of observation, as observed with instruments such as light, electron or scanning electron microscopes, is the considered particle size. [28]

ECSS-E-ST-35-06C deals with the cleanliness requirements for spacecraft propulsion hardware systems. It contains specifications for compliance with limit values for particle quantities divided into three cleanliness classes. The basis for the different cleanliness classes is the diameter of the outer pipes of the system through which the fluid flows. The following classes are defined:

- "Class 1, which applies for propulsion systems, or sections thereof with external tube sizes up to 20 mm ($\frac{3}{4}$ ").
- Class 2, which applies for propulsion systems, or sections thereof with external tube sizes between 20 mm and 50 mm ($\frac{3}{4}$ " – 2").
- Class 3, which applies for propulsion systems, or sections thereof with external tube sizes exceeding 50 mm (>2")." [28]

A table with an overview of the particle quantity limits of the various cleanliness classes can be found in Appendix A. The quantity specifications for particle limits always refer to 100 cm³ of a liquid or 1 m³ of a gas [28].

An alternative cleanliness specification can be found in [29]. It is shown in Tab. 2.2 and shows the particle cleanliness requirements for the Vulcain Engine:

Circuit	Pneumatic actuators	Fuel/ oxidiser lines	Hot gas lines
Size	Max number		
15-25 μm	1000	2000	40000
25-50 μm	100	200	400
50-100 μm	10	20	40
100-500 μm	1	2	4
>500 μm	0	0	0

Tab. 2.2.: Particle cleanliness requirements of the Vulcain Engine [29]

The lower limit value of the particle size that does not require regulation is therefore < 15 μm (see table 2.2) or < 6 μm (see ECSS-E-ST-35-06C Rev.2, Annex A).

Practical experience with standard hydraulic and pneumatic systems has shown that particles under 5 μm are not critical [28, 29].

2.3.2. Continuous Procedures

In continuous processes, particles that are moved along in a fluid are analysed. Possible measured variables are particle quantity, size and shape. In addition, the time dependent output of the particles can be measured.

If particles are entrained in a fluid, this is referred to as disperse two-phase flow [30].

A relevant parameter for characterising these flows is the volume fraction of the disperse phase β_p [-]. It is defined as the volume of all particles in a unit of volume element divided by the units total volume. [31].

$$\beta_p = \frac{V_{Particles}}{V_{Total}} \quad (2.15)$$

The flow states dependent on the β_p are shown in 2.10.

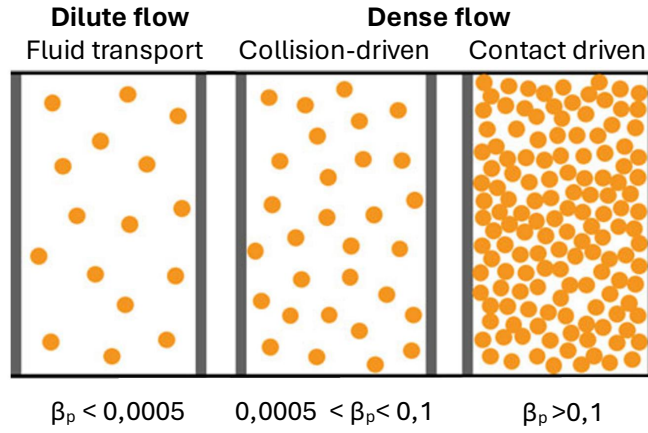


Fig. 2.10.: Schematic of the states of a disperse two-phase flow dependent on the volume fraction of the disperse phase; changed based on [31]

In dilute disperse flows, particle transport is mainly determined by flow forces as well as by external field forces (e.g. gravity and electric force); see Fig. 2.10 on the left. In denser disperse systems, the particle movement is additionally influenced by fluid mechanical interactions between the particles as well as by their collisions; see Fig. 2.10 middle. If the volume fractions of the particles are greater than $\beta_p = 0.1$, this is referred to as contact-driven [31].

An alternative indication of the particle concentration in fluids can be made using the number concentration β_n and the mass concentration β_m [32].

The number concentration in m^{-3} relates the number of particles N [-] in a unit volume to the unit volume of the fluid:

$$\beta_n = \frac{N_{\text{Particles}}}{V_{\text{Total}}} \quad (2.16)$$

The mass concentration relates the sum of the masses m in kg of the particles in a unit volume to the unit volume of the fluid:

$$\beta_m = \frac{m_{\text{Particles}}}{V_{\text{Total}}} \quad (2.17)$$

Approaches to convert masses and number concentration of particles into each other with known density and size distribution of the particles can be found in [32].

Light Extinction Particle Counter (LEPC)

The measuring principle of a LEPC is based on the reduction of the intensity of a light beam caused by the interaction of the light with individual particles. This phenomenon is also known as light blockage or light obscuration. A LEPC, also referred to as an automatic particle counter, can be used to monitor the cleanliness level of e.g. fluids circulating in hydraulic systems or packaged stock fluids. It can also be used to monitor the progress of a flushing operation [33].

Specifications for determining the particle contamination level of a liquid sample with an LEPC can be found in the ISO 11500 standard [33].

Light Scattering Airborne Particle Counter (LSAPC)

The measuring principle of LSAPC is based on the detection of light that is scattered and shadowed by a particle when a particle passes through an incident light beam. The particle size is determined from the intensity of the scattered light and the number of particles from the number of light pulses scattered by individual particles. For this purpose, the light signal is displayed via a photoelectric converter and a pulse strength analyser after it has shone on the particles. When used in cleanrooms, the air to be analysed is drawn in through a vacuum system [34].

An example of the schematic structure of an LSAPC is shown in Fig. 2.11.

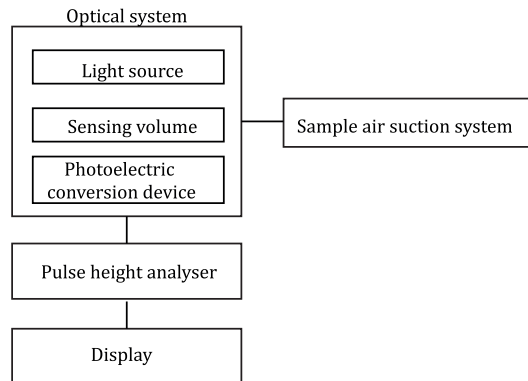


Fig. 2.11.: schematic of the LSAPC working principle [34]

The typical size range of particles measured with this method is between $0.1 \mu\text{m}$ and $10 \mu\text{m}$ particle size. The optical particle size measured with the LSAPC is the light scattering equivalent particle size and not the geometric size. In order to carry out measurements with an LSAPC, the device must be calibrated with particles of a known size distribution. For example, polystyrene latex particles or quartz dust is used for this purpose. [34, 35]

Specifications for determining the particle size distribution for airborne particles with light-scattering particle counters for use in cleanrooms are regulated in the ISO 21501-4 standard [34].

2.3.3. Discontinuous Procedures

The discontinuous methods presented below are the manual, microscopic method and the automatic methods of sieving and the gravimetric method.

Gravimetric Method

In the gravimetric method, the mass concentration of particles is determined by filtering a certain volume of liquid under vacuum conditions through a filter membrane. The increase in mass of the membrane after filtration represents the content of solid impurities. The method is suitable for mass concentrations of at least 3 mg/l . Specifications for the determination of particle contamination by the gravimetric method are regulated in the ISO 4405 standard. The specifications refer to the application for hydraulic fluids. If the method is carried out according to the standard, filter membranes with a pore size of $0.8 \mu\text{m}$ are used for filtering. Examples of suitable filters of different brands that can be used are given in the standard:

- Millipore (Type AAWP04700)

- Pall (Type GN4-08 μm Metrical MCE)
- Sartorius (item name: Zelluloseacetat-Filter 0.8 μm)

To carry out the measurement, the unused filter is first conditioned by soaking it several times with solvent, which is then vaporised. This process is repeated until the filter no longer changes its weight as determined by weighing. A sample diluted in solvent is then drawn through the filter using a vacuum and the solvent is evaporated again. The filter is weighed again and the differential weight is determined [36].

The mass concentration β_m can be determined in accordance with equation 2.17. The $m_{particle}$ value in the equation corresponds to the difference in weight of the filters. V_{total} corresponds to the total volume of the filtered sample.

If β_m falls below the limit value of 3 mg/l specified above, the method is not applicable [36].

Microscopic Method

In the microscopic method, particle contamination is determined by counting the particles deposited on the surface of a membrane filter using an optical microscope. With the microscopic method, particles with a size $\geq 2 \mu\text{m}$ can be measured and counted. The resolution and accuracy depend on the optical system used and the skills of the observer. In order to be able to analyse a sample using the microscopic method, the particles are separated from the liquid in the sample by vacuum filtration. The filter is removed, dried and the particles on it are fixated. The number of particles can then be counted.

For manual counting a gridded filter membrane is used. Particles are only counted in a number of grid fields specified in the used standard. This count is used to calculate the total number of particles captured in the filter and, accordingly, in the sample. [37]

The number concentration can be determined in accordance with (2.16) using the number of particles counted and the volume of the sample.

Another method is automatic counting using image analysis. For this purpose, an optical image of the particles on the filter is created digitally and on the basis of the difference in grey contrast between the particle and the background image the number of particles and their sizes is calculated. [37].

Specifications for the determination of particle contamination by the counting method using an optical microscope are regulated in the ISO 4407 standard. The specifications refer to the application for hydraulic fluids. [37]

Sieving

Sieving methods are suitable for characterising bulk materials. This means that the particles to be measured must be in dry form. Various possible sieving methods offer different possible resolutions. Basically, the particles are sorted and separated in the sieving process by sorting them through sieves with different known mesh sizes. [38, 39]

The measuring ranges of the various sieving methods for different particle size ranges are shown in Figure 2.12.

Since particles below a size of 20 μm are of particular interest for the application of particle measurement for qualification in space applications (see 2.3.1), only the air jet sieving method is explained in more detail below, which is the only sieving method providing sufficient resolution.

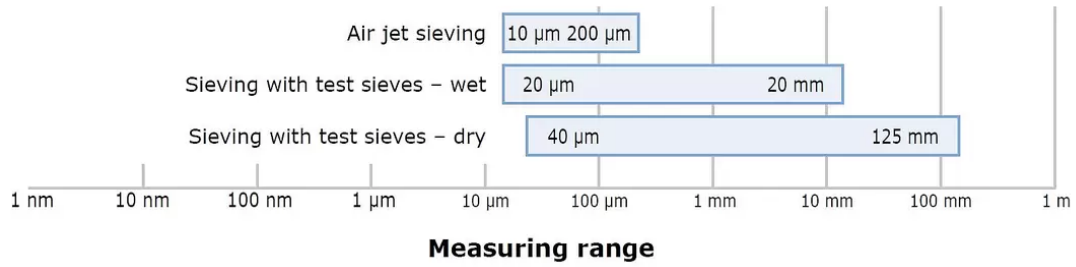


Fig. 2.12.: Suitability of the various sieving methods for analysing different particle sizes [39]

During the Air Sieving Process a series of sieves with different mesh sizes are used. In each step the sample material is placed on the sieve and a jet of air is passed through the sieve from below and disperses the material on the sieve. This dispersion causes fine particles to pass through the sieve, where they are extracted and, if necessary, captured by a cyclone filter. The material to be sieved is then weighed and placed on a sieve with a larger mesh size and the size distribution of the particles can be determined by calculating the weight difference. With this form of sieving, the sieve itself is not moved. [38]

3. Methodology

This chapter presents and explains the methods used in this work. This includes the methodology of the selection procedure used in this work for the evaluation of different design concepts is described in this chapter. Furthermore the inputs for the numerical calculation of the pressure distribution within the bearings lubrication gap, which result in the quantification of the bearings load-bearing capacities, are described. Subsequently the experimental setup for a first evaluation and testing procedure for material-inherent particles occurring in CMC-Material is presented.

3.1. Systematic Selection Procedure

The selection procedure is divided into the following steps:

1. Creating the Model Concepts
2. Creating Evaluation Criteria
3. Preference Analysis
4. Selection

The procedure used for the assessment is based on the VDI 2225 standard [40]. The steps for the procedure, as carried out in this work, are explained below:

1. Creating the Model Concepts

With the requirements defined for the purpose in mind, different concepts are created. The functionality of these must then be verified. The concepts are created based on fundamental considerations of functionality with regard to the application. Care is taken to cover the entire spectrum of technical possibilities. An attempt is made to create concepts impartially towards different approaches and to include new possibilities that have not yet been tested.

Nevertheless, concepts that cannot fulfil a requirement under any circumstances are directly excluded from the further procedure.

2. Creating Evaluation Criteria

The next step is to create evaluation criteria that consider the various design requirements as completely as possible, ensuring that the procedure provides the most accurate result possible. Subjectively important or unimportant criteria should not be evaluated or discarded.

3. Preference Analysis

To make a well founded decision, weighting up the selected evaluation criteria is an essential step. There are multiple options for this process available. The method used in this case is the preference analysis. With this procedure the number of n criteria counted by index k are

compared in pairs with each other and a decision is made as to which is more important for the defined objective. Based on these decisions a weighing factor C_k [-] is determined for each criteria. The procedure is purely subjective as the decision maker makes the comparative decisions purely subjectively. Based on the count of decisions fallen towards one criteria a rank S_k [-] is assigned. To calculate the weighing factor, the reversed rank S_k^{-1} corresponding to the reversed order of the rank is assigned. The weighing factor is calculated as follows:

$$C_k = \frac{\sum C_k}{\sum S_k} \cdot S_k^{-1}. \quad (3.1)$$

The sum of the weighing factors in equation 3.1 can be freely defined. If set to one, this results in a percentage value, which can be used to compare the relevance of the various factors.

4. Selection

For the selection process, the l number of concepts are awarded a number of evaluation points P_{kl} for their fulfilment of the previously defined k number of criteria, for each concept and criteria. The Point scale used is:

- 1 Point : Very bad fulfilment of the criteria
- 2 Points : Bad fulfilment of the criteria
- 3 Points : Satisfactory fulfilment of the criteria
- 4 Points : Good fulfilment of the criteria
- 5 Points : Excellent fulfilment of the criteria

These ratings are then weighted using the previously determined weighing factors, creating the partial utility value p_{kl} for the respective concept and criteria:

$$p_{kl} = C_k \cdot P_{kl}. \quad (3.2)$$

The total utility value K_l of a concept l is calculated using the following formula:

$$K_l = \sum_{k=1}^n C_k \cdot P_{kl}. \quad (3.3)$$

This means that the total utility value is calculated as the sum of partial utility values concerning one concept l .

The results can be presented either on the same point scale or as a percentage of the maximum number of points. The different concepts can be sorted by ascending score and the one with the highest score of the total utility value K_l can then be selected for further investigation.

3.2. Numerical Fluid Mechanical Calculation of CMC Fluid Film Bearings

This chapter documents the parameters used for the numerical calculation of the CMC-Bearings calculated as part of this work. The calculation principles have been explained in the theory and fundamentals section 2.1. The software used is based on the described methods as they were explained. All parameters used in the calculations are summarised below.

For the initial design presented in the results and discussion chapter (see 4.2.1) the parameters for the calculation are set to the values shown in 3.1. In tab. 3.1 the indices J and T are introduced to differentiate between the parameters used for journal and thrust bearings. The determination processes for the values, chosen for each parameter, are explained below:

- For the journal bearing the width of the non-porous CMC is set to 1% of the bearing length z_J . For the thrust bearing the thickness of the non-porous CMC is set to 1% of the bearing thickness resulting from $R_{T,2} - R_{T,1}$. The reason for the small layer thickness of the non-porous parts is the intention to build the bearing without them, saving construction space. Instead, the end faces could be sealed with graphite. The non-porous parts are nevertheless included in the numerical calculation, as the available numerical simulation tools do not allow to exclude them from the simulation. For this reason, no values for b_j , $R_{T,0}$ and $R_{T,3}$ are given in table 3.1.
- The mesh resolution for the journal bearing was chosen, to 50 by 50 grid points, because it was shown that this resolution is sufficient in order to get an accurate solution of the model equation 2.10 [18]. Based on the assumption that the same grid resolution is an accurate solution for the calculation of the thrust bearings, the same resolution was chosen for the thrust bearing.
- The pump speed is set to the nominal speed of the pump (compare 4.1).
- α is set to a typical value for C/C-Material taken out of [10].
- μ is estimated on the basis of the substance values of Rocket Propellant 1 (RP-1), published in [41] and [42].
- The length z_J , the gap height of the journal bearing h_0 and the radii $R_{J/T,i}$ are determined for the journal bearing, taking into account manufacturability and available space.
- The exhaust pressure p_e as boundary condition for the calculation is set to the pump inlet pressure on the assumption that it will be possible to feed the bearing supply mass flow back into the pump inlet flow.
- The supply pressure p_s is then set at a pressure difference of 20 bar, because this value is in the intermediate range what has proven to work for CMC-Bearings in [10] and the available pressure difference of the pumps inlet and outlet pressure of 44.16 bar for the fuel pump.

The decisions are resulting in the input values for the numerical calculation summarized in tab. 3.1.

The resulting pressure distributions of this calculation for an eccentricity of the journal bearing of $0.6 \cdot h_0$ and a gap height of the Thrust bearing of $h = 0.01$ mm are shown in fig. 4.6 and fig. 4.7.

In order to get the load-carrying capacities of the bearings dependent on their operating point, the numeric calculation with the parameters in tab. 3.1 is repeated several times.

For the journal bearings the simulation is repeated for an eccentricity ranging from 10% of the gap height up to 90% of the gap height, with 18 calculation points, linearly spaced across this range of eccentricity.

For the thrust bearings the simulation is repeated for a gap height ranging from 5 to $45 \mu\text{m}$, with 18 calculation points, linearly spaced across this range of gap height. These parameters are used for the calculation results shown in fig. 4.5.

These parameters are used for all numerical calculations whose results are given in this work unless changes are explicitly stated. Deviations are summarised below:

Parameter	Unit	Value
n	[1/min]	40000.0
α	[$\cdot 10^{-14}$]	3.5
p_s	[10^{-5} Pa]	4.14
p_e	[10^{-5} Pa]	20.14
μ	[10^{-3} Pa \cdot s]	1.2
Journal		
h_0	[mm]	0.05
z_R	[mm]	15.0
$R_{R,0}$	[mm]	7.45
$R_{R,1}$	[mm]	7.5
$R_{R,2}$	[mm]	13.5
nx	[-]	50.0
ny	[-]	50.0
Thrust		
z_T	[mm]	6.0
$R_{T,1}$	[mm]	8.0
$R_{T,2}$	[mm]	15.0
NR	[-]	50.0
$N\varphi$	[-]	50.0

Tab. 3.1.: Input values for numerical calculation of the pressure distribution within the bearings lubrication gaps

- For calculating the effect of changing the supply pressure, the supply pressure is varied to $p_s = p_s + \Delta p$ with Δp ranging from -10 bar to $+10$ bar. The results of this calculation are shown in fig. 4.8.
- For calculating the effect of varying lubricating film areas the length of the journal bearing z_j is changed to $z_j = z_j + \Delta z$ with Δz ranging from -4 mm to $+4$ mm and the radial thickness of the thrust bearing $R_{T,3}$ is changed by $R_{T,3} = R_{T,3} + \Delta R$, with ΔR ranging from -2 mm to $+2$ mm. The results of this calculation are shown in fig. 4.9.
- For calculating the effect of varying permeabilities, the calculation is repeated with changing permeability parameters $\alpha = \{3.5 \cdot 10^{-15}, 1.5 \cdot 10^{-14}, 3.5 \cdot 10^{-14}, 5.5 \cdot 10^{-14}, 3.5 \cdot 10^{-13}\}$. The results of this calculation are shown in fig. 4.10.
- For calculating the effect of changing the thickness of the journal bearing, the outer radius of the porous bearing $R_{J,2}$ gets changed to $R_{J,2} = R_{J,2} + \Delta R$. For this calculation ΔR ranges from minus two millimetres to plus two millimetres. For calculating the effect of changing the thickness of the thrust bearing z_T , it gets changed to $z_T = z_t + \Delta z$. Δz ranges from minus two millimetres to plus two millimetres. The results of this calculation are shown in fig. 4.11.
- For calculating the effect of varying the fluid viscosity the viscosity μ gets changed to $\mu = \{1.2 \cdot 10^{-4}, 0.2 \cdot 10^{-3}, 1.2 \cdot 10^{-3}, 2.2 \cdot 10^{-3}, 1.2 \cdot 10^{-2}\}$ [Pa \cdot s]. The results of this calculation are shown in fig. 4.12.
- For calculating the effect of varying the gap height h_0 of the journal bearing, the gap height is changed. The values used are $h_0 = \{0.03 \text{ mm}, 0.04 \text{ mm}, 0.05 \text{ mm}, 0.06 \text{ mm}, 0.07 \text{ mm}\}$. The results of this calculation are shown in fig. 4.13.
- The following changes were made to the calculation of the load bearing capacities of concepts

C, I and A:

- The calculation is done with a supply pressure p_s with the maximum available pressure of 48.3 bar.
- h_0 is set to 0.03 mm.
- The geometry is varied according to table 3.2.

The results of these calculations are shown in fig. 4.15.

Parameter	Unit	Design C	Design I	Design A
Journal				
z_R	[mm]	25.0	23.0	9.0
$R_{R,2}$	[mm]	7.5	7.5	7.5
$R_{R,3}$	[mm]	13.5	11.5	11.5
Thrust				
z_T	[mm]	-	3.0	4.0
$R_{T,1}$	[mm]	-	7.5	8.8
$R_{T,2}$	[mm]	-	11.5	13.8

Tab. 3.2.: Geometry changes for numerical calculation the journal and thrust bearing design variants C,I and A.

3.3. Experimental Investigation of Material-Inherent Particles

To investigate the material-inherent particle pollution, material samples are ultrasonically cleaned, the released particles are filtered out. Subsequently the filters with the residue particles are examined by a weighting or a counting method.

The first test procedure for the investigation of material-inherent particles is based on the counting method using an optical microscope regulated in the ISO 4407 standard. The standard specifies this procedure for the determination of particle contamination in hydraulic fluid systems. [37] In the following this method is referred to as microscopic method. It is selected from the particle measurement methods presented in chapter 2.3, because it can be implemented with a manageable effort and is able to map all particle sizes required. As only a small number of samples is to be analysed, it was assumed that it is not necessary to use an automatic process, but rather to count the particles manually. However, the experiment results exhibited a high number of particles which made the introduction of an automatic counting method using image analysis necessary.

In addition to this method a second evaluation method for estimating particle pollution is used. In order to estimate the particle mass in the samples, a simplified form of the gravimetric method specified in the ISO 4405 standard is used [36]. The microscopic method is still necessary, because it is not possible to predict beforehand whether the critical particle quantity for applying the gravimetric method is reached and because it does not provide any information about the size distribution of the particles.

The steps of the experiments are explained below.

3.3.1. Sampling Method - Filtration

The process arrangement for filtration is carried out in two steps:

- I. Extraction of particles by ultrasonic cleaning
- II. Filtration in filtration device

Fig. 3.1 shows a simplified scheme of the experimental setup and procedure.

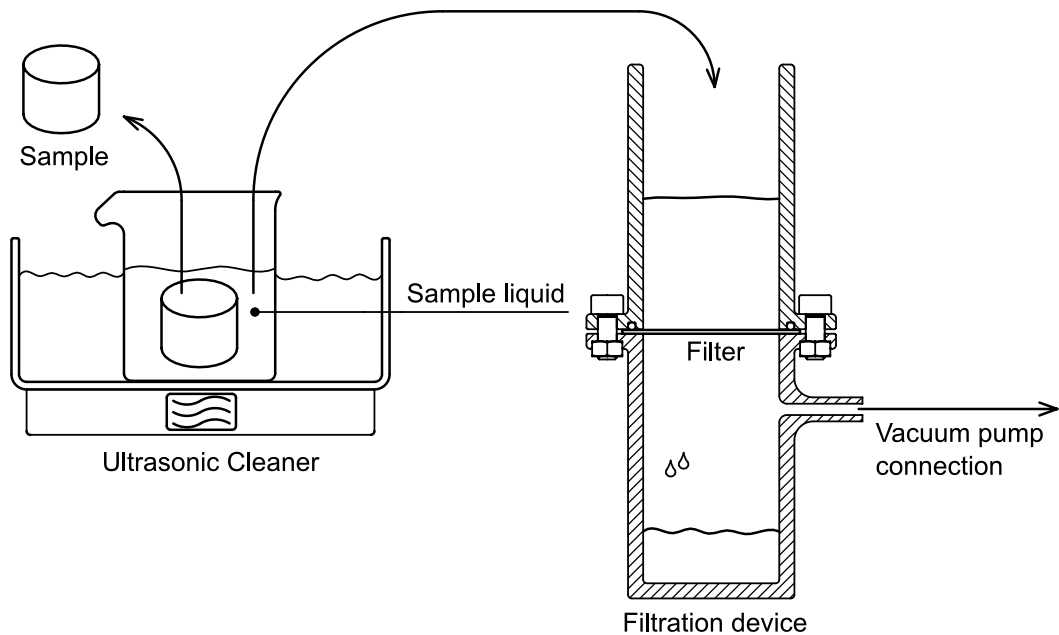


Fig. 3.1.: Illustration of the filtration procedure with a 3D-Printed filtration device.

The following test materials are required:

- Ultrasonic cleaning device
- Beaker
- Distilled water
- Gridded round filters
- Filter holder
- Vacuum pump
- Connecting hoses
- Pliers
- Stop-watch
- Tweezers
- Samples

The samples used have a cylindrical shape with a diameter of 30 mm and a height of 32 mm. The three samples are referred to as sample one, two and three and have the following properties:

Sample 1: C/C CMC-Sample cut out of an C/C-Plate according to fig. 2.9. This sample is therefore closest to the shape of an actual CMC journal bearing sleeve.

Sample 2: C/C CMC-Sample cut out of an C/C plate perpendicular to the alignment as shown in fig. 2.9

Sample 3: Sample cut out of an oxidic fibre ceramic to be investigated for the application with the same fibre orientation as sample 2

The ultrasound device used is the SW45H from Sono Swiss with a nominal power of 2000 W. All filtrations are performed with white, gridded 47 mm round Supor[®] filters with 0.8 μm pore size, obtained via Pall Corporation (LOT 64277530).

All equipment used is carefully cleaned with distilled water before use. Gloves are worn during the entire experiment. Care is taken to store the filters in airtight, closed containers between the

experiment and the evaluation of the microscopic investigation in order to minimize contamination by dust. The step by step particle extraction and filtration procedure is as follows:

1. The beaker is rinsed with distilled water and filled with 75 ml of distilled water.
2. The sample is carefully placed in the beaker filled with distilled water using pliers. The cylindrical sample is placed on its cylindrical surface and is completely submerged.
3. The beaker with the sample is placed in the ultrasonic tank. The water level in the ultrasonic tank is matched with the water level inside the beaker.
4. The ultrasonic device is switched on for the defined test period. The time is stopped with a stopwatch.
5. The beaker is removed from the ultrasonic tank.
6. The sample is carefully removed from the beaker using pliers and held shortly over the beaker to catch excessive fluid located on the sample. The sample is then placed on a dry clean paper towel.
7. The contents of the beaker are poured into the filter assembly.
8. To remove any residue of particles within the beaker 10 ml of distilled water is poured into the beaker. After a short swirl by hand the contents are also poured into the filter assembly.
9. With a manually operated vacuum pump a vacuum is created every 30 seconds in the lower part of the filtration device, causing the water to be sucked through the filter. The total time of the filtration is measured and documented; the end of the filtration process is reached when no water is left on the upper side of the filter. The vacuum does not exceed 20 mmHg as indicated on the hand vacuum pump.
10. The filter assembly is unscrewed and the filter carefully removed with tweezers and placed on the side for further examination.
11. The components are cleaned and screwed back together with a new filter for the next test.
12. The procedure can be repeated with the next sample.

3.3.2. Microscopic Analysis

For microscopic analysis, the gridded filters are placed under an optical microscope and the particles of different sizes within the individual fields are counted.

The counting procedure is based on the ISO 4407 standard [37]. The Pattern shown in fig. 3.2 is used, to name the fields that are counted. The size distribution for classification of the particle sizes is based on the specifications from ECSS-E-ST-35-06C [28], (see annex A). The microscope used is the Keyence VHX Digital Microscope VHX-500.

Due to the large number of particles that were extracted out of the material samples in the experiment, the count of the particles is not carried out by hand in deviation from the ISO 4407 standard, but is determined using the microscope-related Keyence VHX-500 software. This software uses the colour differences in the recorded image data to determine the number of particles within a selected area and their maximum diameter. This data is then analysed. A visualisation of the steps in the analytic process of one grid square can be found in figures shown in fig. 3.3, 3.4 and 3.5. In each case the grid squares 1, 3, 5, 7 and 9 are analysed and the number of particles counted is referred to as N , indexed by the grid square number.

Due to the fact that a high number of particles is released in the first ultrasonic cleaning process

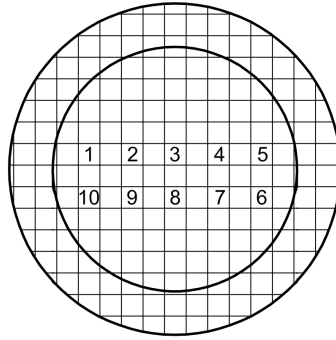


Fig. 3.2.: Counting pattern for ten locations According to the ISO 4407 standard [37]

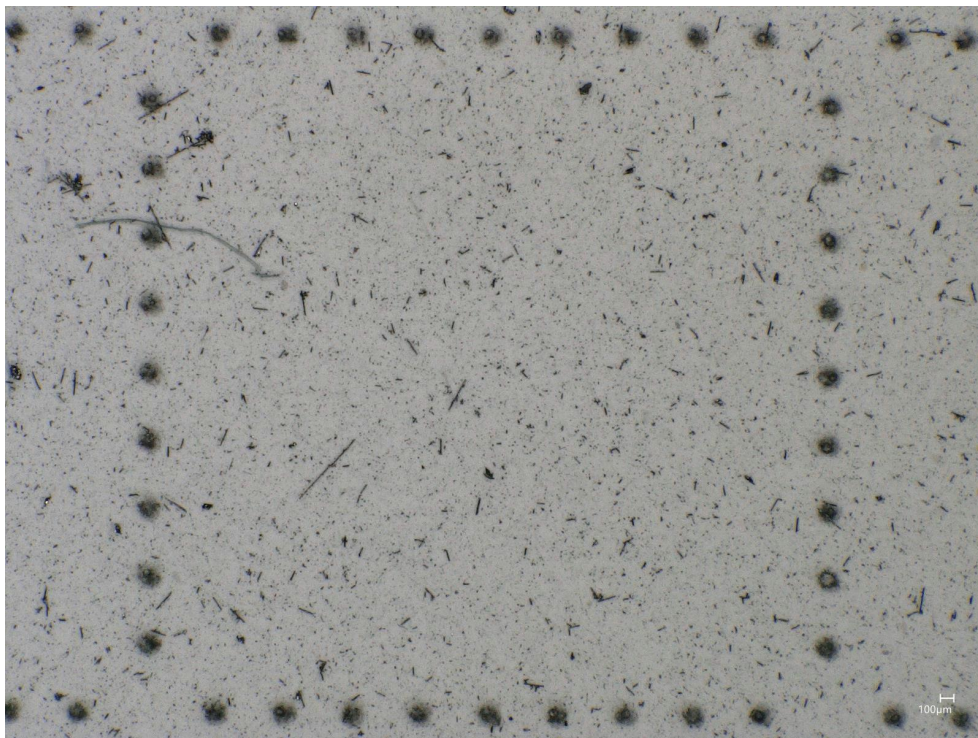


Fig. 3.3.: Image of filter grid square under the microscope, sample 1, 64 minutes (total of 124 minutes) of ultrasonic cleaning time

so that the grid is no longer visible and analysing all filters is not adding valuable information, only individual filters are examined, in cases where the grid is still visible.

In order to analyse and compare the test results to regulation standards, the number of particles counted within a certain size range and grid field is converted into a particle population value as a concentration in the used test liquid. Therefore the volume of the sample within the beaker which is used in the experiment $V_{sample} = 75$ ml multiplied by the number of particles in the sample liquid within in a certain size range is divided by the volume of the sample that the concentration should refer to $V_{reference, sample}$ (100 ml in the ECSS standard). The number of particles within a certain size range in the sample liquid is calculated by extrapolating the numbers counted within the grid field to the whole filtration area. This results in the following equation:

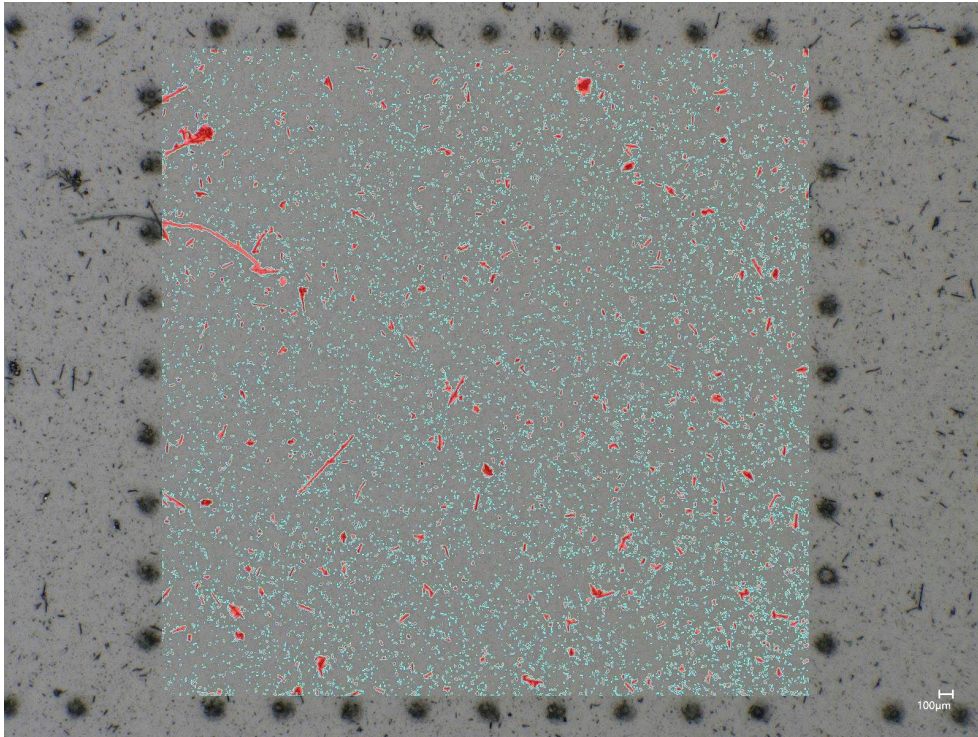


Fig. 3.4.: Superimposition of the image with the computer-aided particle analysis image, sample 1, 64 minutes (total of 124 minutes) of ultrasonic cleaning time

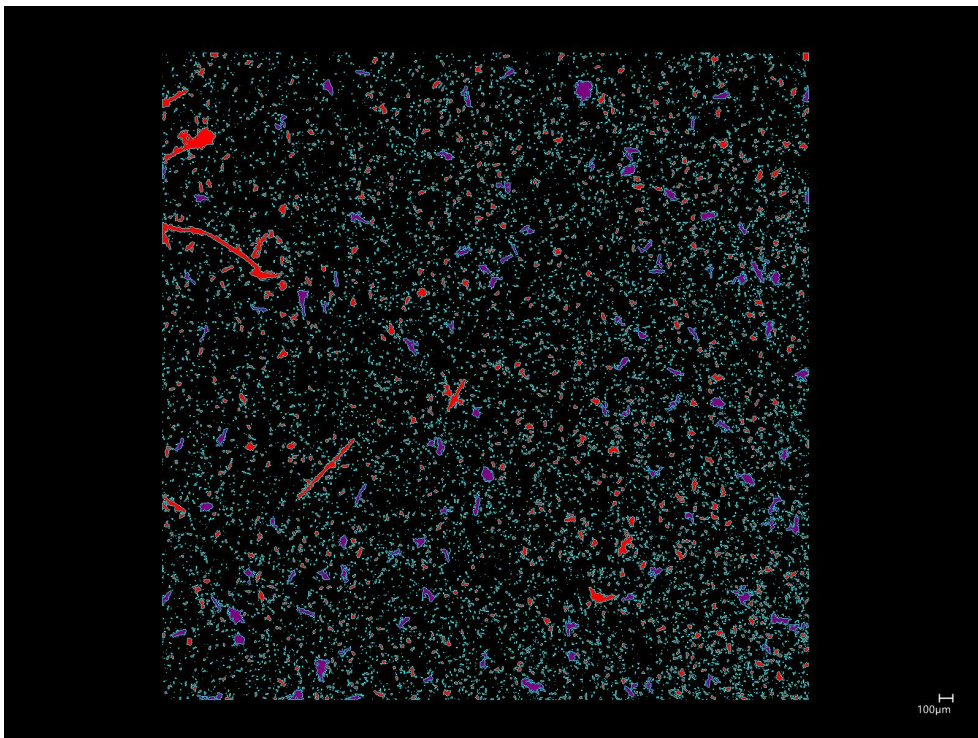


Fig. 3.5.: Image of computer-aided particle analysis, sample 1, 64 minutes (total of 124 minutes) of ultrasonic cleaning time; detected particles are outlined in turquoise; particles of size ranging from $101\mu m$ to $200\mu m$ are marked purple, others red

$$\begin{aligned}\beta_n &= \frac{V_{reference, sample}}{V_{sample}} \cdot N_{extracted\ particles} \\ &= \frac{V_{reference, sample}}{V_{sample}} \cdot \frac{A_{filtration\ area}}{A_{grid\ fields\ counted}} \cdot \sum N_{counted\ particles} \\ &= \frac{100\ \text{ml}}{75\ \text{ml}} \cdot \frac{\pi \cdot (13\ \text{mm})^2}{5 \cdot 3\ \text{mm} \cdot 3\ \text{mm}} \cdot (N_1 + N_3 + N_5 + N_7 + N_9) \\ &\approx 15.73 \cdot (N_1 + N_3 + N_5 + N_7 + N_9).\end{aligned}\tag{3.4}$$

3.3.3. Gravimetric Analysis

A simplified method, based on the ISO 4405 standard is used for the gravimetric analysis. [36] For the process, the filters are weighed before and after filtration using a precision scale.

To do this, the step by step procedure can be described as follows:

1. The filter is removed from its sterile packaging and carefully placed on the precision scale using tweezers. The weight is documented.
2. The filtration process is carried out according to the procedure described in 3.3.1.
3. The used filter is placed in an airtight plastic container for storage.
4. The microscopic analysis is carried out according to the procedure described in 3.3.2.
5. The opened container open is placed in an oven, the filters are dried at 50° C for one hour. The ventilation of the oven is switched off to minimise contamination.
6. The filters are again carefully placed on the precision scale using tweezers. The weight is documented.

An ABJ 220-4NM precision scale from Kern & Sohn is used for all weighing. It has an uncertainty of ± 0.5 mg for the weight range it is used within the experiments.

4. Results and Discussion

The results of the investigations, carried out in order to adapt the technology of CMC fluid film bearings for the application in the turbopump designed for rocket engines, are presented and discussed in the following chapter.

Firstly, the compiled operational loads of the bearing are presented and explained. The concept creation and evaluation, selection, design and construction of the bearing components is then presented. Finally, the results of the preliminary evaluation of the particle emissions of the CMC-Components within the bearings are discussed.

4.1. Collection of Operative Specifications

The basic specifications of the electric turbopump design by the LCRA as provided by the LCRA and summarized for this work are presented in tab. 4.1. The LCRA plans to build two electric turbopumps, one for a fuel similar to RP-1 and one for Liquid Oxygen (LOX). The same geometry of the casing and a similar rotational speed of 40000 rounds per minute is planned for both turbopumps.

Parameter	Unit	Fuel Pump	LOX Pump
Pump Speed	[1/min]	40000 nominal; 50000 max.	40000 nominal; 50000 max.
Nominal Discharge Flowrate	[kg/s]	0.78	1.4
Pump Inlet Pressure	[bar]	4.14	4.14
Pump Discharge Pressure	[bar]	48.3	44.8
Estimated Power	[kW]	9.0	12.0
Bearing Bore Diameter	[mm]	15.0	15.0

Tab. 4.1.: Basic specifications of the electric turbopumps developed by the LCRA.

In the original Design from the LCRA, the bearing arrangement consists of a conventional double-row bearing arrangement with one fixed and one floating bearing as explained in the theory and fundamentals section 2.1. The bearings and their parameters used for the original design are shown in tab. 4.2. The goal is to replace these bearings with the CMC fluid film bearings. The steps taken to achieve this goal are explained below, starting with a simplified determination of the approximate loads occurring.

4.1.1. Load requirements

For the development and selection of bearing concepts and in order to be able to adequately assess their load-bearing capacities, it is necessary to estimate the loads that occur. The following summarises the data from the calculations and provided by the LCRA and describes the calculation procedure used in this work for an approximate load estimation.

At first the estimation of axial loads for the thrust bearing F_T is described. This is followed by

4 Results and Discussion

	Fuel Pump	LOX Pump
Bearing Manufacturer	Schaeffler	Carter
Part Number	XC7002-C-T-P4S-UL	Custom, based on: Schaeffler XC7002-C-T-P4S-UL
Ring Material	Cronidur-30	Cronidur-30
Ball Material	Silicon nitride	Silicon nitride
Bore Diameter [mm]	15	15
Outer Diameter [mm]	32	32
Width [mm]	9	9
Dynamic Load Rating in [kN]:	5.85	-
Static Load Rating in [kN]:	1.70	-

Tab. 4.2.: Specifications of the Bearings used in the original design.

the estimation of the radial loads for the journal bearing F_J , done with formulas provided by [6, 12].

Axial Loads

The LCRA has estimated the axial loads F_T within a range of $F_T = 400 \text{ N} - 1800 \text{ N}$ depending on the approach used for calculation with the direction of the axial forces oriented only in the direction of the pump inlet.

A simple possibility for an estimation is considered to be to assume the resulting pressure force on the projection surface of the impeller as the axial load on the bearing, assuming a linear increase of pressure from pump inlet pressure to pump outlet pressure over the radius. This assessment was not carried out as the load data from the LCRA was considered sufficient for an initial assessment and dimensioning.

Radial Loads

An estimate was made for the radial loads based on the weight of the shaft and the induced loads due to imbalances. For this purpose a simplified Computer Aided Design (CAD) Model of the shaft was created. A cross section drawing of the shaft and its components is shown in fig. 4.1.

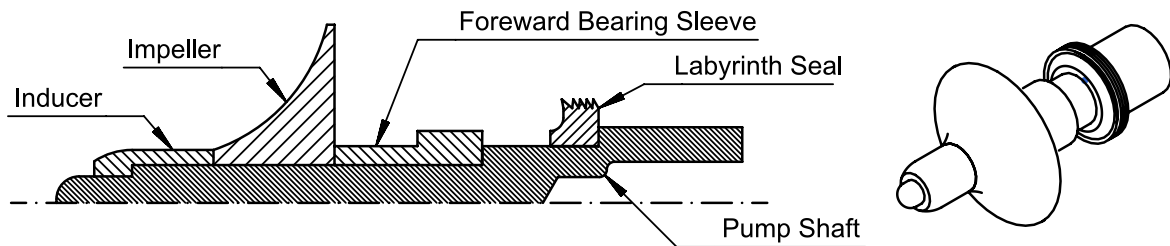


Fig. 4.1.: Components of the shaft assembly for radial load assumptions

The total mass of the shaft assembly required for the calculation is calculated as the sum of the masses of the individual components. These are determined as the product of the volume of the individual components measured in the CAD-Model with the density of the material from which

they are to be built. The results of these calculations and the density used in each case are shown in tab. 4.3.

Part	Volume [mm ³]	Material	Density [kg/m ³]	Mass m [g]
Labyrinth Seal	1916	IN-718	8.2	15.7
Foreward Bearing Sleeve	2835	IN-718	8.2	23.2
Pump Shaft	10754	IN-718	8.2	88.2
Inducer	1290	Ti 6Al-4V	4.43	5.7
Impeller	8580	Ti 6Al-4V	4.43	38.0
			Σ	170.9

Tab. 4.3.: Determination of the weight of the shaft assembly

The gravitational force of the Shaft $F_{J,g}$ was calculated using equation 4.1:

$$F_{J,g} = g_0 \cdot \sum m = 1.676 \text{ N.} \quad (4.1)$$

A load multiplication factor of $L = 10$ is introduced to ensure that the bearing is able to withstand the loads occurring during the launch. In addition, a safety factor of $s = 2$ for a conservative approach is also included.

For the final design, the specifications for the dimensioning and design verification of spaceflight hardware according to the ECSS (here in particular ECSS-E-ST-32-10C [43]) for determining the load multiples and the safety factors should be complied with. As the procedure described here is only intended to determine the approximate magnitude of the forces occurring, it is not covered in detail here. The focus of the design should rather be to design a bearing that is as simple as possible and has a load-bearing capacity as high as possible within the available installation space. The resulting Load $F_{J,g}$ was therefore calculated as:

$$F_{J,g} = g_0 \cdot L \cdot s \sum m = 33.52 \text{ N.} \quad (4.2)$$

To further improve the accuracy of the calculation, the load induced by unbalances is calculated. The comparisons of the calculations allow an assessment which forces are the main influence on radial loads. The loads caused by unbalance are calculated using equation 4.3 [12] and are displayed in fig. 4.2 depending on the unbalance. For a conservatively assumed unbalance of $m_u = 10 \text{ mg}$ placed at the most outer position possible at the shaft ($r = a_4 = 24.44 \text{ mm}$; see fig. 4.3) the radial loads due to unbalance result in:

$$F_{J,u} = m_u \cdot r \cdot \omega^2 = u \cdot r \cdot (2\pi n)^2 = 4.281 \text{ N.} \quad (4.3)$$

Calculating with the same safety factor of $s = 2$ for a conservative approach, a maximum force, resulting from an unbalance, of $F_{J,u} = 8.562 \text{ N}$ is calculated resulting in a maximum combined radial Force as sum of $F_{J,u}$ and $F_{J,g}$ of 42.08 N . This value is set as a minimum radial load carrying capacity for the bearing to be designed.

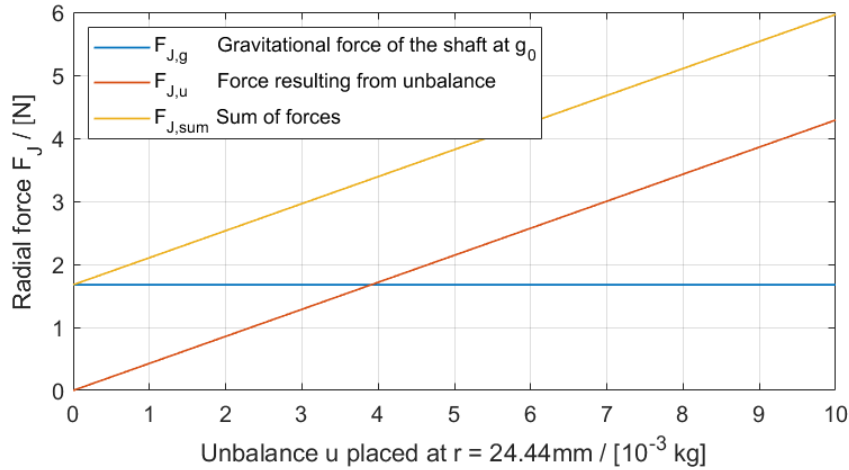


Fig. 4.2.: Calculated Forces based on gravitational weight and unbalance

4.2. Design and Construction

The first step in creating the design is to construct a working model using CAD-Software.

As the load ratings of the original bearings on the fuel side are known and the development of the fuel pump has a greater priority to the LCRA, the construction and design of the fuel pumps bearing is mainly considered in this work. A technical design drawing from the LCRA served as the starting point for the design process. The conventional setup from the LCRA consists of two ball bearings: a floating bearing on the impeller side and a fixed bearing on the opposite site of the impeller. The working model of the turbopump was created using the CAD Software Siemens NX 12 with the help of the information from the LCRA.

A drawing of the reconstructed turbopump section is shown in figure 4.3 with the given reference measurements shown in tab. 4.4.

An image of the Model rendered using the CAD-Software can be found in annex C.

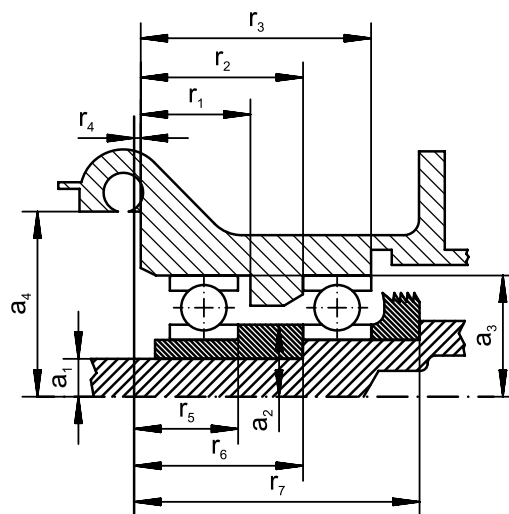


Fig. 4.3.: Reference measurements of the current turbo pump design state

Index	1	2	3	4	5	6	7
Radial r in [mm]:	14.48	21.41	30.41	0.88	13.74	22.31	37.69
Axial a in [mm]:	5.0	7.5	9.51	24.44			

Tab. 4.4.: Reference measurements for the turbopump housing.

4.2.1. Initial Design

An initial design consisting of a journal and a thrust bearing and thus absorbs axial forces in one direction and radial forces is created and calculated with the values summarized in the methodology chapter 3.2 in tab. 3.1.

A cross-section of the geometry is shown in 4.4.

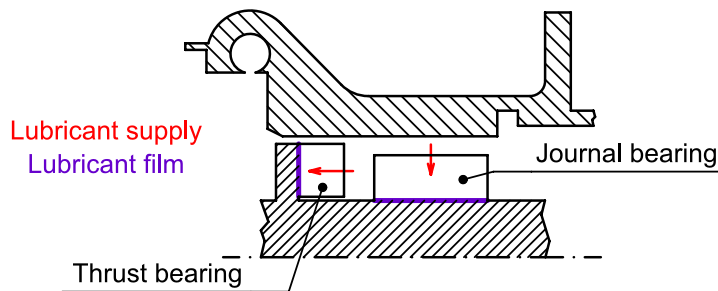


Fig. 4.4.: First iteration cross section

The idea of the creation and numerical calculation of this first design is to obtain a basic idea of the load-bearing capacities that can be expected for a CMC fluid film bearing that can be realised within the space available for the bearing inside the turbopumps casing and the parameters planned for the operation of turbopump. Based on this calculation, the design parameters are varied in order to be able to predict the influences of different parameters on the load-bearing capacity accurately and take them into account in the design. The various parameters of the calculation are varied as described in the methodology chapter (see 3.2) in order to be able to qualitatively assess the influence of design changes on the load-bearing capacity. The results of these calculations are shown below.

The calculated load carrying capacities of the bearings according to 3.2 are shown in fig. 4.5.

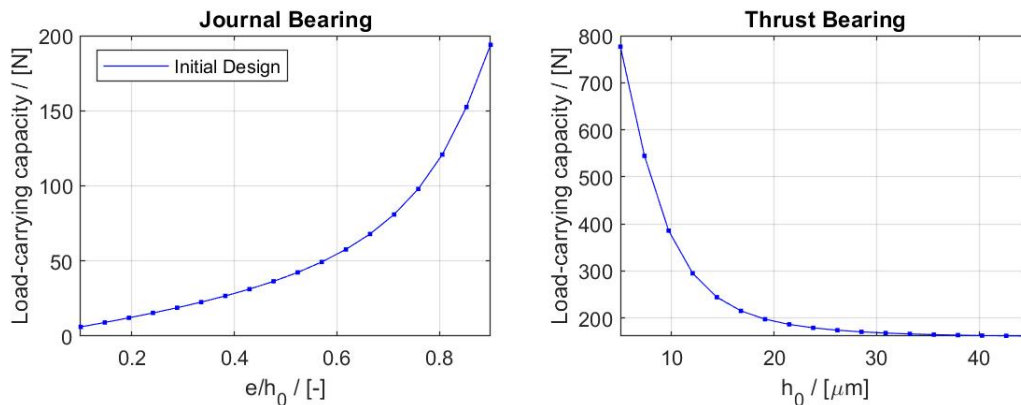


Fig. 4.5.: Load carrying capacities of the Initial Bearing Design

4 Results and Discussion

For the Journal Bearing the pressure distribution within the Bearing is shown in 4.6

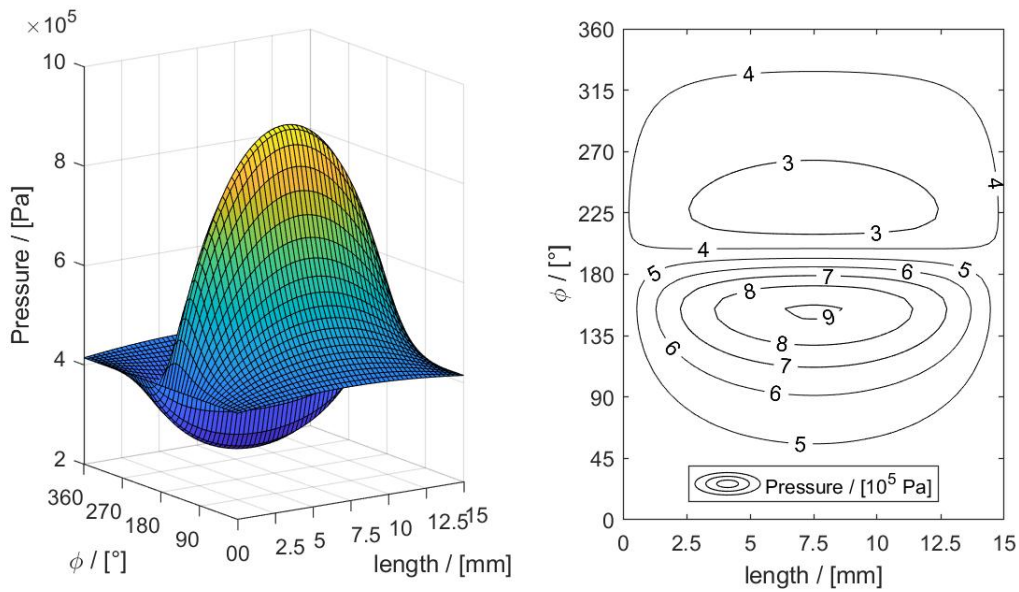


Fig. 4.6.: Calculated pressure distribution within the Journal Bearing for the Initial Design

For the Thrust Bearing the pressure distribution within the Bearing is shown in 4.7

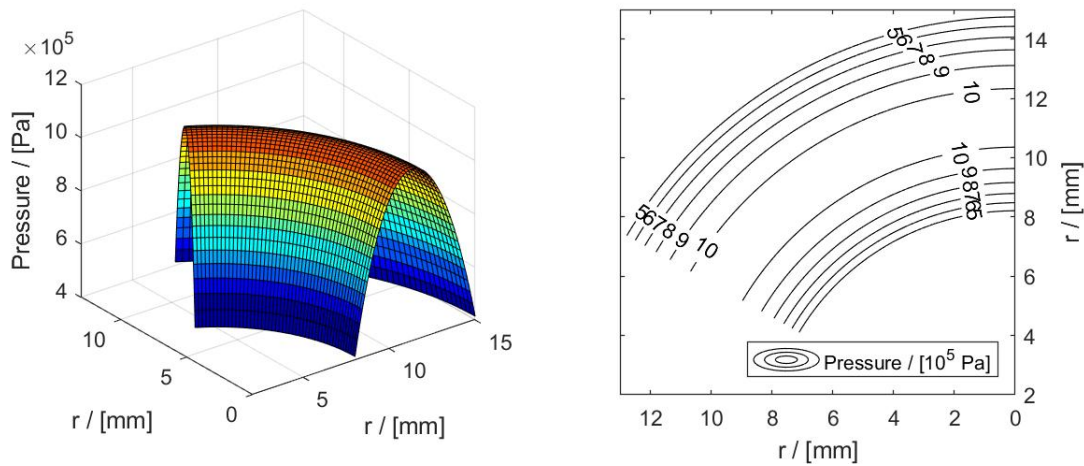


Fig. 4.7.: Calculated pressure distribution within the Thrust Bearing for the Initial Design

The calculated Load carrying capacities for different differential supply pressures Δp are shown in fig. 4.8.

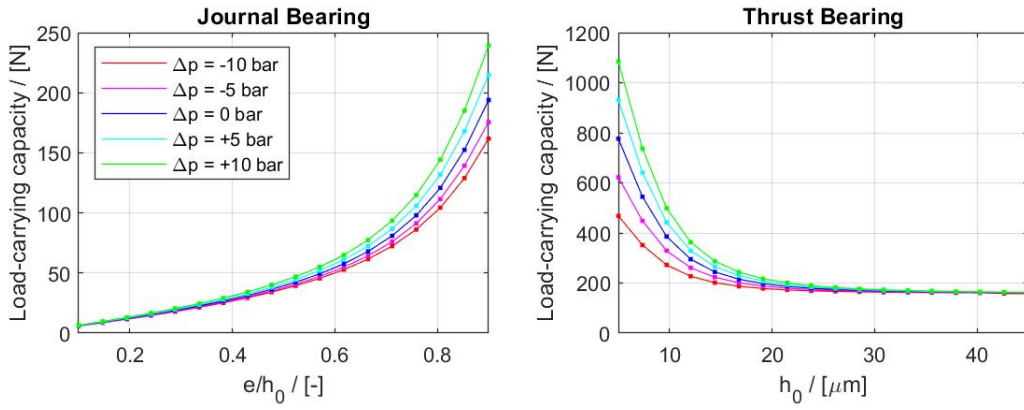


Fig. 4.8.: Effect of changing the supply pressure difference on the Load carrying capacities of the bearing

The effect of increasing the lubricating film width by increasing z_J or $R_{T,3}$ is shown in fig. 4.9.

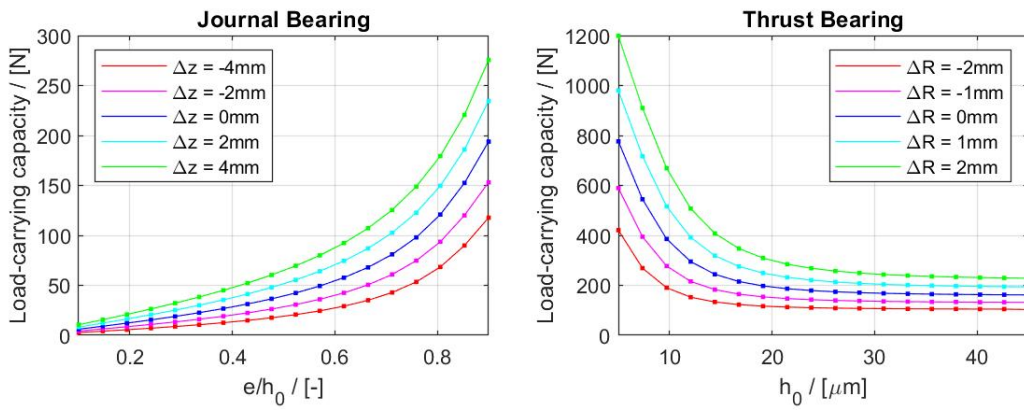


Fig. 4.9.: Effect of increasing the lubricating film area by increasing z_J or $R_{T,3}$

The effect of changing permeability is shown in fig. 4.10.

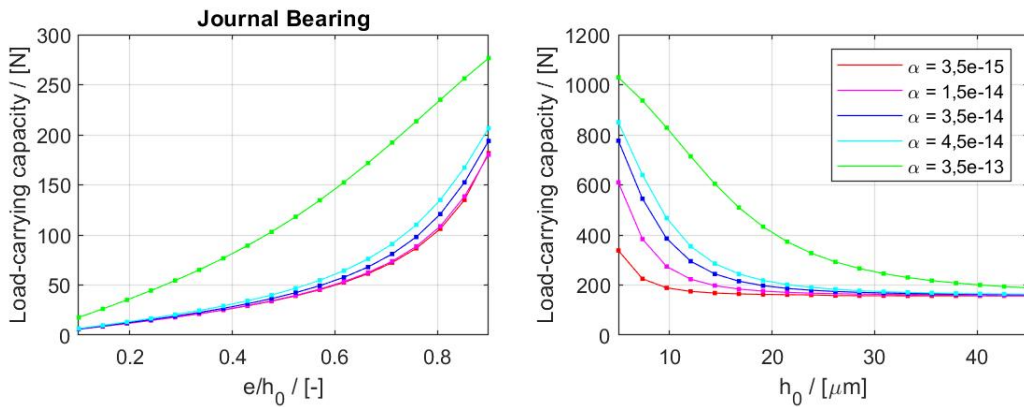


Fig. 4.10.: Effect of changing permeability.

The effect of changing the thickness of the ceramic bearings is shown in fig. 4.11.

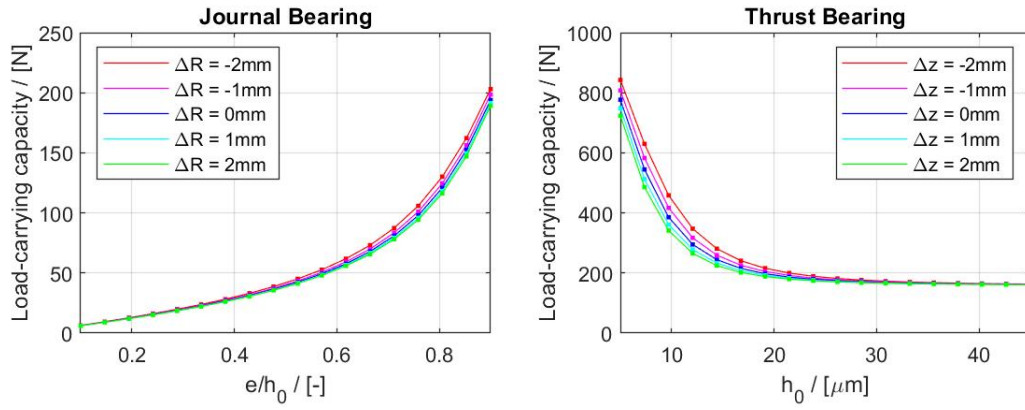


Fig. 4.11.: Effect of changing the thickness of the bearings z_T and R_J , 2.

The effect of changing the viscosity is shown in fig. 4.12.

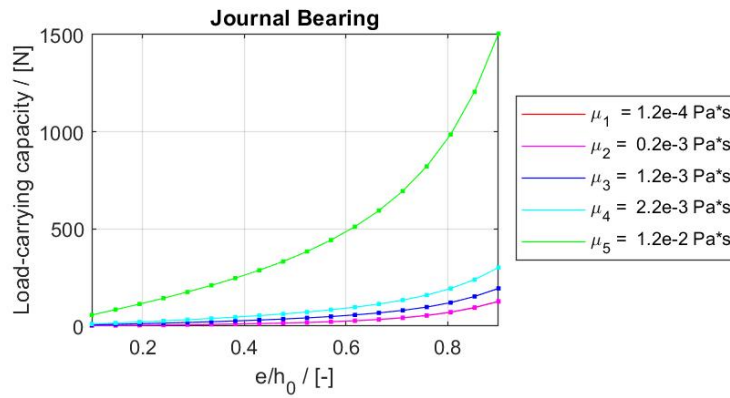


Fig. 4.12.: Effect of changing the viscosity μ .

The effect of changing the gap height h_0 of the Journal Bearing is shown in fig. 4.13.

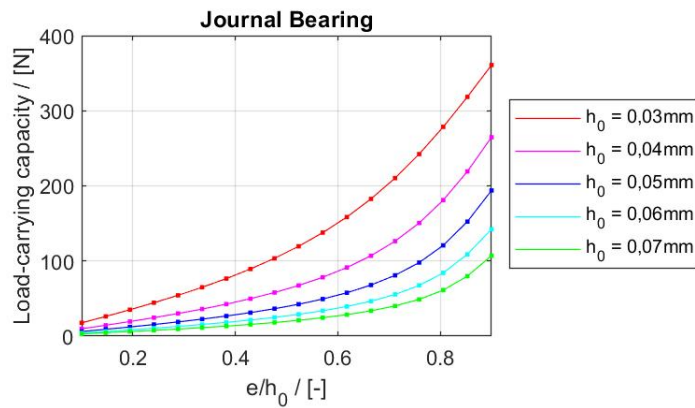


Fig. 4.13.: Effect of changing the gap height h_0 .

4.2.2. Concept Development and Selection

With the elaboration of the load requirements and the knowledge gained from the calculation of the initial design, the next step is to develop various concepts for the construction of a CMC-Bearing and to evaluate them for use in the current application. The results of the Initial design were taken into account in order to assess which parameters are of particular importance for estimating the load-bearing capacities and bearing properties. The procedure used is explained in the methodology chapter, see 3.1.

Creating the Model Concepts

The bearing concepts developed are shown in fig. 4.14. The concepts can be divided into groups with straight and inclined geometry and into those, that can absorb the same axial forces in both directions and those that can absorb more axial forces in one direction than the other. They are labelled from A to M for the following selection procedure. The simplified CMC-Components concepts in an isometric view and a cross-section view of the respective geometry for each concept are shown in fig. 4.14. A qualitative comparison of the estimated loads that can be absorbed is shown in fig. 4.14 in the form of red arrows. The way used to determine this estimate is explained below when the evaluation criteria are defined.

Creating Evaluation Criteria

The evaluation criteria created and used are shown in tab. 4.5 and explained below.

Categorisation	Number	Description
Development	I	State of research
Loads	II	Axial
	III	Radial
	IV	Modal behaviour
Production	V	Geometric Complexity and Tolerances CMC
	VI	Assembly
	VII	Complexity of the fluid flow

Tab. 4.5.: Evaluation criteria selected to identify the best suitable concepts.

- **Development**

Criteria I assesses the current state of the art research and development of CMC fluid film bearings. Configurations that have been partially tested are ranked with a higher score than those not built or tested before. The reason for this is that it is assumed that fewer problems and unforeseen results can be expected during operation, construction and design with more investigated design options.

- **Loads**

Criteria II & III evaluates the load-bearing capacities for axial and radial loads of the bearing. For criteria II the radial length of the fluid film is seen as an indicator for the magnitude of the axial load support. For III the axial length of the fluid film area is seen as an indicator for the magnitude of the radial load support. These assumptions are made based on the results shown in 4.2.1. The lengths for the specific design concepts are measured from the concept drawing shown in fig. 4.14. The estimated magnitude of the

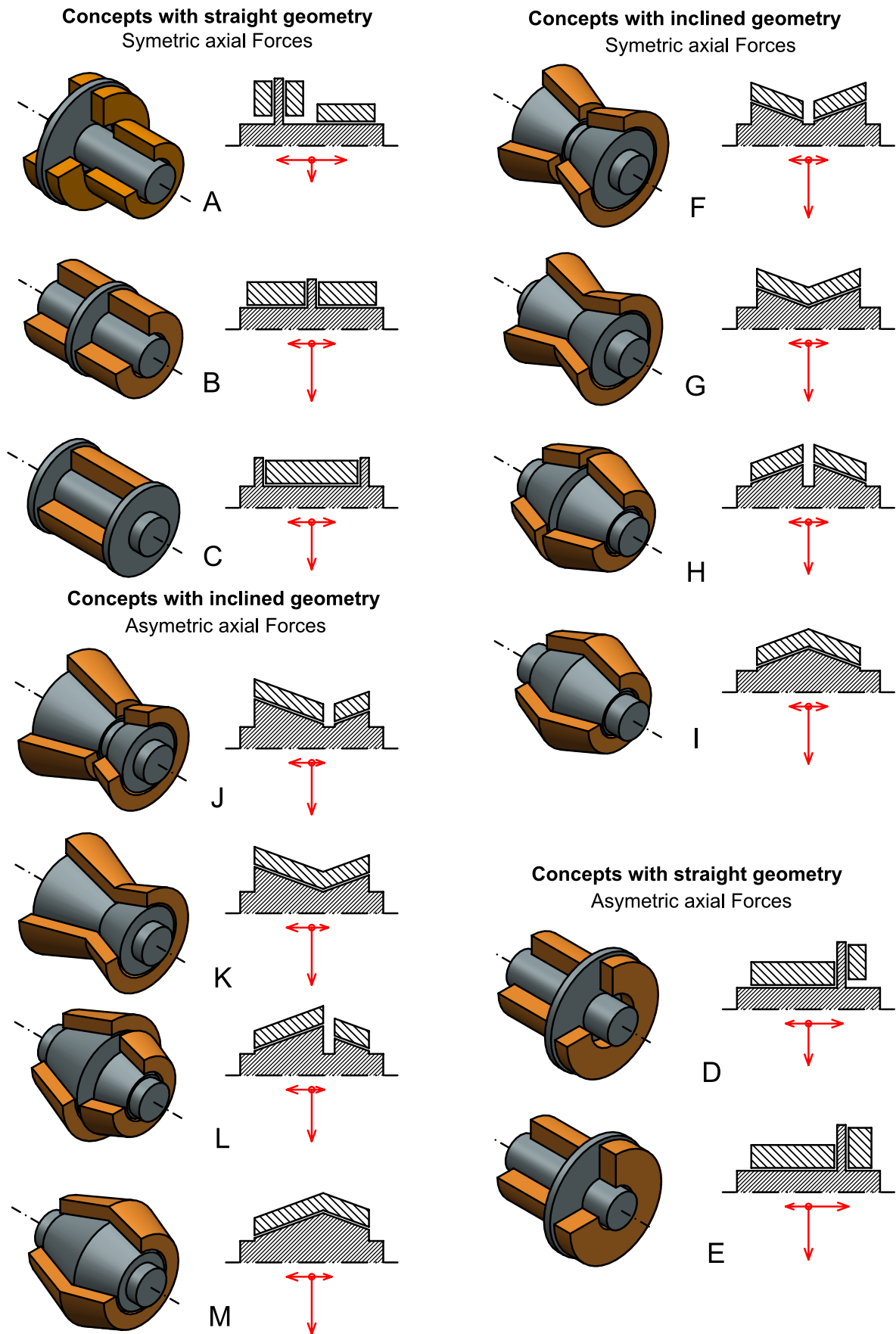


Fig. 4.14.: Various concepts developed for the combination of journal and thrust bearings for absorbing radial forces and axial forces in both directions within one bearing setup.

forces that can be absorbed corresponds to a qualitative estimation using this method. The resulting load-bearing capacities are shown on the drawing as red arrows. To improve the visualisation, the length of the radial forces was changed by a factor of 0.5 in relation to the described axial length of the lubricating film.

Criteria IV evaluates the concepts regarding their modal behaviour and therefore the occurring loads. It is assumed that increasing the mass of the axle and increasing the radial dimensions of the axle has an unfavourable effect on the modal behaviour and increasing the strain on the bearing. Therefore, concepts with a low axle volume and radial dimensions are assessed better than those with a high axle volume and a large cross-section.

- **Production**

Criteria V evaluates the geometric complexity and tolerances for the CMC-Components of the bearing setup. It is assumed that inclined geometry bearings are more difficult to produce within the small tolerances needed for the bearings gap heights. It is assumed that this will be even more difficult for joining two inclined CMC-Components which differ in the angle of inclination without a gap, therefore increasing production cost and effort. Concepts with more individual CMC-Parts with different geometric dimensions of the CMC-Component are evaluated less suitable because they are increasing the complexity and therefore also resulting in higher costs. It is assumed that increased complexity not only increases production costs and effort, but also generally makes successful implementation of the bearing more difficult. This is why it has a negative impact on the assessment.

Criteria VI assesses the potential assembly difficulties. Since it has already been investigated that misalignment of the shaft influences the performance of externally pressurised journal bearings and is usually caused by incorrect assembly [44], the feasibility of assembly is given particular attention with this criteria. The concepts are evaluated according to the number of parts in which the axes must be divisible and the number of CMC-components that must be installed separately in the bearing housing. The lower the sum of these parts, the higher the rating.

Criteria VII evaluates the complexity of the fluid flow. The number of input areas needed for pressurizing the CMC-Component is therefore added to the number of outlet areas needed for the lubrication fluids flow. The lower the sum of these areas, the higher the rating, reducing the complexity for flow guidance and sealing and the space required for these constructive measures.

Preference Analysis

The results of the preference analysis are shown in tab. 4.6. The procedure is carried out as explained in the methodology chapter (see 3.1). Particular emphasis is placed on the best possible absorption of radial loads, as the radial load-bearing capacity of the initial design was rather low compared to the axial load-bearing capacity. The complexity of the CMC-Component and the different production-concerning criteria were also highly prioritised in order to achieve the simplest and most robust design possible for a first application of the CMC fluid film bearing within a turbopump developed for use in rocket engines.

4 Results and Discussion

Criteria	Rank	Rank ⁻¹	Weight [%]	
k	S_k	S_k^{-1}	Count	C_k
I	6	2	0	7.14
II	3	5	1	17.9
III	1	7	14	25.0
IV	5	3	0	10.7
V	2	6	5	21.4
VI	7	1	0	3.57
VII	4	4	1	14.3
Σ	28	28	21	100

Tab. 4.6.: Results of the preference analysis.

Selection

The results of the selection process and the resulting ranking is shown in tab. 4.7. The procedure and calculation is carried out according to the description in 3.1. For the final ranking, the concepts are categorised into four groups for better comparability. They are divided into straight and inclined geometry and into those that can absorb symmetrical or asymmetrical axial forces. The individual groups can be seen in fig. 4.14.

Straight Geometry - Symetric									
Concept l	Weight	A		B		C			
Criteria k	C_k [%]	P_{kl}	p_{kl}	P_{kl}	p_{kl}	P_{kl}	p_{ij}		
I	7.14	5	0.357	2	0.143	2	0.143		
II	17.9	5	0.893	1	0.179	1	0.179		
III	25.0	1	0.250	5	1.250	4	1.000		
IV	10.7	5	0.536	5	0.536	4	0.429		
V	21.4	3	0.643	4	0.857	5	1.071		
VI	3.57	2	0.071	3	0.107	3	0.107		
VII	14.3	2	0.286	3	0.429	4	0.571		
Σ	100	23	3.036	23	3.500	23	3.500		
Rank		2		1		1			
Straight Geometry - Asymetric									
Concept l	Weight	D		E					
Criteria k	C_k [%]	P_{kl}	p_{kl}	P_{kl}	p_{kl}				
I	7.14	2	0.143	2	0.143				
II	17.9	4	0.714	5	0.893				
III	25.0	2	0.500	2	0.500				
IV	10.7	5	0.536	5	0.536				
V	21.4	3	0.643	3	0.643				
VI	3.57	3	0.107	3	0.107				
VII	14.3	3	0.420	3	0.429				
Σ	100	22	3.063	23	3.250				
Rank		2		1					
Inclined Geometry - Symetric									
Concept l	Weight	F		G		H		I	
Criteria k	C_k [%]	P_{kl}	p_{kl}	P_{kl}	p_{kl}	P_{kl}	p_{ij}	P_{ij}	p_{ij}
I	7.14	1	0.071	1	0.071	1	0.071	1	0.071
II	17.9	3	0.536	4	0.714	3	0.536	4	0.714
III	25.0	4	1.000	5	1.250	4	1.000	5	1.250
IV	10.7	3	0.321	4	0.429	3	0.321	4	0.429
V	21.4	2	0.429	1	0.214	2	0.429	1	0.214
VI	3.57	2	0.071	3	0.107	3	0.107	4	0.143
VII	14.3	3	0.429	4	0.571	3	0.429	4	0.571
Σ	100	18	2,857	22	3,357	19	2,893	23	3,393
Rank		4		2		3		1	
Inclined Geometry - Asymetric									
Concept l	Weight	J		K		L		M	
Criteria k	C_k [%]	P_{kl}	u_{kl}	P_{kl}	u_{kl}	P_{kl}	u_{kl}	P_{kl}	u_{kl}
I	7.14	1	0.071	1	0.071	1	0.071	1	0.071
II	17.9	3	0.536	4	0.714	3	0.536	4	0.714
III	25.0	4	1.000	5	1.250	4	1.000	5	1.250
IV	10.7	3	0.321	4	0.429	3	0.321	4	0.429
V	21.4	1	0.214	1	0.214	1	0.214	1	0.214
VI	3.57	2	0.071	3	0.107	3	0.107	4	0.143
VII	14.3	3	0.429	4	0.571	3	0.429	4	0.571
Σ	100	17	2.643	22	3.357	18	2.679	23	3.393
Rank		4		3		2		1	

Tab. 4.7.: Selection results of the selection procedure with the total utility values K_l highlighted in red.

4.2.3. Detailed development of the selected concepts

Based on the selection procedure, concept C and I are selected for further investigation and design, due to reaching the highest scores for symmetric and asymmetric designs with straight geometries. Concept B, with a score of 3.5 being as high as the score of concept C is not considered further, because C seems to be more feasible, due to just one CMC-Part needed for realisation. At this point, it is decided that no more concepts with inclined geometry should be pursued for reasons of simplicity, superior experimental experience and manufacturability of CMC fluid film bearings with straight geometry. In addition to that, concept A was further developed due to considerations of easy feasibility.

For each concept, a CAD-Model of a possible construction approach for integration into the turbopump is designed. The goal is to realise a bearing with a great load-bearing capacity within the available space, while being able to accommodate the fluid guidance for the supply of the bearing and to provide installation space for a sealing.

For each design option, the special features of the construction and the presumed advantages and disadvantages are briefly explained in the following.

Cross section drawings of the designs C, I and A are shown in fig. 4.16, 4.17 and 4.18.

A summary of the numerical calculation of the load-bearing capacities of the different designs, executed with the parameters and methods described in the methodology chapter (see. 3.2, is shown in 4.15 and explained below.

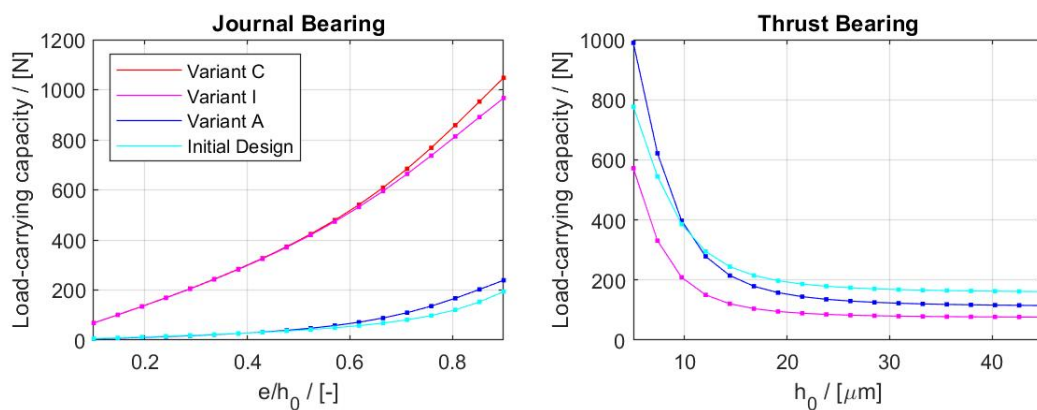


Fig. 4.15.: Comparison of the Load bearing capacities of the bearing designs.

Concept C

Design C consists of only one CMC-Component for the bearing in the form of a journal bearing sleeve with an end piece made of a non-porous CMC-Material on both sides. The idea is that the fluid outflow of the bearing is used as a component which absorbs forces perpendicular to the intended direction. Therefore the sleeve provides radial support and axial support through a lubricant film forming on the shaft shoulders (see fig. 4.16).

The advantages of this are a maximized fluid film surface and correspondingly a high load-bearing capacity for radial forces. In addition, an internal lubricant guide with fluid feed from behind the impeller and backflow through a hollow shaft can be realised. Because of the simplicity of the CMC-Part this can be achieved due to more available construction space while maintaining sufficient component thickness and simplicity of the required components.

The main disadvantage is that the axial load capacity can not be predicted with the used numerical methods.

The load-bearing capacity of the variant C journal bearing is numerically calculated and shown

in 4.15. It is calculated without consideration of possible interaction of the journal bearings fluid mechanical behaviour with the fluid film of the intended thrust bearing, due to the simulation tools available. The load bearing capacity of the thrust bearing is neither calculated nor shown in fig. 4.15, because of this reason. In addition, it could occur that in the event of strong thermal changes during operation with cryogenic media, the shrinkage of the shaft is so high in comparison to that of the CMC-Sleeve due to their different coefficient of thermal expansion that the lubrication gaps between the two shaft shoulders could close. This could become a problem for this design in particular, due to its large axial dimensions.

Another disadvantage is that due to the one-piece design, the running stability during operation and the reaction to misalignment and momentums acting on the bearing cannot be predicted, as it differs greatly from any conventional bearing step up. These points must be taken into account

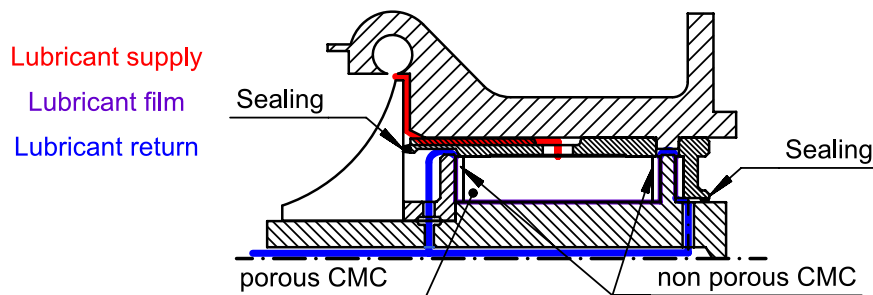


Fig. 4.16.: Integration of concept C into the design.

in any further development. Even if the application is still a long way from realisation, this design could be worth the increased development effort due to its constructive simplicity in which only one CMC-Component has to be used.

Concept I

Design I consists of two CMC-Bearings, a journal and a thrust bearing, both with a non-porous ceramic end piece on both sides. In the same way as with design C, the fluid outflow from the bearing is used to achieve an additional axial support on the journal bearing and an additional radial support on the thrust bearing. This should increase the radial load carrying capacity and also improve the absorption of momentum, due to radial support over greater axial distances. In the axial direction, the forces acting mainly in the direction of the turbopump inflow are absorbed by a conventional CMC thrust bearing. In the opposite direction the forces are absorbed solely by the outflow of the radial bearing. The advantage of this design is that the load-bearing capacity of the radial bearing as well as that of the axial bearing in the main load direction can be calculated using the numerical tools available. Only the influence of the bearing outflow fluid film on the pressure distribution within the bearing can not be taken into account. The calculated load bearing capacities are shown in fig. 4.15. The main disadvantage of this design is that the complexity of the fluid guidance increases due to the two-bearing design. In order to enable internal fluid guidance, complex and filigree mounts and sockets must be manufactured for mounting the bearing sleeves and the fluid supply, if the fluid flow is to be managed internally, as implemented in design I (see fig. 4.17). Another disadvantage is that, due to the asymmetrical bearing design, the running stability during operation and the reaction to misalignment cannot be predicted. This design thus represents a compromise between the simplicity of the CMC-Components as implemented in design variant C and a complete separation of the bearings as

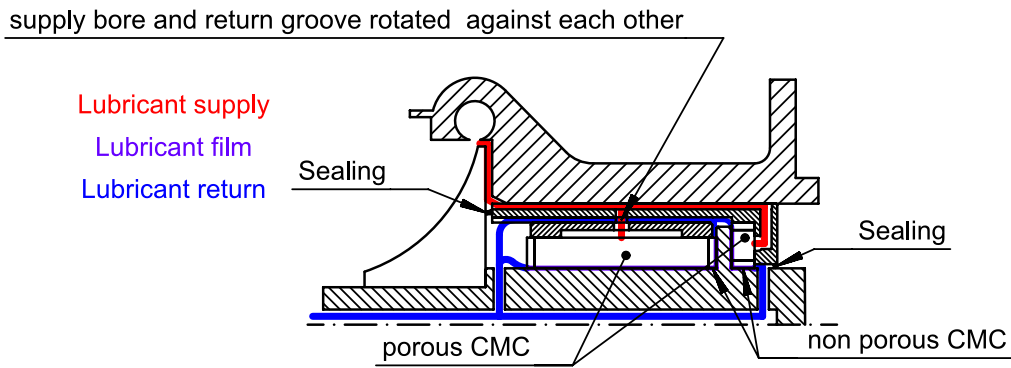


Fig. 4.17.: Integration of concept I into the design.

implemented in design A. This variant is not considered further, primarily due to the lack of predictability of the fluid mechanical behaviour and increased complexity compared to concept C.

Concept A

Design A consists of a bearing layout for the CMC-Bearing based on conventional bearing layouts. Two equally sized central thrust bearings support axial forces in both directions on the shaft shoulder. The two equally sized external radial bearings support radial forces. This design has been configured in such a way that realisation is as simple as possible. For this reason, no internal fluid guidance components was used. The lubricating fluid is supplied and discharged via pressure holes through the housing with pressure connections. This design offers significant advantages:

- The journal and thrust bearings load-bearing capacities can be calculated independently of each other.
- The external lubrication supply simplifies testing and performance measurement. The designed bearings could be tested with both RP-1 and LOX at operating conditions.
- Particle emission tests can be carried out easily, because of the external supply and discharge of the lubrication fluid through the housing. The external fluid supply enables a filtering of the fluid if the tests show a limit-exceeding particle pollution inside the bearing without changing the inner design of the bearing. Another easy possibility to implement in this design is not to feed the lubrication fluid back into the pump inlet.
- Due to the widely spaced radial bearings, occurring momentum can be absorbed well. In combination with the symmetrical design, this contributes to the presumably stable running behaviour of the shaft.
- Due to the short CMC-Sleeves of the journal bearings and the design with one shaft shoulder, changes in the size of the metal parts due to temperature changes can presumably be better accommodated during cryogenic operation.

The following disadvantages are accepted in return:

- For all bearings in this design, the outflow of the lubricating fluid is on one sided due to space constraints. The influence of this on the load carrying capacity and pressure distribution cannot be taken into account in the numerical calculation.
- The potential load carrying capacity, especially radial load carrying capacity, is low compared to the other designs (see 4.15), as no potential advantages from the combination of

axial and radial bearings can be utilised, resulting in smaller bearings. It must be noted that the calculation of the load carrying capacity of the radial bearing in fig. 4.15 refers to the simulation of one of the two bearings; when comparing the bearings, twice the load carrying capacity must be assumed consequently.

- The size of the CMC bearing sleeves is comparatively small, which makes production more difficult.

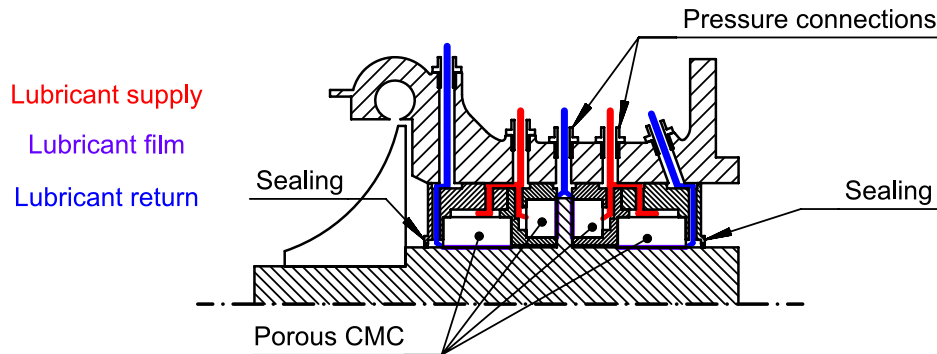


Fig. 4.18.: Integration of Design Concept A

Due to the advantages of design variant C, it will be further developed for testing. The design intends for the bearing sleeves to be press-fitted into the housing. Additional sealing between the fluid-conducting grooves was implemented using O-rings in accordance with the DIN ISO 3601-1 [45] standard. Technical drawings of the central bearing elements can be found in annex B.

The technical drawings are intended to provide an impression of the design and are not all complete in terms of dimensions, surface specifications and tolerances. The tolerances and surface specifications of the CMC-Parts are completely given as target specifications. Tolerances and measurements relating to installation in a LCRA turbopump casing or in a casing for a test setup are given, as are the dimensions required for drilling fluid supply holes and fluid flow holes into the casing. Additional drawings with complete tolerancing required for production of the journal and thrust bearings sleeves are held by the DLR. The information required for integration of the design into the LCRA turbopump or a test setup is completely given.

4.3. Preliminary evaluation of potential particle emission risks

In this chapter, the results of the particle experiments are presented and discussed. The procedure was carried out as explained in the methodology chapter (see 3.3). The potential risks of particle emissions from the CMC-Bearings components into the rocket engine propulsion system is evaluated and an outlook on potential further development steps is given.

4.3.1. Experiment Results

The results of the filtration process are presented first, followed by those of the gravimetric and microscopic methods.

In an initial series of tests, filtering was carried out every 30 seconds until a total time of four minutes was reached. Subsequently, in a second series of tests, the samples were cleaned, doubling the time (4 min, 8 min, 16 min, ...) until a total cleaning time of 256 minutes was reached.

4 Results and Discussion

During filtering, the particles were found to be evenly distributed on the filter paper. In addition, the filtration times did not differ greatly from one another. For this reason, the filtration times for the tests with ultrasonic cleaning times are not documented for the second test series. The filtration times documented for the first test series are shown in tab. 4.8. The weights of the

Extraction time [s]	30	60	90	120	150	180	210	240
Sample 1	4:45	5:04	4:31	4:35	4:39	5:03	4:32	4:36
Sample 2	4:13	4:05	5:01	4:06	4:31	4:25	4:35	4:15
Sample 3	4:03	4:05	4:09	4:31	4:20	4:01	4:32	4:09

Tab. 4.8.: Filtration times in [min].

three material samples before and after testing are shown in tab. 4.9.

For longer ultrasonic times, it is observed that the surface of the samples is attacked. Parts of

Sample	Pre Test Weight [g]	Post Test Weight [g]	Weight difference [mg]	m_d [%]
1	31.5703	31.5338	-36.5	-0.116
2	31.4023	31.3903	-12.0	-0.038
3	31.7108	31.5785	-132.3	-0.417

Tab. 4.9.: Material sample weights before and after ultrasonic cleaning tests.

the matrix between the tissue layers appear to detach. This is true for all samples.

Gravimetric experiment results

The resulting measurements of the particle filtration and analysis of the filters using the gravimetric method are shown in tab. 4.10.

Extraction time [s]		30	60	90	120	150	180	210	240
Sample 1	Pre-Test	69.8	70.3	70.2	69.6	69.4	69.7	69.8	70.4
	Post-Test	78.9	73.9	72.2	71.4	70.4	70.3	70.5	70.2
Sample 2	Pre-Test	68.9	69.5	69.7	69.4	69.8	69.7	69.4	69.2
	Post-Test	73.0	71.5	70.5	70.3	70.0	69.9	69.5	69.3
Sample 3	Pre-Test	69.9	69.5	69.4	69.5	69.0	69.8	69.1	67.5
	Post-Test	99.0	86.5	79.5	75.8	72.9	73.0	709.8	69.5

Tab. 4.10.: Measured filter weights in [10^{-6} kg] before and after filtration.

The values from tab. 4.10 are analysed in fig. 4.19. Therefore the weight of the filter pre-test is subtracted from the weight of the filter post-test and the extracted particle mass at this point in time is added up. This produces the values shown in fig. 4.19, which can be approximated by an exponential saturation function of the form

$$m_{\text{particles extracted}} = a \cdot (1 - e^{-bt}). \quad (4.4)$$

The parameters a and b are approximated to equation 4.4 using the Matlab R2020a software and the `nlinfit()` function. The results are shown in tab. 4.11.

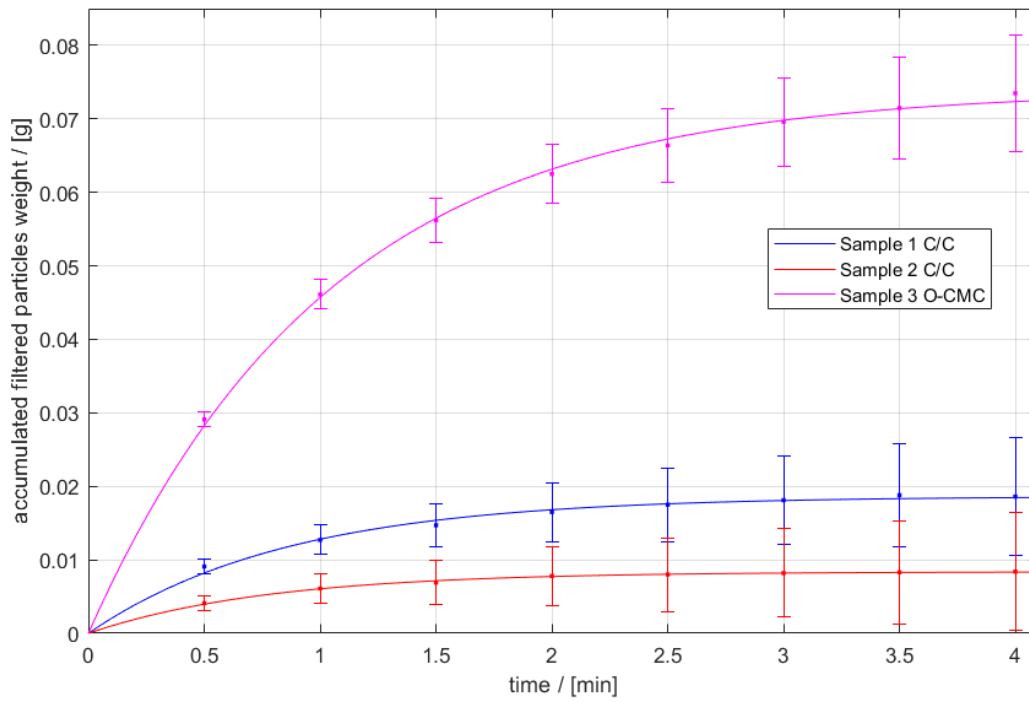


Fig. 4.19.: Results of particle mass quantity measurements using the gravimetric method.

Sample	a [mg]	b [1/s]	Sample weight difference $ m_d $ [mg]	Deviation of a from m_d [%]
1	18.647	1.1598	36.5	-48.9
2	08.374	1.2849	12.0	-30.4
3	73.926	0.9629	132.3	-44.1

Tab. 4.11.: Parameters a and b for the fitted function and comparison of factor a with actual weight difference m_d of the material samples.

Microscopic analysis results

Fig. 4.20 shows the digital microscope image of a typically observable particle population on the filter after filtering a C/C-Sample. Particles can be found on the filter in all size ranges relevant for qualification according to ECSS-E-ST-35-06.

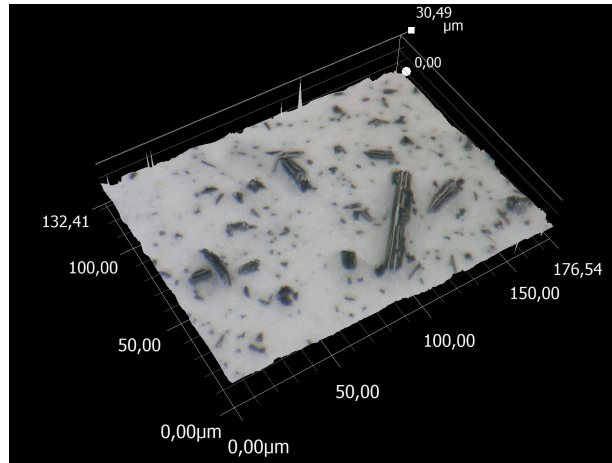


Fig. 4.20.: Digital microscopic image with three-dimensional image capture, Filter residues from Sample 1, Ultrasonic cleaning time of 64 min (total of 128 min).

The microscopic analysis provides a particle quantity distribution displayed in a histogram shown in fig. 4.21.

In 4.21 the particle population, which was determined with an image analysis method, is displayed. The particles are grouped according to the maximum determined diameter into bins corresponding to a $4 \mu\text{m}$ range and in bins according to ECSS-E-ST-35-06 Class I, subclass G. Class I, subclass G refers to the propellant or reference liquid that is to be used in the operation of the pump.

The actual number of particles exceeded the limit values specified in ECSS-E-ST-35-06 class I, subclass G by a factor of several hundreds. In order to be able to qualitatively compare the particle size ranges in which the limits are exceeded the most, the respective limits were scaled. For scaling, the number of particles for the first size range ($6 \mu\text{m}$ to $10 \mu\text{m}$) was divided by the limit value specified by the standard. The resulting factor was used to scale all other limit values. The scaled limits are shown in histogram 4.21.

The distribution is analysed analogously to fig. 4.21 for both C/C-Samples (sample 1, sample 2), each after an ultrasonic cleaning time of 30s (240s in total) and 64 min (128 min in total). The additional diagrams can be found in annex D.

It is not possible to analyse the oxidic CMC-Sample using the image analysis software with the used procedure, as the contrast of the white particles on the white filter is not strong enough. From the subjective impression of the observer, a particle population similar to that of the C/C samples is expected.

4.3.2. Conclusions

The qualitative comparison of the results leads to the following conclusions

- After ultrasonic cleaning, the test liquids contain particle concentrations that exceed the permissible limit values by a multiple in all size ranges.

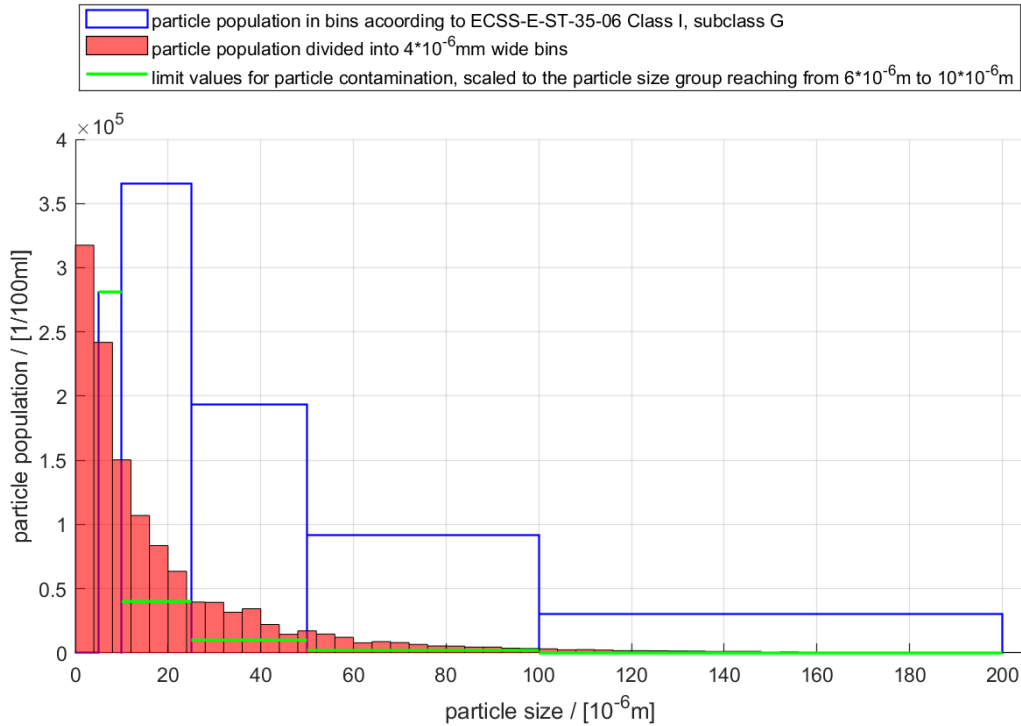


Fig. 4.21.: Particle distribution of the cleaning fluid of sample 1, ultrasonic cleaning time 30 s (total of 240 s).

- The larger the size of the particles in the group under consideration, the higher the factor by which the values are exceeded. This means that larger sized particles (e.g. 51 - 100 μm) could pose a more significant problem than smaller sized particles (e.g. 6 - 10 μm), when trying to comply with particle pollution standards in an actual application.
- Particles in the size range between 101 and 200 μm occur, but should not be present in the propellant or reference liquid according to the ECSS-E-ST-35-06 standard.
- Longer ultrasonic cleaning times do not lead to a reduction in particle contamination, but instead leads to damage of the material. The damage could be observed on the surface of the sample. The initially smooth material increasingly showed particle breakouts on the surface after long cleaning times. It was not possible to determine whether this damage also occurs inside the sample using this method.
- Although the particle concentrations measured in the test exceed the permitted concentrations by a multiple, it is not possible to predict if the limits during application will be exceeded based only on these results. The reason for this is the fundamental difference between the application and the test. During testing the particles are accumulated in the reference liquid over a long period of time, whereas in the actual application the liquid flows through the bearing continuously. Furthermore, it cannot be predicted whether the mere flow of liquid will release the particles from the material to a greater or lesser extent than the ultrasonic bath.
- It is necessary to determine how many particles are flushed out into the lubrication fluid under potential operating conditions.

4.3.3. Discussion and Outlook

This chapter discusses the uncertainties of the results, as well as the advantages and disadvantages of the methods used and makes suggestions for improving the execution of the experiments.

For the gravimetric analysis, the uncertainty can be estimated using the uncertainty of the scale. The scale has an uncertainty of ± 0.5 mg. For added and subtracted values, the accuracies are added up for each case, resulting in a error range, presented as error bars. Both is shown in fig. 4.19.

For the microscopic analysis, no precise statement can be made about the uncertainty due to the unknown error of the automatic counting method using digital image processing. It has been noticed that particles which are close to each other are sometimes counted as one particle of larger diameter. As a result, the accuracy decreases if the particle density on the surface of the filter is too high. In some cases small particles ($5 \mu\text{m}$) are not recognised. However, the resulting error is not substantial, as particles smaller than $5 \mu\text{m}$ do not have to be taken into account for regulatory purposes.

The filtration setup proved to be appropriate for the investigations. The filtration works without leakage and is reproducible with an observed uniform distribution of particles on the filter. The even distribution of the particles is also reflected in the fact that the counted particles of the same filter in different fields do not deviate greatly from each other.

To further improve the results, ultrasonic cleaning and filtration could be carried out under cleanroom conditions to avoid possible contamination. Another possibility would be to use an ultrasonic device whose frequency can be varied in order to find a method in which the material is not damaged even during prolonged exposure. To enable the observation of oxidic CMC-Particles under the microscope, the filters can be replaced with darker ones to create an observable contrast or to colour the particles with a contrast agent.

The gravimetric method has proven to be useful for determining the total quantity of rinsed-out particles. However, it is not suitable for the particle quantities expected in applications compiling with regulations, as the differences in mass of the filters would be too small. The method could be further improved by using a finer scale. However, it is doubtful that the information gained from this will provide any added value.

The microscopic method proved to be well suited for determining the particle quantity in all particle size groups categorised according to ECSS-E-ST-35-06. If the particle quantity in the test fluid exceeds the limit values by a multiple, manual counting is not possible. Manual counting provides more accurate results, which is why an attempt should be made to reduce the amount of particles in the samples in further tests. The automatic counting method has advantages in terms of possible automation and standardisation of testing and approval procedures. It is therefore recommended that the method be retained for further qualification of the material for the application.

Outlook

The results of these experiments have led to the following summarized conclusions concerning the potential risk factor of particle contamination in fluid film CMC-Bearings:

- The material contains particles of sizes which are critical for operation.
- A testing procedure must be developed to ensure that only a amount of particles within the limits given by the ECSS-E-ST-35-06 standard are emitted through the bearing during operation.

For this reason, further testing is proposed to ensure that a testing process can be developed to qualify the CMC-Bearings for space applications. Two tests are proposed for this purpose:

1. Perform a flush test of the bearing component under or similar to the operating conditions. This test can be done with the Method IV “Liquid flow test under operating conditions” according to ECSS-E-ST-35-06 11.1.5 0200339 [28]. Since the combination of LOX with the C/C-Components in particular creates potential hazards due to the possible reaction between the carbon and oxygen, it is suggested that these tests be carried out with other gases. Table 4.12 shows various possible gases in conditions of interest for the application. The material data for Liquid Nitrogen (LN2), Gaseous Nitrogen (GN2) and LOX were acquired via the database of the National Institute of Standards and Technology (NIST) Chemistry WebBook [46]. The temperatures selected were those at which the gas is cryogenic at atmospheric pressure. The material data for pressure and dynamic viscosity of dry air originates from linear interpolation from the tables of the Association of German Engineers (Verein deutscher Ingenieure) (VDI)-Wärmeatlas [47].

Medium	Temperature [K]	Pressure [10 ⁵ Pa]	dyn. Viscosity μ [10 ⁻⁶ Pa · s]	Density ρ [kg/m ³]
Air	293.15*	4.0	18.26	4.77
		40.0	18.83	48.11
GN2	293.15*	4.0	18.23	46.24
		40.0	30.84	368.11
LN2	77.0	4.0	173.24	817.22
		40.0	260.85	878.99
LOX	90.19	4.0	196.24	1142.8
		40.0	271.88	1149.6

Tab. 4.12.: Fluid properties at different potential operation points for future liquid flush tests.

It is assumed that viscosity in particular is the decisive fluid property for the release of particles from the material, as it has a major influence on the flow behaviour within the material. Therefore it is proposed that initial tests could be performed with GN2 due to feasibility and further testing with LN2, which potentially gives comparable results to a test with LOX, but with considerably less effort.

2. Perform a filtering test of the fluid flowing out of the bearing of the running test set-up under load to ensure that no particle emissions are caused due to wear and friction or cavitation under running conditions.

Based on the results of the first test, it is proposed to develop a process to remove the particles in the material using a cleaning process consisting of ultrasonic cleaning and or flushing with fluid. Ultrasonic cleaning can only be used to a limited extent due to the partial destruction of the material after prolonged exposure. This should help to limit the amount of particles present in the structure of the material due to the manufacturing, also limiting the particle released during operation.

Based on the results of the second test, the design and operating parameters may be adjusted to prevent the degradation of the CMC-Components, resulting in additional particle pollution, during operation.

If no possibility can be found to meet the regulatory levels through these measures, other options may be considered:

*Corresponds to a room temperature of 20°C

- Attaching the particles within the material by flushing with a fixative liquid.
- Cleaning the lubricant before recirculation, for example by filtering.
- Not recirculating the fluid into the fuel or oxygen cycle.

5. Summary

In order to advance the development and demonstration of the functionality and superior properties of CMC fluid film bearings for use in rocket turbopumps, various aspects are examined in the present work for the adaptation of the bearings to the test propellant turbopump of the Canadian space research initiative LCRA.

5.1. Design and Construction of the Bearing Components

In order to enable the design and layout, as well as the adaptation of the bearings to the turbopump, the operating parameters were first summarised. The turbopumps developed by Launch Canada are electrically driven turbopumps for a fuel similar to RP-1 and for LOX. The pumps run at a nominal 40000 rounds per minutes with an estimated power of 9 kW and 12 kW respectively. The original design of both pumps utilises a setup of two conventional groove ball bearings (fixed and floating) for axial and radial load support. These are to be replaced by the CMC fluid film bearing.

The axial loads relevant for the design were provided by the LCRA. The radial loads were determined using the estimated shaft weight and an assumed imbalance of the shaft. A CAD working model of the conventional bearing setup was created using reference dimensions of the turbopump design. The resulting concepts were constructed within the limits defined by the geometry of the model created.

The design of the bearings was realised using a software tool developed in a dissertation on the subject of aerostatic journal bearings. The basics of the calculations were researched and are explained in more detail in the theoretical section. The numerical calculation method calculates the REHL for the application of journal and thrust bearings and, from the resulting pressure distribution in the lubrication gap of the bearings, the radial and axial loads that can be absorbed.

In order to investigate the influence of various design parameters on the load-bearing capacity of the bearings, the operating parameters for a simple bearing that can be realised in the available installation space were determined and estimated in the best possible way. A series of numerical calculations were carried out to determine the influence of various parameters on the load-bearing capacity of the bearings.

These calculations show that the lubricant film width for thrust and journal bearings has the greatest influence on the load-bearing capacity. In addition, an increase in the supply pressure significantly increases the load-bearing capacity, especially but not exclusively for thrust bearings. An increase in the permeability of the material also has a positive effect on the load-bearing capacity. Reducing the thickness of the CMC-Components only leads to a small increase in load-bearing capacity. For the journal bearing, an increase in the viscosity of the lubricant and a reduction in the gap height of the bearing also leads to an increased load-bearing capacity.

With the help of the knowledge gained, thirteen different concepts A - M were created, which represent different configurations to absorb radial and axial loads. Different strategies for combined load support are the potential combination of radial and axial load absorption by combining

load-bearing lubricating films on individual ceramic components or inclined geometries of CMC-Components.

The concepts promise various advantages and disadvantages in terms of manufacturability, ease of assembly, complexity and load-bearing capacity while maintaining similar dimensions.

These advantages were systematically evaluated using a weighted selection process and three concepts (C, I, A) were selected for more detailed consideration.

Even though inclined geometries offer potential advantages, their development was not pursued further due to their higher complexity. However, many of the concepts could be interesting for further consideration and other applications.

The load-bearing capacities of the three design proposals were calculated, as far as possible, with the aid of numerical calculations and the various advantages of the designs were weighed against each other. Design C and A in particular stand out. Design C is characterised by the use of a single porous CMC-Component absorbing both radial and axial loads. The long lubrication gap in the radial bearing results in potentially good load absorption in radial direction. If the design is used, the axial load capacity must be determined, which cannot be calculated with the available numerical tools. It must also be analysed whether the thermal expansion of the components during cryogenic operation could potentially lead to jamming of the bearing. Concept A is a more conservative approach that combines four separate CMC-Components in separate bearings to support axial and radial loads. The loads that can be absorbed were determined numerically and are close to the required design loads. For these reasons, the design was selected to develop a prototype together with the partner Launch Canada Rocketry Association and the startup Black Engine Aerospace in co-operation with DLR to determine the load capacity and running characteristics of the bearing. Technical drawings of the design were created. Drawings that give an impression of the design can be found in Appendix B. The prototype can then be integrated into LCRA's turbopump. It can also be used to carry out further investigations to determine the actual particle pollution caused by the CMC fluid film bearing during operation.

5.2. Evaluation of the Risk due to Particle Pollution

Particles within components of fluid-carrying systems represent a risk for every spacecraft. In order to be able to assess the potential hazards caused by the particle pollution from the CMC-Bearing, the existing standards and specifications for particle contamination in spacecrafts and the various options for measuring particles were first researched in a literature review. The results are presented in the theory and fundamentals chapter.

Based on this research, an experiment was planned and carried out with the aim of determining the occurrence and size distribution of particles in the CMC-Material. For this purpose, material samples were repeatedly cleaned in an ultrasonic water bath. The particles emitted into the water were filtered out with a developed filter device and analysed. The selected method is a combination of gravimetric and microscopic analyses, in which the quantity of particles is determined by weighing and the size distribution is determined by observation and counting of particles under a microscope. The procedures were each carried out considering ISO standards for aerospace regarding hydraulic systems and analysed according to the ECSS-Specifications for particle limits in propellants of liquid rocket engines.

The analyses show that a large number of particles in all critical size ranges can be easily extracted from the material. The presence of larger particles in particular poses a potential risk to the operation of the bearing. For this reason, the possibilities for further investigation and methods for material improvement are discussed in detail. Proposals for further tests and potential measures to reduce particle emissions were presented. These include a test in which the release of particles

from the material is investigated in a flow-through sample under operating conditions and a test of a prototype using the devolved design variant A.

With the help of these tests, it should then be possible to develop a design which fulfils the specifications for particle pollution to enable safe operation of the bearing. This should enable the full exploitation of the bearings potential advantages in terms of load-bearing capacity and service life.

Finally it can be concluded, that further material treatment and investigation is essential in order to prevent critical particle emissions.

Bibliography

- [1] Teske, B.: “Preparing Commercial Space Companies for Safety Management System Implementation (Secondary Research Topic: Determining Whether High Reliability Theory Attributes Exist in an Airline Safety Management System Environment)”. PhD thesis. University of North Dakota, 2020.
- [2] Ortelt, M.: *Black Engine CMC Space Propulsion Technology*. 2019. URL: https://elib.dlr.de/132612/1/2019_09_24_DLR_Ortelt_htcmc10_presentation.pdf.
- [3] Ortelt, M. Hald.H; Greuel, D.: *Experimentelle thermophysikalische Betrachtung poröser Innenliner aus Faserkeramik in effusiv gekühlten Raketenbrennkammern*. 2007.
- [4] Gardiner, G.: *Multi-composite thrust chamber aims to boost rockets, reduce cost for New Space economy*. URL: <https://www.compositesworld.com/articles/multi-composite-thrust-chamber-aims-to-boost-rockets-reduce-cost-for-new-space-economy>.
- [5] ESA Publications Division, ed.: *Tribology in Liquid Oxygen of SIC/SIC Ceramic Matrix Composites in Connection with the Design of Hydrostatic Bearing: Proceedings of the 9th European Space Mechanisms and Tribology Symposium*. 2001. ISBN: 92-9092-761-5.
- [6] Wagner, B.: “Untersuchungen zu Sekundärsystemen in Turbopumpen für Flüssigkeitsraketenantriebe”. In: (2016).
- [7] Xu, J. et al.: “An Overview of Bearing Candidates for the Next Generation of Reusable Liquid Rocket Turbopumps”. In: *Chinese Journal of Mechanical Engineering* 33.1 (2020). ISSN: 1000-9345. DOI: 10.1186/s10033-020-00442-6.
- [8] Seiler, H. Ortelt, M.; Böhle, M.: “Development of a hydrostatic journal bearing with micro porous CMC material”. In: *Liquid propulsion ; Volume 2 of 2* (2019). URL: <https://elib.dlr.de/130052/>.
- [9] Launch Canada: *Rocket Turbopump Project*. URL: <http://www.launchcanada.org/rocket-turbopump-project>.
- [10] Schimpf, A.: *Aerostatic Journal Bearing based on an Orthotropic Layered Porous Structure*. Kaiserslautern-Landau: Rheinland-Pfälzische Technische Universität Kaiserslautern-Landau, 2023. DOI: 72421.
- [11] Matek, W. Muhs, D.; Roloff, H.: *Maschinenelemente*. 18. Aufl. Viewegs Fachbücher der Technik. Braunschweig: Vieweg, 2007. ISBN: 9783834802620.
- [12] Akademischer Verein Hütte Czichos, H.; Hennecke, M.: *HÜTTE - Das Ingenieurwissen*. 34. Aufl. 2012. aktualisierte. Berlin, Heidelberg: Springer Berlin Heidelberg and Imprint: Springer, 2012. ISBN: 978-3-642-22849-0.
- [13] Ortelt, M.: *Aufgabenstellung Bachelorarbeit: Anwendungskonforme Anpassung innovativer faserkeramischer Fluidlager an eine Forschungstreibstoffförderpumpe für kryogene Raumfahrtantriebe: Aufgabenstellung Bachelorarbeit*. Stuttgart, 2023.
- [14] Cieslicki, K., ed.: *Investigations of the effect of inertia on flow of air through porous bearing sleeves*. 1993. DOI: 10.1016/0043-1648(94)90301-8.

- [15] Durazo-Cardenas, I. S. Corbett, J.; Stephenson, D. J.: “The performance of a porous ceramic hydrostatic journal bearing”. In: *Proceedings of the Institution of Mechanical Engineers, Part J: Journal of Engineering Tribology* 224.1 (2010), pp. 81–89. ISSN: 1350-6501. DOI: 10.1243/13506501JET570.
- [16] Belforte, G. et al.: “Permeability and Inertial Coefficients of Porous Media for Air Bearing Feeding Systems”. In: *Journal of Tribology* 129 (2007), pp. 705–711. ISSN: 0742-4787. DOI: 10.1115/1.2768068. URL: https://asmedigitalcollection.asme.org/tribology/article/129/4/705/468579?casa_token=sYfyom7QhfkAAAAA:Y49f9XGcdTPCAihMjj9B6uSeGI4-vF45x_cnX5HbYEGESAWEot4od7d6VzHYMoog59x6XCEc.
- [17] Schimpf, A. et al.: “Experimental Investigation of Aerostatic Journal Bearings Made of Carbon Fiber-Reinforced Carbon Composites”. In: *Journal of Tribology* 144.4 (2022). ISSN: 0742-4787. DOI: 10.1115/1.4052747.
- [18] Böhle, M. Gu., Y.; Schimpf, A.: “Two flow models for designing hydrostatic bearings with porous material”. In: *AJKFLUIDS Engineering Division Summer Meeting*.
- [19] Schimpf, A. Gu, Y.; Böhle, M.: “Analysis of Flow Models for Aerostatic Thrust Bearings with Porous Material”. In: *Journal of Physics: Conference Series* 1909.1 (2021), p. 012039. ISSN: 1742-6588. DOI: 10.1088/1742-6596/1909/1/012039.
- [20] Hamrock, B. J.: *Fundamentals of Fluid film Lubrication: NASA Reference Publication 1255*. Columbus, Ohio: National Aeronautics and Space Administration, Office of Management, Scientific and Technical Information Program, 1991.
- [21] Singh, M. et al., eds.: *Oetra - Optimized Ceramic for Hypersonic Application with Transpiration Cooling: Advances in High Temperature Ceramic Matrix Composites and Materials for Sustainable Development; Ceramic Transactions*. Vol. CCLXIII. 2017. ISBN: 978-1-119-40728-7. DOI: 10.1002/9781119407270.ch37.
- [22] Mainzer, B.: *Manufacturing and Design of nonoxide Ceramic Matrix Composites for Gas Turbine Applications*. Ed. by University of Cambridge, Department of Materials Science & Metallurgy. URL: <https://www.ccg.msm.cam.ac.uk/system/files/documents/poster-no-3-by-d-koch.pdf>.
- [23] Chawla, K. K.: *Composite Materials: Science and Engineering*. 4th ed. 2019. Springer eBook Collection. Cham: Springer International Publishing and Imprint Springer, 2019. ISBN: 9783030289836. DOI: 10.1007/978-3-030-28983-6.
- [24] M. Leuchs, A. M.: *Ceramic Matrix Composite Material in Highly Loaded Journal Bearings: Proceedings of ASME TURBO EXPO*. Amsterdam, The Netherlands, 2002.
- [25] Heidenreich, B.; Göring, J.: *Die CMC-Werkstoffe des DLR und ihre Einsatzmöglichkeiten*. 2008. URL: https://dlr.de/Portaldata/35/Resources/dokumente/Die_CMC-Werkstoffe_des_DLR_und_ihre_Einsatzmoeglichkeiten.pdf.
- [26] Kitsche, W.: “Pollution Control on a test facility for a cryogenic rocket engine”. In: *3rd European conference for Aerospace Sciences* (2009).
- [27] International Organization for Standardization: *ISO 5884: Aerospace series — Fluid systems and components — Methods for system sampling and measuring the solid particle contamination in hydraulic fluids*. Vernier, Geneva, Switzerland, 2018.
- [28] European Cooperation for Space Standardization: *Space engineering: Cleanliness requirements for spacecraft propulsion hardware*. Noodwijk, The Netherlands, 2020. URL: <https://ecss.nl/standard/ecss-e-st-35-06c-rev-2-cleanliness-requirements-for-spacecraft-propulsion-hardware-7-april-2020/>.

-
- [29] Kitsche, W.: *Operation of a cryogenic rocket engine: An outline with Down-to-Earth and Up-to-Space remarks ; with 19 tables*. Berlin: Springer, 2011. ISBN: 9783642105647.
- [30] Sommerfeld, M. René Oliemans; Berend van Wachem: *ERCOfTAC best practice guidelines for computational fluid dynamics of dispersed multi-phase flows*. Brussels [S.D.]: ERCOfTAC, 2008. ISBN: 978-91-633-3564-8.
- [31] Sommerfeld, M.: “L3.1 Bewegung fester Partikel in Gasen und Flüssigkeiten”. In: *VDI-Wärmeatlas*. Ed. by Stephan, P. et al. Springer Reference Technik. Berlin, Heidelberg: Springer Berlin Heidelberg, 2019, pp. 1543–1559. ISBN: 978-3-662-52988-1. DOI: 10.1007/978-3-662-52989-8{\textunderscore}88.
- [32] Merkisz, J.; Pielecha, J.: *Nanoparticle Emissions From Combustion Engines*. 1st ed. 2015. Vol. 8. Springer Tracts on Transportation and Traffic. Cham: Springer International Publishing and Imprint: Springer, 2015. ISBN: 9783319159287.
- [33] International Organization for Standardization: *ISO 11500: Hydraulic fluid power — Determination of the particulate contamination level of a liquid sample by automatic particle counting using the light-extinction principle*. Vernier, Geneva, Switzerland, 2022.
- [34] International Organization for Standardization: *ISO 21501-4: Determination of particle size distribution — Single particle light interaction methods*. 2018.
- [35] Buettner, H.: “Measurement of the Size of Fine Nonspherical Particles with a Light-Scattering Particle Counter”. In: *Aerosol Science and Technology* 12.2 (1990), pp. 413–421. ISSN: 0278-6826. DOI: 10.1080/02786829008959356.
- [36] International Organization for Standardization: *ISO 4405: Hydraulic fluid power — Fluid contamination — Determination of particulate contamination by the gravimetric method*. Vernier, Geneva, Switzerland, 2022.
- [37] International Organization for Standardization: *ISO 4407: Hydraulic fluid power — Fluid contamination — Determination of particulate contamination by the counting method using an optical microscope*. Geneva, Switzerland, 2002.
- [38] RETSCH GmbH Haan, ed.: *Siebanalytik: Qualität aufs Korn genommen*. 2016. URL: <https://www.retsch.de/files/8881/expert-guide-sieben.pdf>.
- [39] *Proceedings of AJKFLUIDS 2019 Fluids Enginerring*.
- [40] Verein deutscher Ingenieure: *VDI 2225: Technisch-wirtschaftliches Konstruieren - Technisch-wirtschaftliche Bewertung*. Düsseldorf, Germany, 1998-11.
- [41] Abdulagatov, I. M.; Akhmedova-Azizova, L. A.: “Viscosity of rocket propellant (RP-1) at high temperatures and high pressures”. In: *Fuel* 235 (2019), pp. 703–714. DOI: 10.1016/j.fuel.2018.08.073.
- [42] Outcalt, S. L. Laesecke, A.; Brumback, K. J.: “Thermophysical Properties Measurements of Rocket Propellants RP-1 and RP-2”. In: *Journal of Propulsion and Power* 25.5 (2009), pp. 1032–1040. ISSN: 0748-4658. DOI: 10.2514/1.40543.
- [43] European Cooperation for Space Standardization: *Space engineering: Structural factors of safety for spaceflight hardware*. 2019.
- [44] Markho, P.: “An Experimental Investigation of the Effect of Misalignment and Directionality on the Performance of an Externally-Pressurized, Orifice-Compensated Air Journal Bearing”. In: (1979).
- [45] Deutsches Institut für Normung e.V.: *DIN ISO 3601-1: Fluidtechnik - O-Ringe -Teil 1: Innendurchmesser, Schnur Stärken, Toleranzen und Bezeichnung*. Berlin, Germany.

Bibliography

- [46] Linstrom, P.: *NIST Chemistry WebBook, NIST Standard Reference Database 69*. 1997. DOI: 10.18434/T4D303. URL: <https://webbook.nist.gov/chemistry/fluid/>.
- [47] Stephan, P. et al., eds.: *VDI-Wärmeatlas*. Living reference work, continuously updated edition. VDI Springer Reference. Wiesbaden: Springer, 2019. ISBN: 9783662529911. DOI: 10.1007/978-3-662-52991-1.

A. Excerpts from standards

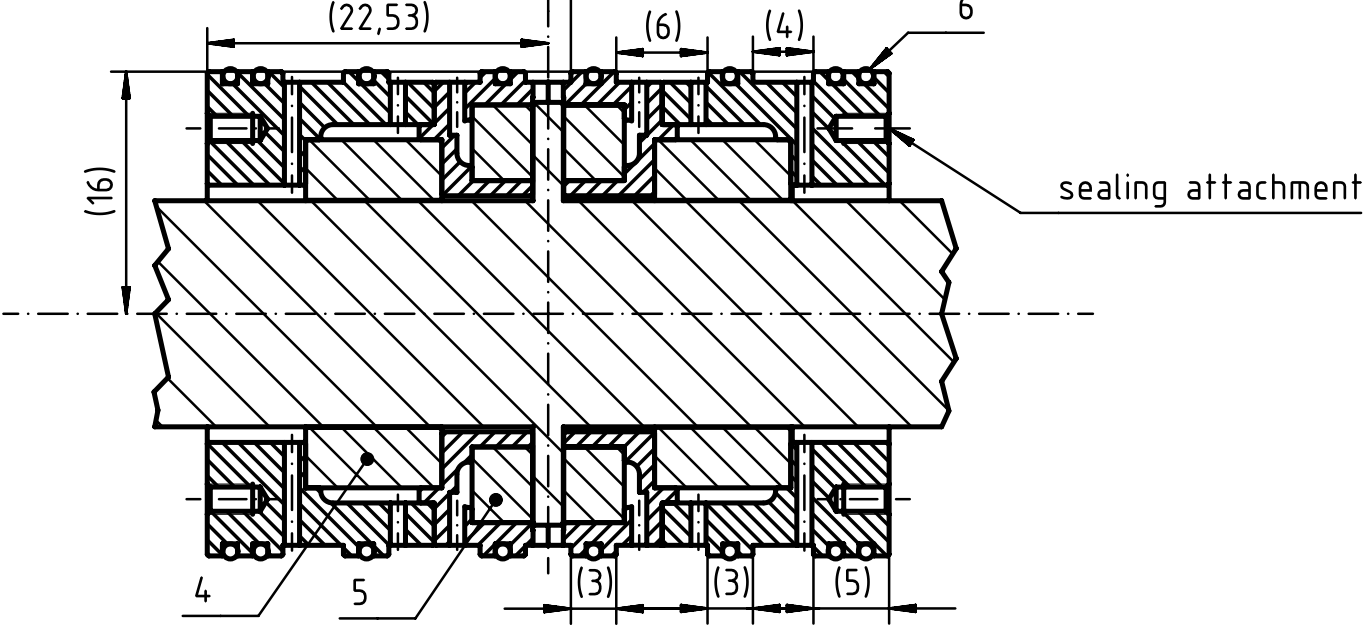
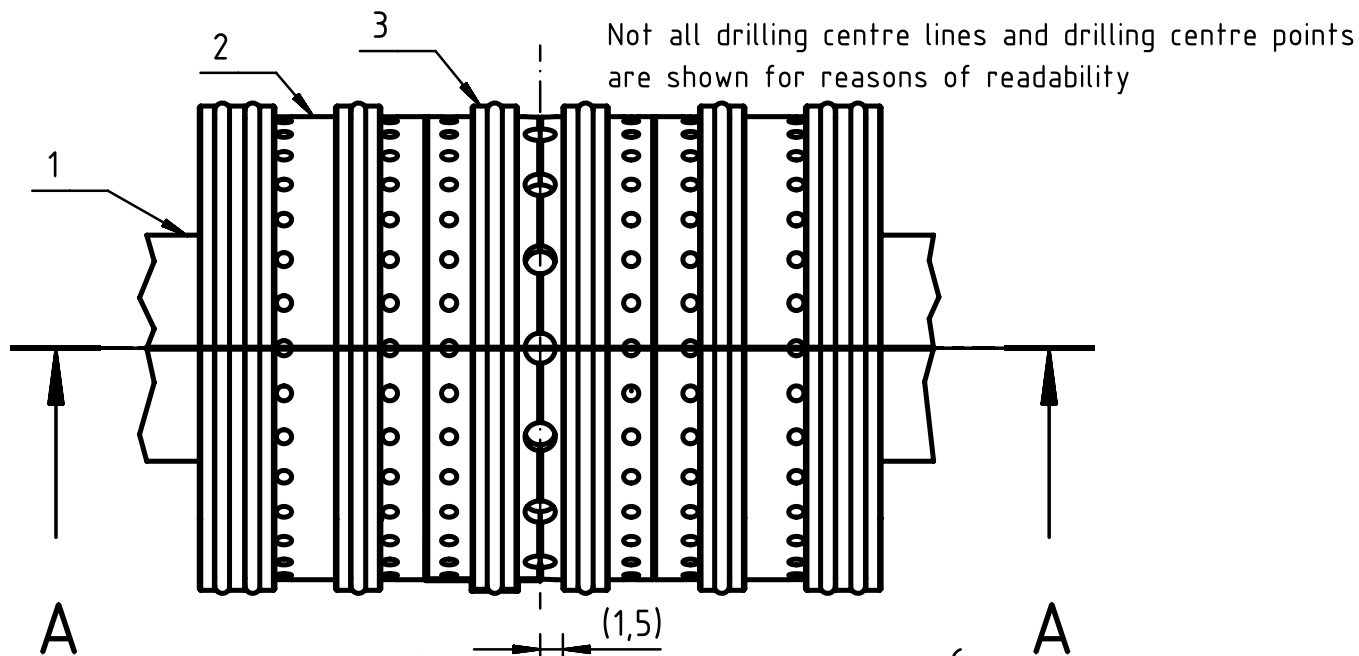
Table 4-1: Cleanliness classes

Hardware, propellant, gases, packaging	Class 1										Class 2										Class 3									
	Range of particle sizes (µm) ^a										Range of particle sizes (µm) ^a										Range of particle sizes (µm) ^a									
	0-5	6-10	11-25	26-50	51-100	101-200	0-5	6-10	11-25	26-50	51-100	101-200	0-5	6-10	11-25	26-50	51-100	101-200	0-5	6-10	11-25	26-50	51-100	101-200	201-500	501-1000				
Single part components	Do not count										Do not count										Do not count									
Multi part components	60	140	600	1200	6	1	0	0	0	0	0	140	600	1200	1000	250	60	15	40	6	1	0	0	0						
Subsystems	60	140	600	1200	6	1	0	0	0	0	0	140	600	1200	1000	250	60	15	40	6	1	0	0	0						
Systems	60	140	600	1200	6	1	0	0	0	0	0	140	600	1200	1000	250	60	15	40	6	1	0	0	0						
Test fluid	60	140	600	1200	6	1	0	0	0	0	0	140	600	1200	1000	250	60	15	40	6	1	0	0	0						
Components with moving parts having clearances of:	Do not count										Do not count										Do not count									
25 µm-40 µm	5	20	80	140	60	1	0	0	0	0	0	10	30	100	600	140	20	10	0	0	0	0	0	0						
40 µm-65 µm	5	20	80	140	60	1	0	0	0	0	0	10	30	100	600	140	20	10	0	0	0	0	0	0						
65 µm-90 µm	5	20	80	140	60	1	0	0	0	0	0	10	30	100	600	140	20	10	0	0	0	0	0	0						
Propellant or reference liquid	5	20	80	140	60	1	0	0	0	0	0	10	30	100	600	140	20	10	0	0	0	0	0	0						
Gas ^b	5	20	80	140	60	1	0	0	0	0	0	10	30	100	600	140	20	10	0	0	0	0	0	0						
Precision packaging material	5	20	80	140	60	1	0	0	0	0	0	10	30	100	600	140	20	10	0	0	0	0	0	0						

^a The particle count is related to a sample of 100 cm³ of liquid or 1 m³ of gas in conformance with clause 6.2.3, no metallic particles > 50 µm are allowed

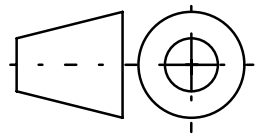
^b Propellant, pressurant and simulant

B. Technical Drawings




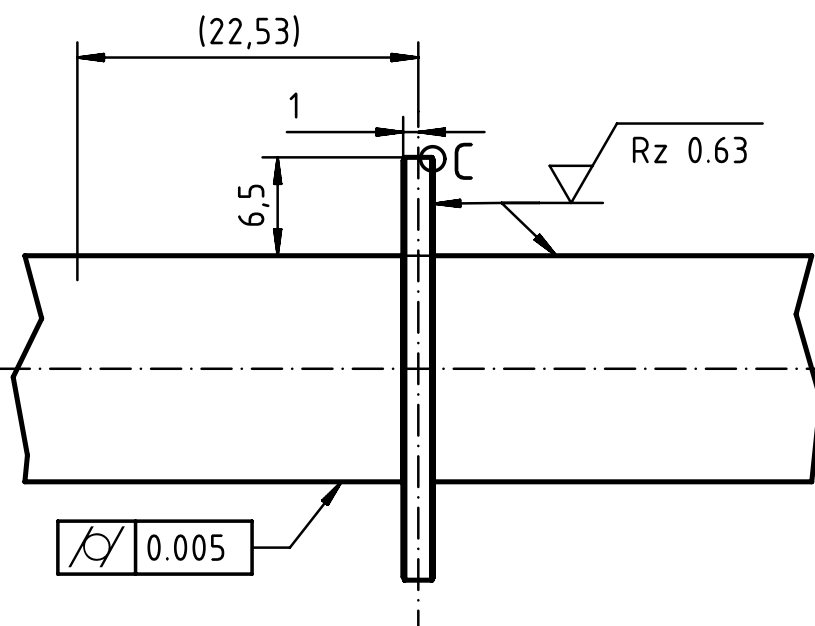
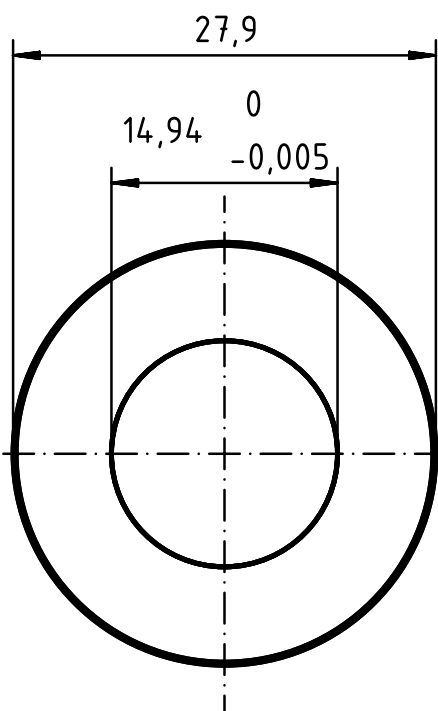
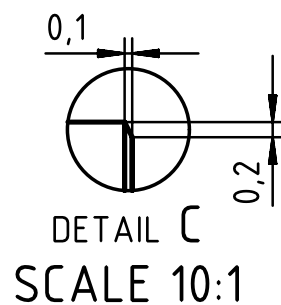
SECTION A-A

This technical drawing is intended to provide an impression of the design and is not complete in terms of dimensions, surface specifications and tolerances. The information required for integration of the design into the Launch Canada turbopump or a test setup is given.

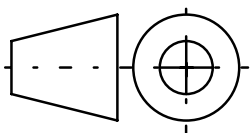


6	Pcs	8	O-Ring Sealing	O-Ring-ISO3601-1A-011A-30,4x1-CS	Nitrile Butadienne Rubber
5	Pcs	2	Thrust Bearing	MB20240006	C/C
4	Pcs	2	Journal Bearing	MB20240005	C/C
3	Pcs	2	Thrust Sleeve	MB20240004	IN-718
2	Pcs	2	Journal Sleeve	MB20240003	IN-718
1	Pcs	1	Shaft	MB20240002	IN-718
Pos. 1	Amount 2	Unit 3	name 4	Part number 5	Material 6


Max. Tolerance		Surface		Scale	2:1	Mass	-
-		-		material blank no.	-		
-		-		model no.	-		
	Date	Name		Design A			
Work.	15.03.2024	M. Beitinger					
Check							
Norm							
Supervisor: M. Ortelt							
				Drawing number	MB20240001		Page
				File: -		1/6	
Resp.	Change	Date	Name				

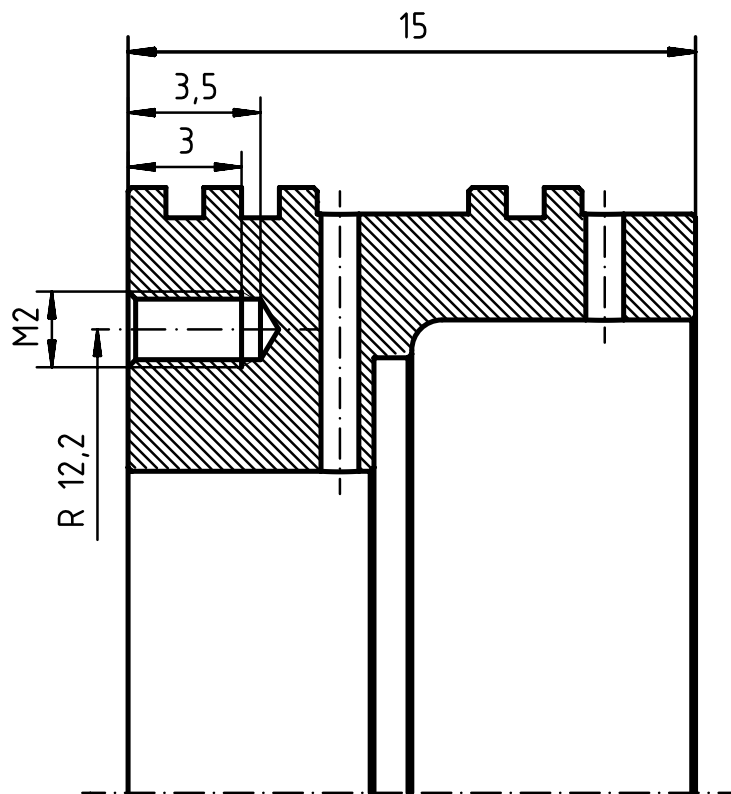
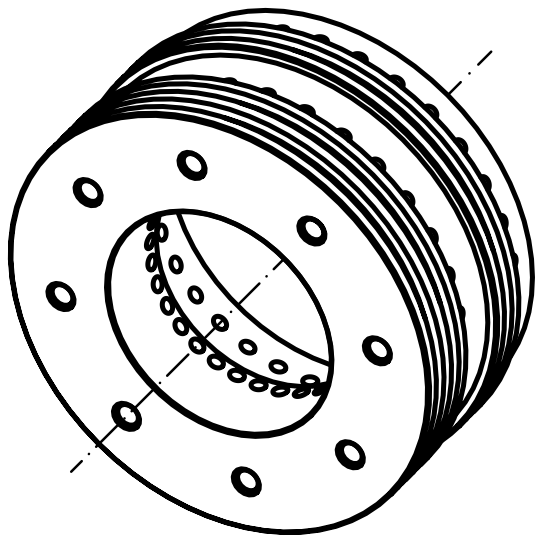


Outside the installation space of the bearing, changes to the shaft geometry and surface quality are possible



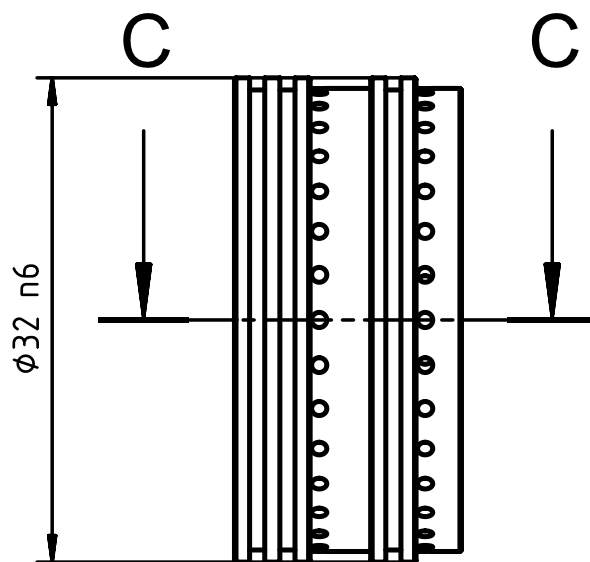
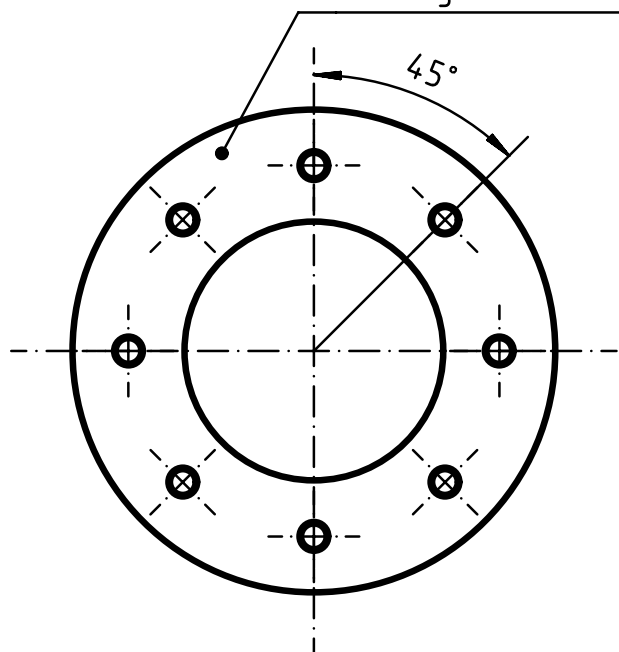
This technical drawing is intended to provide an impression of the design and is not complete in terms of dimensions, surface specifications and tolerances. The information required for integration of the design into the Launch Canada turbopump or a test setup is given.

				Max. Tolerance	Surface	Scale	2:1 (10:1)	Mass	-	
				-	-	material	IN-718			
					Date	Name	Name			
				Work.	15.03.2024	M. Beitinger	Shaft			
				Check						
				Norm						
				Supervisor: M. Ortelt						
							Drawing number	MB20240002	Page	2/6
Resp.	Change	Date	Name				File: -			

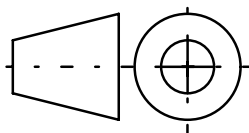


sealing attachment surface


SECTION C-C 5:1

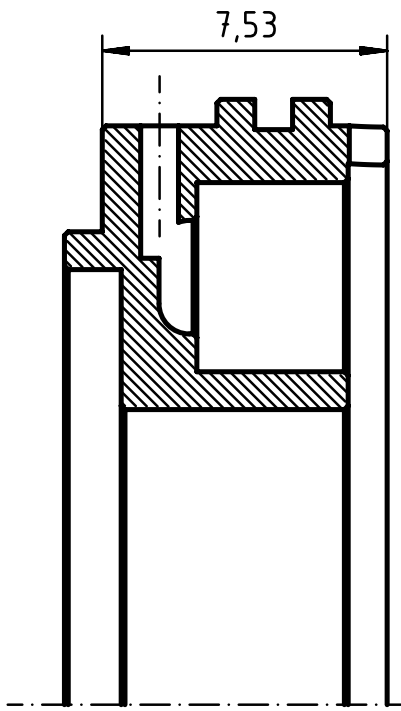


Installation in housing with diameter $\phi 32\ H5$

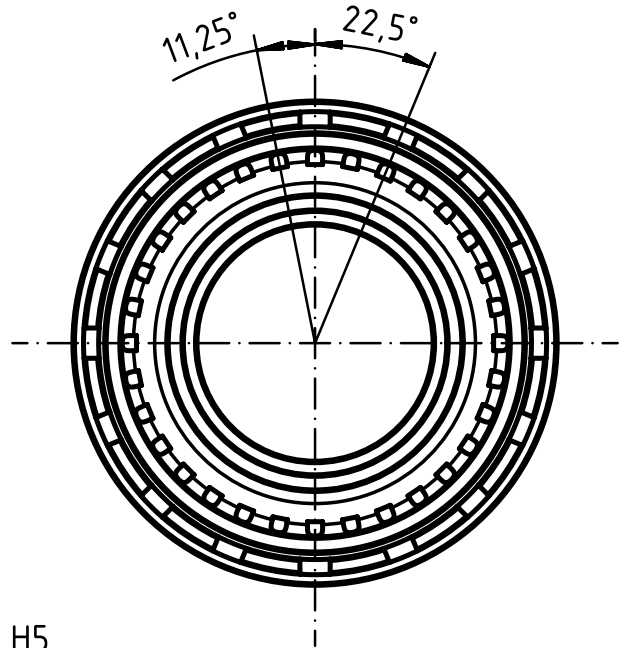
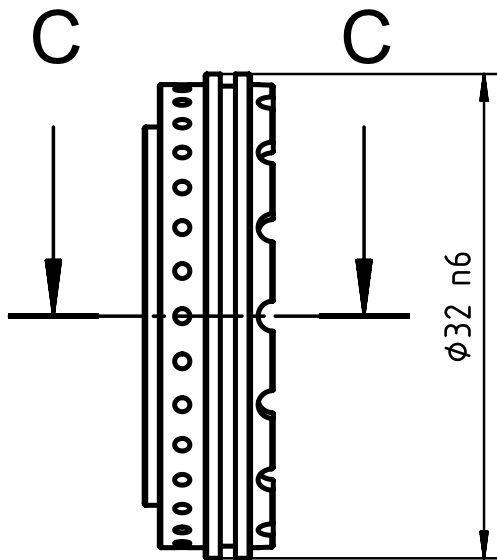
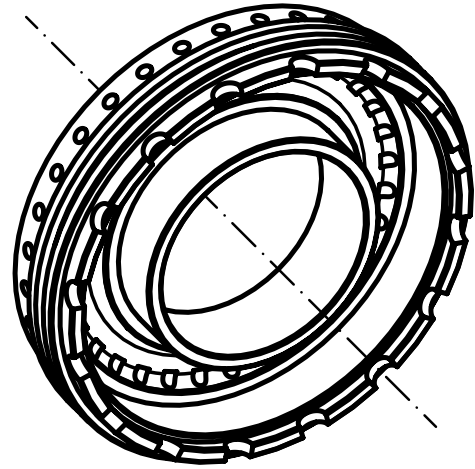


This technical drawing is intended to provide an impression of the design and is not complete in terms of dimensions, surface specifications and tolerances. The information required for integration of the design into the Launch Canada turbopump or a test setup is given.

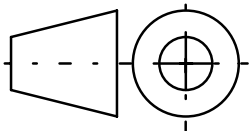
		Max. Tolerance	Surface	Scale	2:1 (5:1)	Mass	44,9g
		-	-	material	IN-718		
				blank no.			
				model no.			
		Date	Name	<p style="text-align: center; font-size: 24px; margin: 0;">Journal Sleeve</p>			
		Work.	15.03.2024 M. Beitinger				
		Check					
		Norm					
		Supervisor: M. Ortelt					
				Drawing number	MB20240003	Page	3/6
Resp.	Change	Date	Name	File: -			




SECTION C-C 5:1

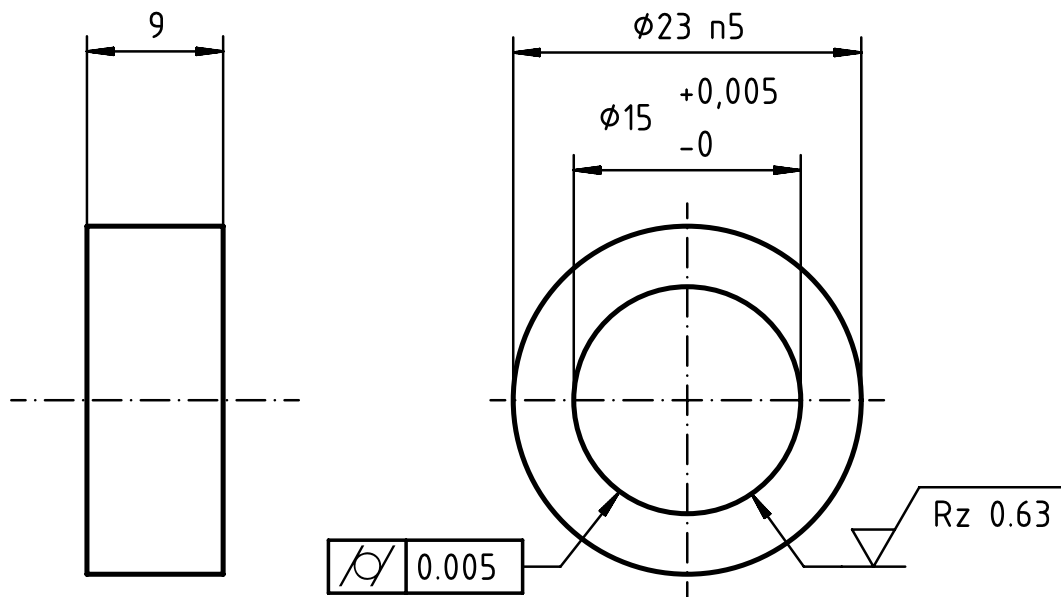


Installation in housing with diameter $\phi 32\ H5$

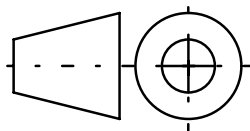


This technical drawing is intended to provide an impression of the design and is not complete in terms of dimensions, surface specifications and tolerances. The information required for integration of the design into the Launch Canada turbopump or a test setup is given.

			Max. Tolerance	Surface	Scale	2:1 (5:1)	Mass	14,9 g
			-	-	material	IN-718		
				Date	Name	Name		
			Work.	15.03.2024	M. Beitinger	<h1>Thrust Sleeve</h1>		
			Check					
			Norm					
			Supervisor: M. Ortelt					
						Drawing number	MB20240004	Page
								4/6
Resp.	Change	Date	Name	File: -				

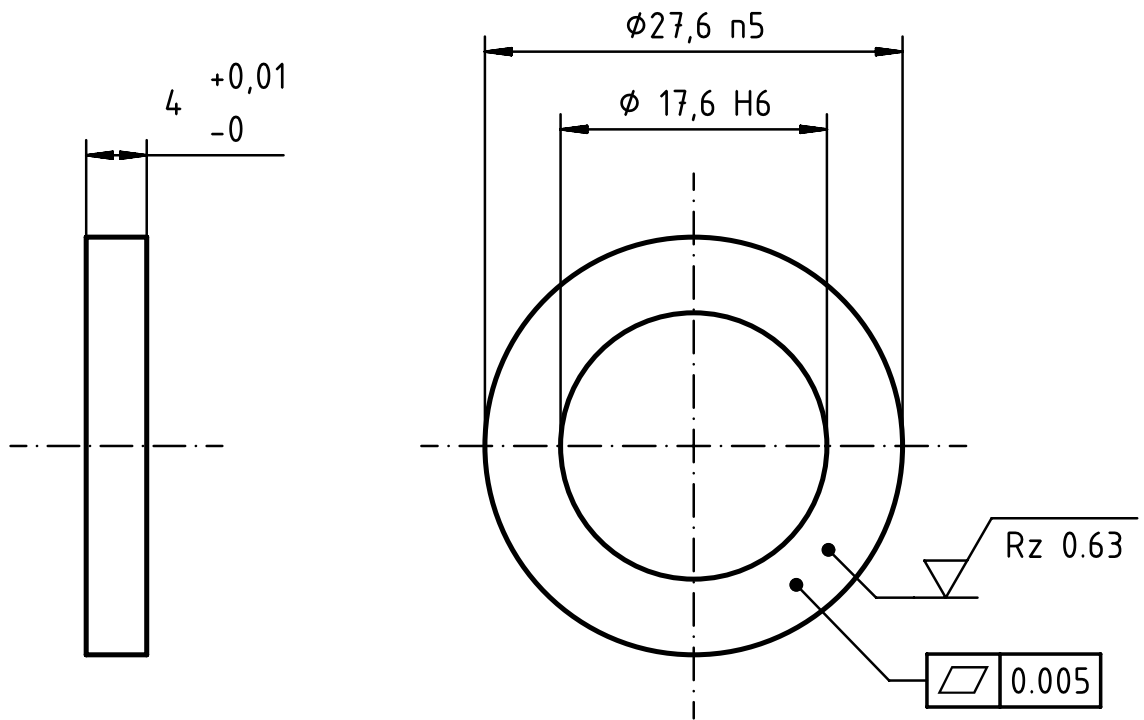


$Rz 6.3$ ($Rz 0.63$)

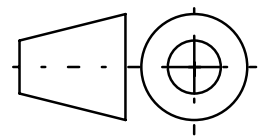


This technical drawing is intended to provide an impression of the design. Given tolerances and dimensions are targets that still have to be proven to be achievable in production. The information required for integration of the design into the Launch Canada turbopump or a test setup is given.

			Max. Tolerance	Surface	Scale	2:1	Mass	2.99 g
			ISO2768-f	-	material	C/C CMC		
				Date	Name	Name		
			Work.	15.03.2024	M. Beitinger	Journal Bearing		
			Check					
			Norm					
			Supervisor: M. Ortelt					
						Drawing number	MB20240005	
								Page
Resp.	Change	Date	Name	File: -				



Rz 6.3 (Rz 0.63)



This technical drawing is intended to provide an impression of the design.
 Given tolerances and dimensions are targets that still have to be proven to be achievable in production.
 The information required for integration of the design into the Launch Canada turbopump or a test setup is given.

				Max. Tolerance	Surface	Scale	2:1	Mass	1.97 g
				ISO2768-f	-	material	C/C CMC		
				Date	Name	blank no.			
				Work.	15.03.2024	model no.			
				Check		Name			
				Norm					
				Supervisor: M. Ortelt					
						Drawing number MB20240006			Page
									File: -
Resp.	Change	Date	Name						

C. Design Renderings

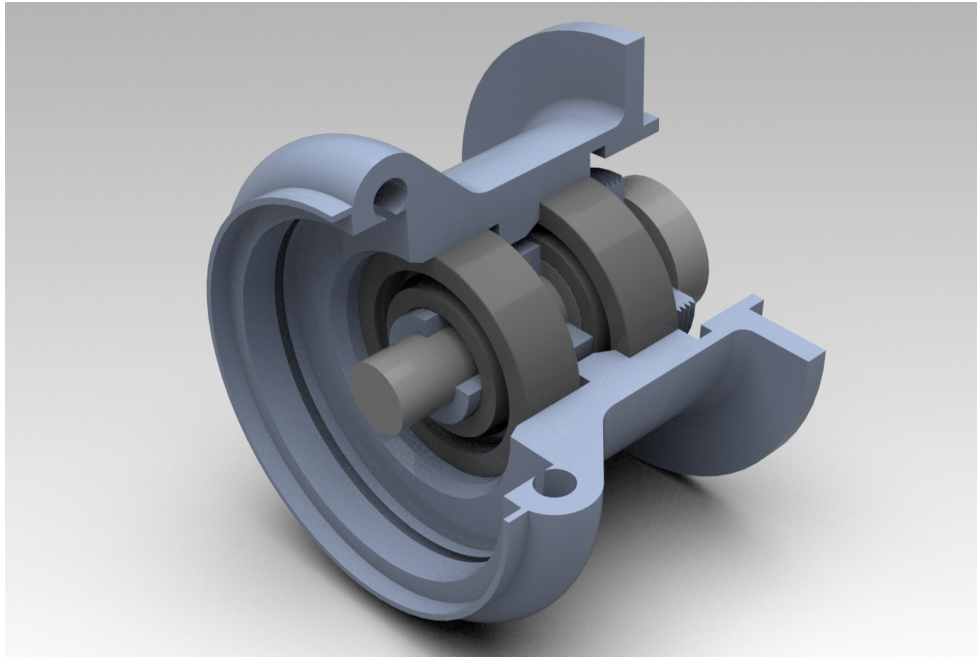


Fig. C.1.: Graphical rendering of the CAD model of the reconstructed bearing setup

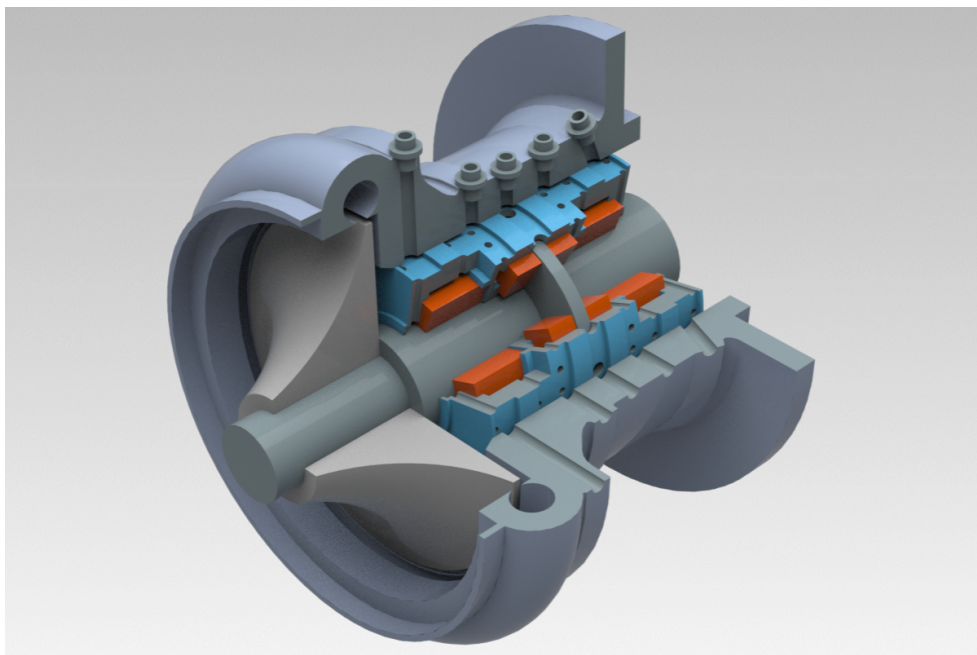


Fig. C.2.: Graphical rendering of design variant A

D. Experiment Documentation

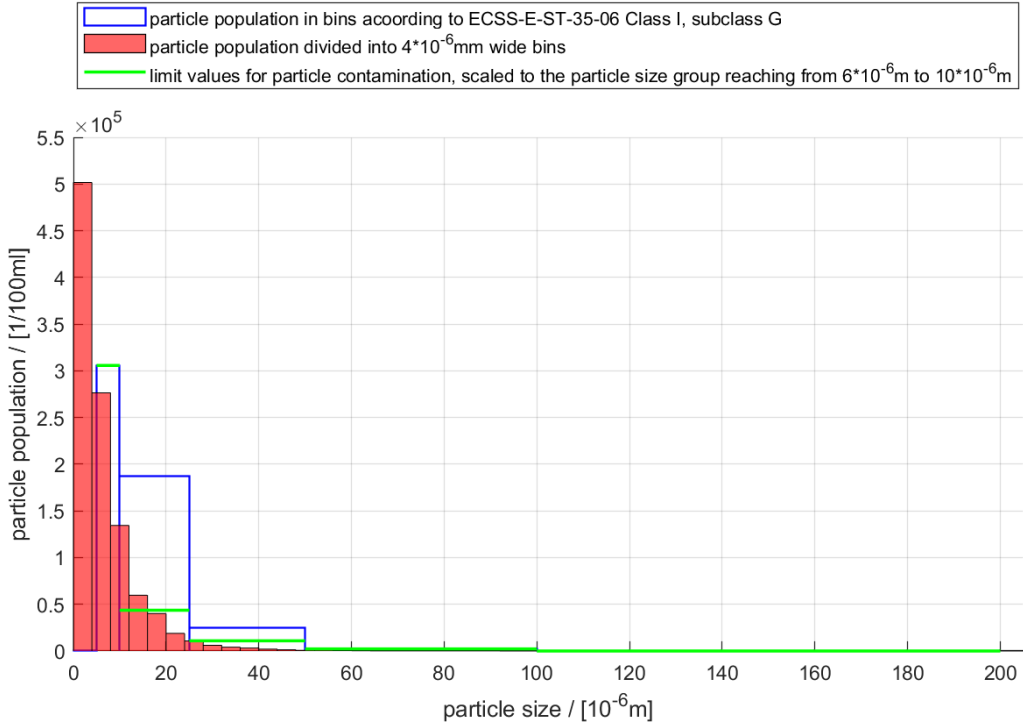


Fig. D.1.: Particle distribution within the sample fluid of sample 2, with an ultrasonic cleaning time of 30s (total of 240s)

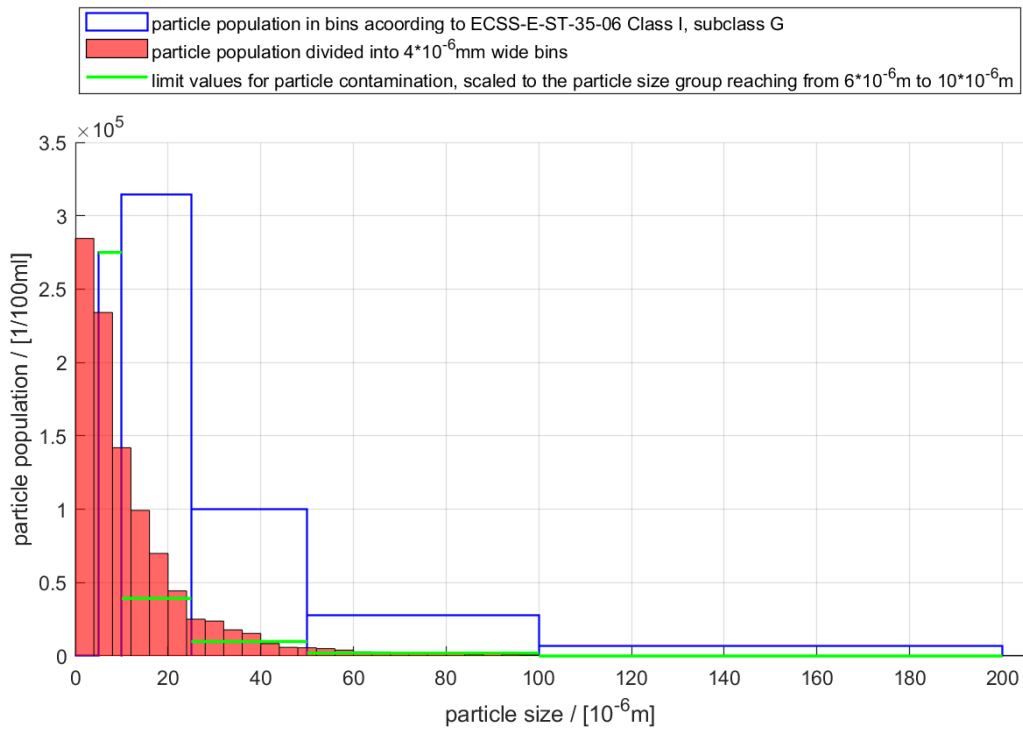


Fig. D.2.: Particle distribution within the sample fluid of Sample 1, with an ultrasonic cleaning time of 64 min (total of 128 min)

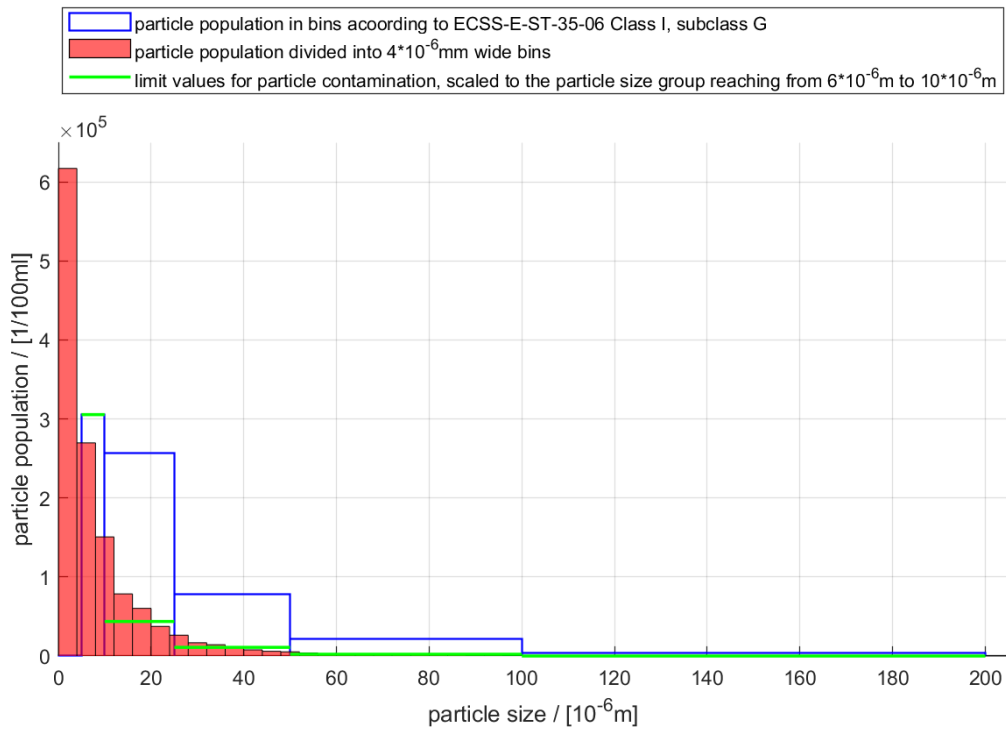


Fig. D.3.: Particle distribution within the sample fluid of sample 2, with an ultrasonic cleaning time of 64 min (total of 128 min)